Dielectrophoresis Study of Electroporation Effects on Dielectric Properties of Biological Cells

by

Elham Salimi

A Thesis submitted to the Faculty of Graduate Studies of
The University of Manitoba
in partial fulfilment of the requirements of the degree of

DOCTOR OF PHILOSOPHY

Department of Electrical and Computer Engineering
University of Manitoba
Winnipeg

Abstract

Electroporation affects the dielectric properties of cells. Dielectric measurement techniques can provide a label-free and non-invasive modality to study this phenomenon. In this thesis we introduce a dielectrophoresis (DEP) based technique to study changes in the cytoplasm conductivity of single Chinese hamster ovary (CHO) cells immediately after electroporation. Using a microfluidic chip, we study changes in the DEP response of single CHO cells a few seconds after electroporation. First, in order to quantify our DEP measurement results and relate them to the cells internal conductivity, we introduce a dielectric model for CHO cells. This is achieved by measuring the DEP response of many individual cells in the β-dispersion frequency region and curve fitting to the measured data. Second, we present quantitative results for changes in the cytoplasm conductivity of single cells subjected to pulsed electric fields with various intensities. We observe that when electroporation is performed in media with lower ionic concentration than cells cytoplasm, their internal conductivity decreases after electroporation depending on the intensity of applied pulses. We also observe that with reversible electroporation there is a limit on the decrease in the cells' internal conductivity. We hypothesize the reason is the presence of large and relatively immobile negative ions inside the cell which attract mobile positive ions (mainly sodium and potassium) to maintain cell electrical neutrality. We monitor the temporal response of cells after electroporation to measure the time constant of changes due to ion transport and observe this ranges from seconds to tens of seconds depending on the applied pulse intensity. This result can be used to infer information about the density and resealing time of very small pores (not measurable with conventional marker molecules). Lastly, we measure the electroporation of cells in media with different

conductivities. Our results show that electroporation in very low conductivity media requires stronger pulses to achieve a similar poration extent as in high conductivity media. The outcome of this thesis can be used to improve our understanding of the dynamics of electroporation as well as its modelling in order to make more accurate predictions or optimize the process for specific applications.

Acknowledgments

This thesis marks the end of my journey in obtaining my PhD, an intriguing and mind sharpening path filled with both joyful and distressing experiences. I am profoundly thankful to the people who have helped and supported me through the ups and downs of this journey.

First and foremost, I thank my advisor, Dr. Greg Bridges, for his continuous support and guidance throughout the project. His expertise and passion for research and science added inestimably to my graduate experience. His involvement in this challenging project motivated me to work harder and remain focused, even in the most distressful times. Every step along the way, from long and insightful discussions about measurement details and results to thorough paper revisions, I learned invaluable lessons I consider the greatest achievements of my PhD experience.

I would like to thank my advisory committee, Dr. Douglas Thomson and Dr. Francis Lin, for their intriguing questions and discussions during the project and their insightful comments on the thesis. I also thank my external examiner, Dr. Pingshan Wang, for reviewing the thesis and providing helpful comments.

I thank Dr. Michael Butler for allowing me to work in his microbiology lab and generously sharing his knowledge and vision about the biological aspects of this project.

I thank Dr. Katrin Braasch, from Dr. Butler's lab, for frequently providing me with biological cell samples and patiently teaching me how to work with different apparatus in the lab. Special thanks go out to my labmates and research group members, Marija Nikolic Jaric, Tim Cable, Graham Ferrier, Bahareh Saboktakin, Ashlesha Bhide, Samaneh Afshar

Delkhah, Azita Fazelkhah, and Kaveh Mohammad, for all the stimulating discussions, late night and early morning experiments, and all the fun memories we made out of frustrating failed experiments. I also thank Vincent Jung, James Dietrich, Dwayne Chrusch, and Cory Smit for their technical assistance.

I gratefully acknowledge the University of Manitoba, the Natural Sciences and Engineering Research Council (NSERC), Canada Foundation for Innovation, and CMC microsystems for financial support of this work.

Last but certainly not least, I would like to thank my parents, my sister, and my brother for supporting and encouraging me every moment along the way. Words cannot express how grateful I am to have their endless love and support. I would also like to thank my friends for being my second family in Winnipeg, helping me whenever and wherever I needed them.

Dedicated to my wonderful parents

Table of Contents

List of Tables

List of Figures

List of Copyrighted Materials for which Permission was Obtained

- E. Salimi, and D.J. Thomson, G.E. Bridges, " Dielectric model for Chinese hamster ovary cells obtained by dielectrophoresis cytometry", Biomicrofluidics, vol. 10, no. 1, pp. 014111, 2016. Chapters 3 and 4 of this thesis contains materials from this paper.
- K. C. Smith, “A Unified Model of Electroporation and Molecular Transport,” Massachusetts institute of Technology, 2011.

Chapter 1. Introduction

1.1 RESEARCH RATIONALE AND OBJECTIVES

Electroporation is the formation of conductive pores in the membrane of biological cells as a result of exposure to intense pulsed electric fields. The cell membrane polarizes in a strong electric field resulting in an increase in the electric potential across it. Above a certain threshold the lipid bilayer molecules of the membrane rearrange themselves and form pores through which impermeable molecules and ions can pass in and out of the cell [1]–[3]. The phenomenon has various biological and biomedical applications such as electrogenetherapy, electrochemotherapy, bacterial decontamination, and irreversible electroporation of cancerous cells [4]–[18]. Research studies and application methodologies employ pulses with various durations and amplitudes ranging from sub-millisecond to nanosecond and sub-kV/cm to MV/cm [19]. Long duration pulses (microsecond to millisecond) can result in a host of physiological effects such as necrosis, reversible, or irreversible permeabilization. Electroporation using nanosecond duration

pulses, such that the pulse duration is less than the cell membrane charging time-constant, has shown to effect the cell internal organelles and induce apoptosis in cells [20]–[28].

In studies of electroporation, direct measurements of the pores is challenging since the size of the pores is very small (nanometer radius) and they are formed in a short period of time (nanosecond to millisecond range). Therefore, measurements on the secondary effects of electroporation such as transport of impermeable ions and molecules through the membrane [29]–[33], increase in the membrane conductance [34]–[37], and changes in the physiological state of cells (e.g. apoptosis [20], [21]) mostly form the basis for understanding the process of electroporation and modelling it.

Electroporation starts with a large electric field that creates conductive pathways in the cell membrane. During the existence of pores the electric force along with diffusion transport ions in and out of the cell. As a result the dielectric properties of a cell exposed to electroporating pulses are affected during and after electroporation. The conductivity of the membrane is significantly higher during electroporation [2], [38]–[40] and the cell's internal conductivity is impacted by influx and efflux of ions [41], [42]. Therefore, dielectric measurement techniques can be used as a tool for detecting and characterizing electroporation of cells. Being label-free, non-destructive, and integratable with electroporation apparatus make dielectric study techniques suitable for investigating the extent of electroporation in applications such as bacterial decontamination or irreversible electroporation of cells. In addition, studying electroporation from an electrical point of view can provide valuable information on the mechanism and timing of ion transport and improve our insight into the dynamics of electroporation. Measurements of changes in the ionic content of cells induced by electroporation along with the conventional optical

techniques can provide information on the density of pores, their size, and their resealing time. Using ions rather than larger dye molecules has the advantage that information about very small size pores (smaller than conventional dye molecules) can be inferred experimentally. In [33] the uptake of Thallium cations by cells preloaded with a fluorescent marker is measured to obtain information about the density and lifetime of nanopores created by nanosecond pulsed electroporation. Dielectric study techniques have the potential to perform similar measurements without requiring marker molecules.

Quantified measurements of changes in dielectric parameters of cells during and after electroporation and incorporating them into the theoretical and numerical models of electroporation can improve the accuracy of their predictions. The necessity of considering a dynamic membrane conductivity in modeling the response of cells to a single electroporating pulse has been discussed in several studies [43]–[48]. Cytoplasm conductivity is another parameter which can be dramatically influenced by electroporation. In multiple pulse applications (with slow repetition rate) this can change the charging time constant of the cell internal structures and impact the electroporation process. With some knowledge of how the dielectric properties of a cell is affected after pulse exposures the pulse parameters can be optimized for various applications in multiple pulse electroporation protocols.

Dielectric based techniques have been employed in several studies to investigate the electroporation of a bulk suspension of biological cells. Changes in the conductivity of cell pellets before and after electroporation with microsecond and millisecond pulses are reported in [40], [49]. Frequency-domain impedance measurement over the range 100 Hz to 100kHz is used in [50] to study the change in the conductivity of a suspension of mouse

melanoma cells (B16F1) due to electroporation. Time-domain reflectometry (TDR) is employed in [41], [51]–[53] to study changes in the electrical properties of HL-60 (Human promyelocytic leukemic cell line) and Jurkat cells subjected to microsecond and nanosecond pulses. Studying the electroporation of cells subjected to microsecond pulses using a dielectrophoresis (DEP) technique, based on monitoring the cross-over frequency or by field-flow fractionation, is reported in [42], [54]–[56].

Bulk electroporation and studying the response of a suspension of cells provide the overall response of a distribution of cells with different sizes, shapes, and possibly physiological state. Single cell studies, however, have the advantage of being able to examine the response of a cell with a known shape and size and without the influence of neighboring cells or aggregation effects. . In a recent study, the dielectric properties of individual HeLa cells before and after electroporation has been investigated using an electric impedance spectroscopy technique. In their study cells are exposed to high intensity continuous sinusoidal electric fields as they pass through a set of poration electrodes [57]. In their case the cells are exposed to numerous strong pulses (more than 1000 pulses) which cause dramatic changes to the cell structure and membrane.

The objective of this work is to dielectrically study the effects of electroporation at single cell level and obtain quantitative results on how the internal conductivity of cells is affected by electroporation. We develop a microfluidic based setup and measurement technique to simultaneously electroporate single cells and measure their dielectric response within seconds after pulse exposures. Electroporation is performed by applying approximately eight 100 μs duration pulses with various amplitudes similar to the protocols employed in several previous studies [31], [32], [42], [48], [50], [56], [58]–[60].

We employ a DEP cytometry technique to study changes in the cytoplasm conductivity of single Chinese hamster ovary (CHO) cells immediately after electroporation. A microfluidic chip with an array of sensing and actuating electrodes embedded in its microfluidic channel is used to detect single cells, electroporate them, and measure their DEP response before and after electroporation. To achieve the required sensitivity for detection and dielectric characterization of single cells we use a resonator-enhanced microwave interferometer which measures the microwave frequency differential impedance of sensing electrodes as a cell passes over them. Since the dielectric properties of CHO cells are not well-characterized, first, we describe a dielectric model for CHO cells and determine its dielectric parameters using measurements by the DEP cytometer and numerical simulations. Then we employ this model to relate the electroporation induced changes in the DEP response of cells to their internal conductivity. Changes in the cytoplasm conductivity of cells subjected to microsecond pulses with various intensities is reported.

1.2 CONTRIBUTIONS

The main contributions of the author reported in this thesis are as follow:

- A novel dielectrophoresis based technique is introduced to simultaneously electroporate single biological cells and study their dielectric response within seconds after the pulse application. This provides a label-free and non-invasive modality to measure the efficiency of electroporation in applications such as bacterial decontamination or transfection.

- A numerical model is developed to relate the displacement of cells in a microfluidic channel due to a DEP force to the cells dielectric properties. The validity of the numerical model is verified with polystyrene spheres which have known dielectric properties.
- By measuring the DEP response of many individual CHO cells along with numerical simulations, a dielectric model with its parameters is introduced for CHO cells. The model is based on a fairly complicated double-shell structure which includes the cell's nucleoplasm, nuclear envelope, cytoplasm, and membrane. Moreover, the sensitivity of cell dielectric parameters over different frequencies is presented. The developed model can benefit the ongoing studies on dielectric assessment of CHO cells' status for pharmecutical applications and other medical/biological researches.
- Quantified results showing changes in the cytoplasm conductivity of individual CHO cells due to electroporation with pulsed electric fields of various intensities is presented. With electroporation in a low conductivity medium (less than 0.2 S/m), a decrease in the cytoplasm conductivity of cells depending on the intensity of the applied pulses is demonstrated. Also, a limit on the decrease in the internal conductivity of cells after electroporation is observed indicating that beyond a certain intensity, stronger pulses do not lead to further decrease in the cells internal conductivity. The presented results can be used to optimize the electroporation protocol and pulse parameters for various applications. Also, incorporating changes in the internal conductivity of cells into the model of electroporation improves the accuracy of their predictions in multiple pulse applications.

- The temporal change in the cytoplasm conductivity of individual CHO cells exposed to pulsed electric fields with various intensities is presented. It is observed that there is a time constant associated with the cells' internal conductivity change which ranges from seconds to tens of seconds depending on the applied pulse intensity. This observation is in agreement with simulation results reported by others in literature. This result can be used to infer information about the density of minimum-size pores which cannot be assessed by conventional fluorescent markers.
- Studies of the electroporation of individual cells in extremely low conductivity medium (0.001 S/m) is performed. Experimental results suggest that in such media higher intensity pulses are required to achieve a similar poration extent as compared with electroporation in higher conductivity media. In dielectric study of electroporation, very low conductivity media is commonly employed to avoid electrode polarizations. The results presented here can help such studies in properly selecting the pulse parameters.

1.3 THESIS STRUCTURE

The thesis is comprised of seven chapters as follows:

Chapter 1. Introduction

In this chapter the motivations and objectives of the thesis is presented. A comprehensive review of the previous works on dielectric measurement of electroporation is given covering the studies on population of cells and single cells.

Chapter 2. Theory and Background

In this chapter a brief review of the theory of dielectrophoresis and electroporation is presented. Using simulations, the effect of cells' dielectric parameters on the spectrum of the Clausius-Mossotti factor is investigated. This is performed to select the proper frequency range for studying the electroporation of cells.

Chapter 3. DEP Cytometry Apparatus and Measurement Technique

In this chapter our DEP measurement set-up and technique is presented. The microfluidic system along with the microwave interferometer employed to detect cells in the microfluidic channel is described in detail. Then the DEP measurement technique and the numerical simulation method used to obtain $Re\{K_{CM}\}$ is explained.

Chapter 4. Dielectric Model for CHO Cells

In this chapter a dielectric model for CHO cells is presented based on a double-shell model. The measured DEP response of CHO cells in media with different conductivities is demonstrated. Using numerical simulations, the spectra of $Re\{K_{CM}\}$ is calculated from the measured DEP response. After performing a sensitivity analysis to determine the most sensitive cell parameters over our measured frequency range, a dielectric model for CHO cells is obtained by optimization and curve-fitting to the measured date. The results of this chapter is published in:

E. Salimi, and D.J. Thomson, G.E. Bridges, " Dielectric model for Chinese hamster ovary cells obtained by dielectrophoresis cytometry", Biomicrofluidics, vol. 10, no. 1, pp. 014111, 2016.

Chapter 5. Single Cell Cytoplasm Conductivity Change Induced by Electroporation

This chapter presents the results of measuring changes in the cytoplasm conductivity of CHO cells induced by electroporation. The DEP response of several individual cells before and after exposure to electroporating pulses with various amplitudes is presented. Using numerical simulations, the measured data is mapped to the cell's cytoplasm conductivity providing quantitative results on how the cell's internal conductivity is affected by electroporation and its dependence on the pulses amplitude. A discussion relating the results of this chapter to the findings in other literature (obtained by other measurement techniques or modeling) is also presented. A manuscript based on the results of this chapter has been prepared for submission to the journal Biomicrofluidics.

Chapter 6. Effect of Medium Conductivity

Electroporation of cells in moderately high and very low conductivity media is studied in this chapter. The results for single cell and bulk electroporation in a very low conductivity medium, obtained using our DEP cytometer, is presented and compared with the results from a dye exclusion technique.

Chapter 7. Conclusions and Future Work

A summary of the research is presented and possible future work is suggested in this chapter.

Chapter 2. Theory and Background

2.1 DIELECTROPHORESIS

Dielecterophoresis (DEP) is the movement of a polarizable particle in a non-uniform electric field caused by electric dipole forces. The magnitude and direction of a DEP force depends on the dielectric properties of cells with respect to their suspending media and is thus different on various type or state of cells. Dielectrophoretic based techniques combined with microfluidic systems have been used to study stem cells [61], differentiate different types of cells in blood analysis [62], [63], trap and separate DNA [64], [65], study the effect of drugs on cells [66]–[68] separate viable and non-viable cells [69]–[71], isolate circulating tumor cells from a blood sample [72], and detect early stage of apoptosis in a batch culture of CHO cells [73], [74]. Reviews on the theory and applications of DEP can be found in [75], [76].

2.1.1 Theory

In case of particles such as biological cells, a DEP force arises from the accumulation of free (conductive, related to σ) and bound (dielectric, related to ε) charges at the interface of the particle and suspending media due to an alternating electric field and is known as Maxwell-Wagner interfacial polarization. For a homogeneous spherical particle with complex permittivity $\tilde{\varepsilon}_p = \varepsilon_p - j\frac{\sigma_p}{\omega}$ (ε_p and σ_p the particle permittivity and conductivity, respectively) suspended in a medium with complex permittivity $\tilde{\varepsilon}_e = \varepsilon_e - j\frac{\sigma_e}{\omega}$ (ε_e and σ_e the external medium permittivity and conductivity, respectively) and exposed to an electric field, $\boldsymbol{E}$, the equivalent electric dipole moment of the particle (see Fig. 2.1) is obtained by solving the Laplace equation with proper boundary conditions as [77]

$$\boldsymbol{p} = 4\pi\varepsilon_e \frac{\tilde{\varepsilon}_p - \tilde{\varepsilon}_e}{\tilde{\varepsilon}_p + 2\tilde{\varepsilon}_e}\boldsymbol{E} = 4\pi\varepsilon_e R^3 K_{CM}(\omega)\boldsymbol{E}, \tag{2.1}$$

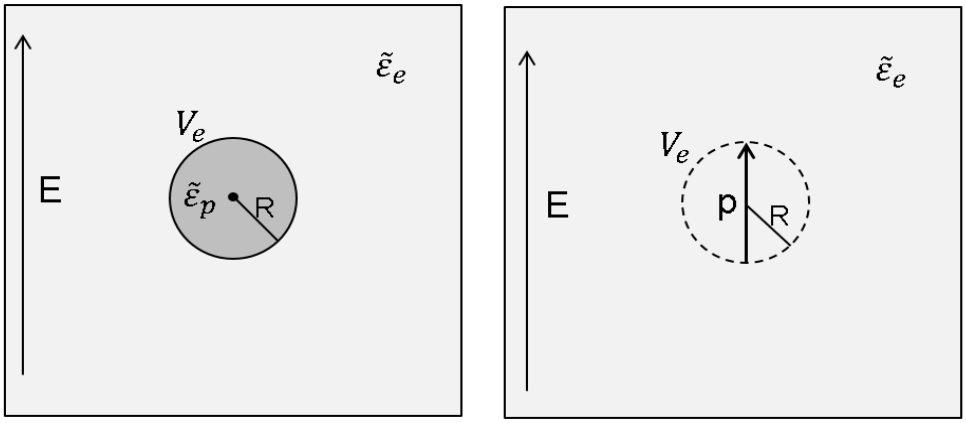

Figure 2.1: *A homogenous spherical particle with complex permittivity ε_p in a medium with complex permittivity ε_e can be replaced by an electric dipole with dipole moment, $\boldsymbol{p}$, such that the electric potential at the boundary of the particle and medium, V_e, remains the same. $\boldsymbol{p}$ is related to ε_p and ε_e through the Clausius-Mossotti factor, K_{CM}.*

where $K_{CM}(\omega)$ is the Clausius-Mossotti factor which is a measure of the cell's polarizability with respect to its surrounding medium at a given frequency and *R* is the particle radius.

In a stationary uniform electric field the equivalent dipole positive and negative charges experience the same electric force resulting in a zero net force on the particle. However, in a non-uniform electric field the positive and negative charges are exposed to forces with different values which leads to a non-zero DEP force on the particle. Under the assumption that the size of the particle is much smaller than the field non-uniformity (so that the dipole approximation is valid) the time-averaged DEP force exerted on the particle is calculated as [77]

$$\boldsymbol{F_{DEP}} = \frac{3}{2}\varepsilon_e V_p Re\{K_{CM}\}\boldsymbol{\nabla}(E_{rms}^2)\,, \tag{2.2}$$

with V_p, $Re\{K_{CM}\}$, and E_{rms} being the particle volume, the real part of K_{CM}, and the rms of the electric field at the centre of the particle. The DEP force is frequency dependent through $Re\{K_{CM}\}$ and is directed with or against the gradient of the square of the electric field depending on the sign of $Re\{K_{CM}\}$. With $Re\{K_{CM}\} > 0$ the force is called positive DEP (pDEP) and the particle is moved towards the high intensity field regions. Whereas with $Re\{K_{CM}\} < 0$ the force is called negative DEP (nDEP) and the particle is repelled from the high intensity field areas. Fig. 2.2 gives $Re\{K_{CM}\}$ versus frequency for a typical viable CHO cell suspended in a medium with conductivity 0.17 S/m. The electrical and geometrical parameters of the cell are the values obtained for CHO cells in chapter 4 (see Table 4.1)

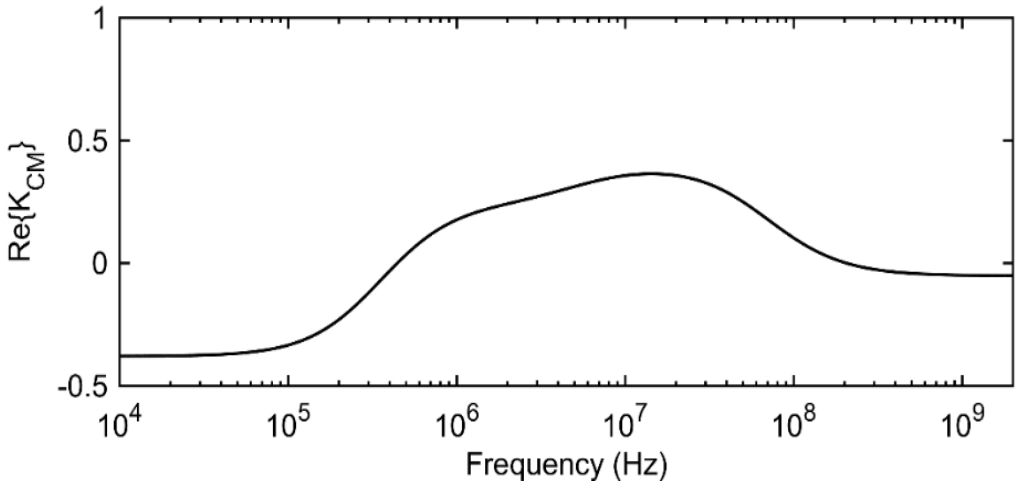

Figure 2.2: *$Re\{K_{CM}\}$ as a function of frequency for a typical viable CHO cell (with parameters given in Table 4.1) suspended in a medium with conductivity 0.17 S/m.*

The DEP force expressed in Eq.(2.2) is derived for a homogenous spherical particle. Although many type of cells (including Chinese hamster ovary (CHO) cells employed in this study) can be geometrically approximated by spheres they are heterogeneous due to their plasma membrane and internal organelles. To estimate the DEP force on cells, they are simplified and represented by a multi-shell model shown in Fig. 2.3. In this study we use a two-shell model to represent a CHO cell containing the nucleus, nuclear envelope, cytoplasm, and plasma membrane. Starting from the innermost layer, the nucleus and the nuclear envelope can be replaced by a homogeneous sphere using the equivalent dipole moment method explained before. Applying the technique progressively to simplify the multi-shell model, as shown in Fig. 2.3, yields the cell equivalent homogeneous sphere with complex permittivity [78], [79]

$$\tilde{\varepsilon}_c = \tilde{\varepsilon}_m \frac{2(1-v_1)+(1+2v_1)E_1}{(2+v_1)+(1-v_1)E_1}, \tag{2.3}$$

where $v_1 = (1 - d/R)^3$ with d the membrane thickness, $\tilde{\varepsilon}_m$ the complex permittivity of the membrane, and R the cell radius and E_1 defined as

$$E_1 = \frac{\tilde{\varepsilon}_i}{\tilde{\varepsilon}_m} \frac{2(1 - v_2) + (1 + 2v_2)E_2}{(2 + v_2) + (1 - v_2)E_2}, \tag{2.4}$$

where $v_2 = (R_n/(R - d))^3$ with R_n the nucleus radius, $\tilde{\varepsilon}_i$ the complex permittivity of the cytoplasm, and E_2 given by

$$E_2 = \frac{\tilde{\varepsilon}_{ne}}{\tilde{\varepsilon}_i} \frac{2(1 - v_3) + (1 + 2v_3)E_3}{(2 + v_3) + (1 - v_3)E_3}, \tag{2.5}$$

$\tilde{\varepsilon}_n$ and $\tilde{\varepsilon}_{ne}$ are the complex permittivity of the nucleoplasm and nuclear envelope, $E_3 = \tilde{\varepsilon}_n/\tilde{\varepsilon}_{ne}$, and $v = (1 - d_n/R_n)^3$ with d_n the nuclear envelope thickness.

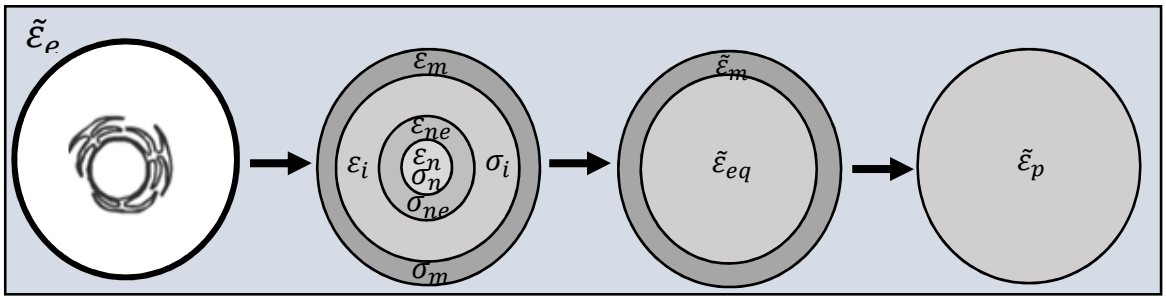

Figure 2.3: *Progressive simplification of a cell with a nucleus into a homogenous sphere using two-shell model and Eq. 2.3-2.5.*

It should be noted that the shell model employed throughout this study is spherically symmetric. Cells may not be completely symmetric and this may slightly effect the extraction of cell parameters from the measured data.

2.1.2 Effect of Cell Parameters on the Clausius-Mossotti Factor

The DEP force acting on a cell is a function of the cell dielectric properties through the real part of the Clausius-Mossotti factor, $Re\{K_{CM}\}$. In this section we investigate the effect of a cells dielectric and geometric properties (permittivity and conductivity of the membrane,

cytoplasm, nuclear envelope, and nucleoplasm, the cell radius and the membrane thickness) on the frequency spectra of $Re\{K_{CM}\}$. In each case one parameter is chosen as variable and the remaining ones take the nominal value provided in Table 4.1.

A. Effect of Membrane Permittivity and Conductivity

We study the effect of changing the membrane permittivity and conductivity on the frequency dependent behavior of $Re\{K_{CM}\}$. The cell membrane is made of phospholipid bilayer with embedded proteins. Thus, it has a very low conductivity (approximately 10^{-6} S/m) and its relative permittivity is substantially less than water (reported in the range 3 to 20 for different type of cells). $Re\{K_{CM}\}$ as a function of frequency for three values of membrane conductivity and permittivity are shown in Fig 2.4a and b, respectively. The broad range of conductivity change (not realistic under normal physiological conditions) is chosen because during electroporation the membrane conductance increases by several orders of magnitude. The graph shows that the membrane conductivity only affects the low frequency (less than 200 kHz) part of $Re\{K_{CM}\}$ spectra. Approximately one order of magnitude increase in the membrane conductivity is required to decrease the low frequency plateau of $Re\{K_{CM}\}$ by 20 percent. The membrane permittivity (effects the membrane capacitance) mostly impacts the first crossover frequency, the frequency at which the sign of $Re\{K_{CM}\}$ changes from negative to positive. Increase in the membrane permittivity results in larger membrane capacitance which shifts the first crossover to lower frequencies. Electroporation may cause an increase in the effective membrane permittivity during the presence of pores since the pores are filled water which has a higher permittivity than the lipid structure of the membrane.

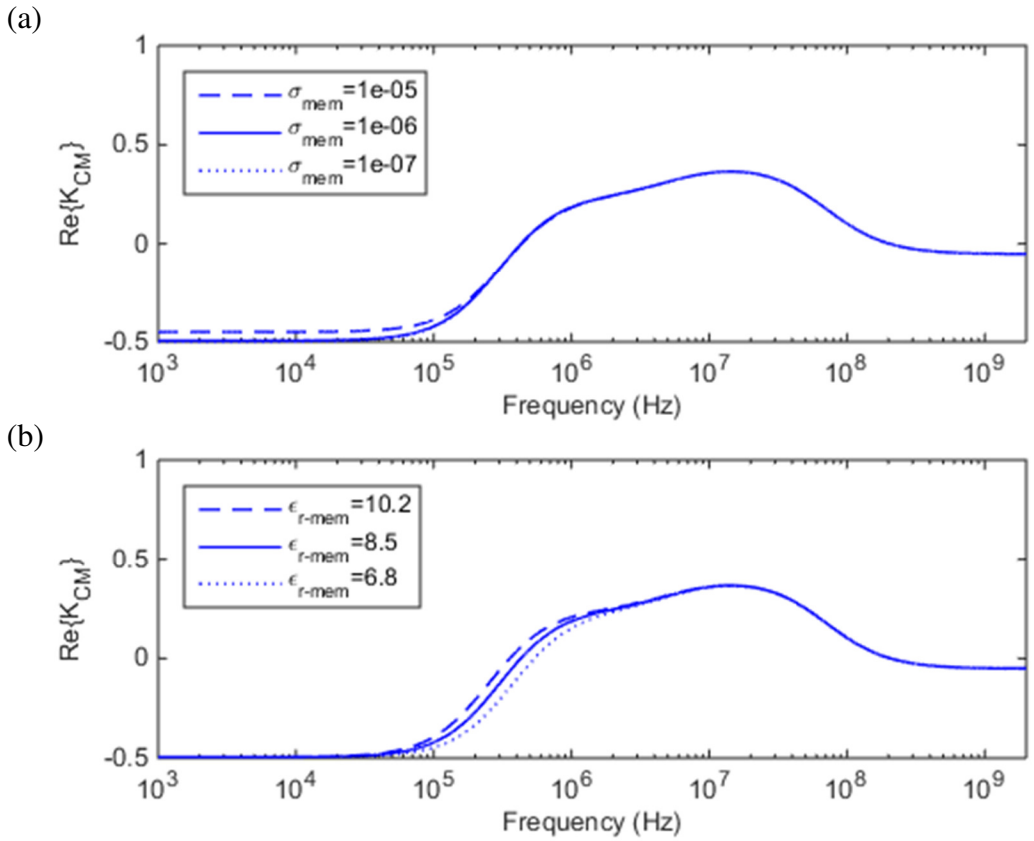

Figure 2.4: *Spectrum of $Re\{K_{CM}\}$ for three values of (a) membrane conductivity and (b) membrane permittivity. Changes in the membrane conductivity have impacts on the low frequency plateau of the spectra whereas the membrane permittivity affects the first crossover frequency.*

B. Effect of Cytoplasm Permittivity and Conductivity

The cytoplasm of cells is dominantly made of water. The presence of various type of proteins and other soluble and insoluble substances makes the relative permittivity of the cytoplasm slightly less than water (approximately 60). Cytoplasm is moderately conductive (ranging from 0.1 to 1.2 S/m for different type of cells) due to the presence of ions and other mobile charged molecules inside the cell. The effect of changes in the cytoplasm conductivity and permittivity on $Re\{K_{CM}\}$ is shown in Fig 2.5. The cytoplasm conductivity affects the spectra between the two crossover frequencies with more impact over 1-50 MHz. A 20 percent decrease in the cytoplasm conductivity leads to 18 percent decrease in $Re\{K_{CM}\}$ at 10 MHz. Changes in the cytoplasm permittivity have impact on the

second crossover frequency and high frequency part of the spectra (higher than 100 MHz). Transport of ions and other molecules through the membrane during and after electroporation may lead to changes in the cytoplasm conductivity and permittivity.

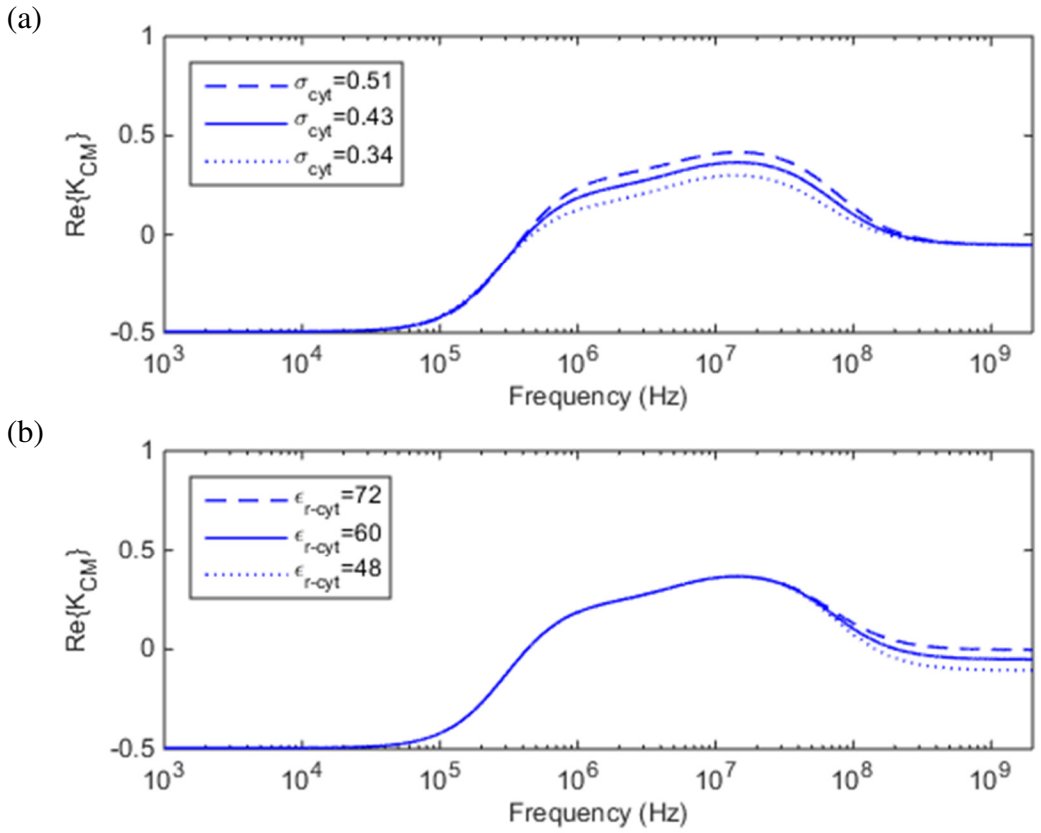

Figure 2.5: *Spectrum of Re{K_{CM} } for three values of (a) cytoplasm conductivity and (b) cytoplasm permittivity. Changes in the cytoplasm conductivity affects the spectra between the two crossovers whereas the permittivity impacts the second crossover frequency and the high frequency part of the spectra.*

C. Effect of Nuclear Envelope Permittivity and Conductivity

Changes in the nuclear envelope permittivity and conductivity only slightly affects the spectra of $Re\{K_{CM}\}$ spectra as depicted in Fig 2.6. Significant increase in the nuclear envelope conductivity (may occur due to internal membranes electroporation) flattens the spectra in the low megahertz range.

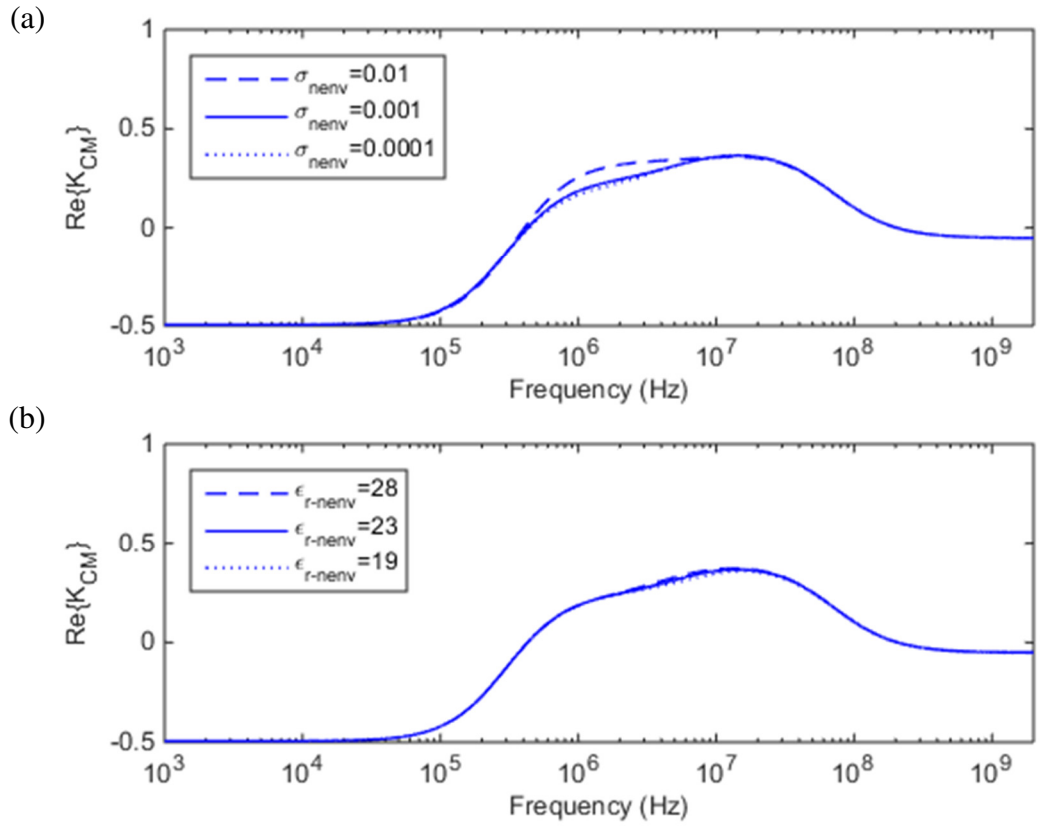

Figure 2.6: *Spectrum of $Re\{K_{CM}\}$ for three values of (a) nuclear envelope conductivity and (b) nuclear envelope permittivity.*

D. Effect of Nucleoplasm Permittivity and Conductivity

As shown in Fig. 2.7a a large decrease in the nucleoplasm conductivity leads to changes in $Re\{K_{CM}\}$ in mid megahertz frequency range, however, it may not be detectable as the effect of the cytoplasm conductivity is more pronounced over this frequency range. Nucleoplasm permittivity has negligible impact on $Re\{K_{CM}\}$ spectra, Fig. 2.7b. In these simulations the volume of the nucleus is approximately 17 percent of the cell volume. Changes in the nucleus properties may occur due to internal electroporation or electroporation induced physiological changes such as apoptosis.

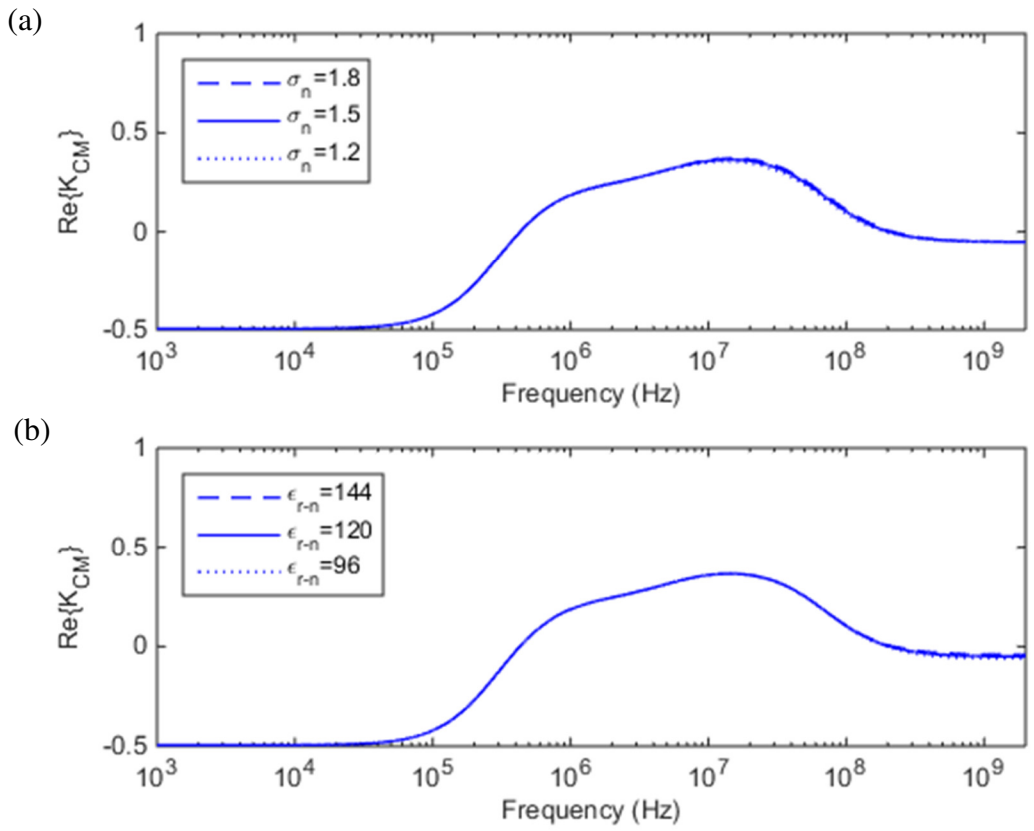

Figure 2.7: *Spectrum of $Re\{K_{CM}\}$ for three values of (a) nucleoplasm conductivity and (b) nucleoplasm permittivity.*

E. Effect of Membrane Thickness and Cell Size

Changes in the thickness of the membrane affects the membrane capacitance and consequently the first crossover frequency, Fig 2.8a. Decrease in the membrane thickness increases the membrane capacitance which results in lower crossover frequency. The effect of cell size on $Re\{K_{CM}\}$ is demonstrated in Fig. 2.8b for 20 percent increase or decrease in the cell radius (73 percent increase or 49 percent decrease in volume). The spectra of $Re\{K_{CM}\}$ is affected by the cell size over the whole frequency range as the cell radius has a direct impact on the cell overall capacitance and conductance. However, the effect on the

spectra between the cross-over frequencies is significantly less than the effect of the cytoplasm conductivity. Electroporation may cause enlargement of cells depending on the amplitude and duration of applied pulses [42], [53], [80], [81]

The simulation results presented in this section show that in DEP study of cells the DEP frequency can be selected to monitor specific changes in cells' electrical parameters, providing an approach to correlate this with physiological changes (e.g. after electroporation). The results suggest that low-frequency DEP (less than 200 kHz) can be used to study cells' membrane conductivity, mid-frequency DEP (1-50 MHz) can be used to study cells' cytoplasm conductivity, and high-frequency DEP application (greater than 100 MHz) can be used to investigate cells' cytoplasm permittivity. The first cross-over frequency provides combined information about the membrane permittivity and thickness. However, it should be considered that the cytoplasm conductivity also affects the first cross-over frequency.

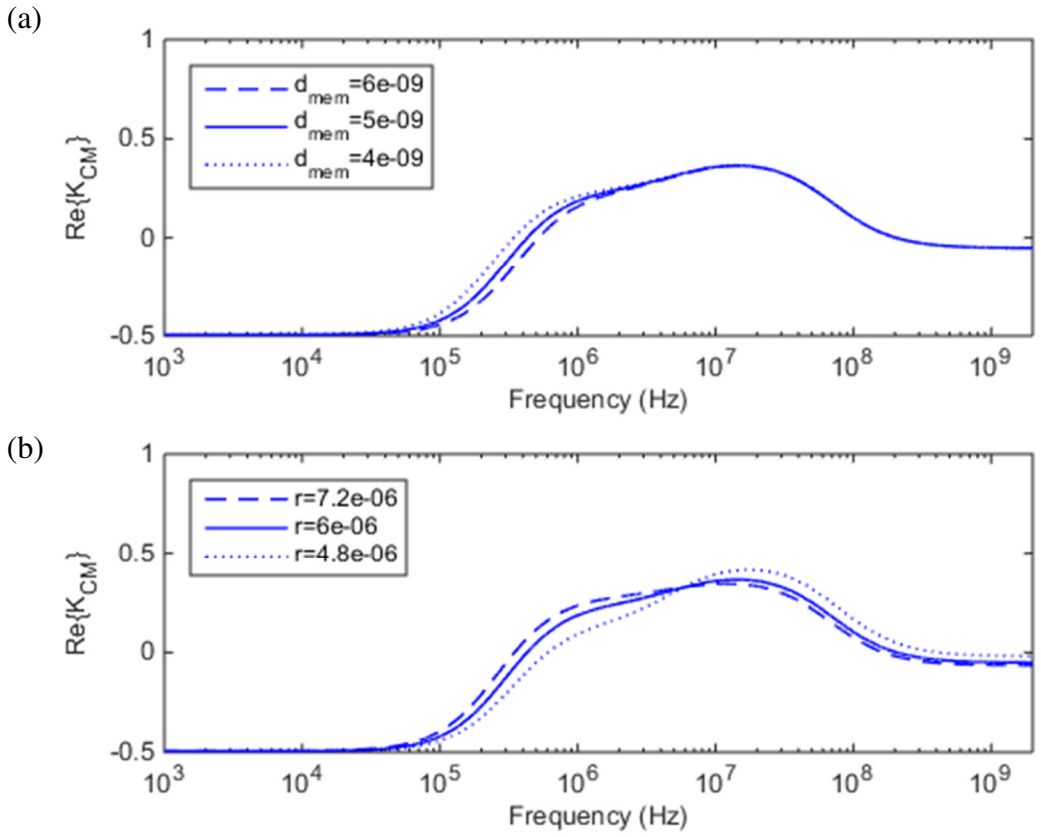

Figure 2.8: *Spectrum of Re{K_{CM} } for three values of (a) membrane thickness and (b) cell radius. Changes in the membrane thickness affects the first crossover frequency whereas the impact of the cell radius is observable over the whole frequency range.*

2.2 ELECTROPORATION

The plasma membrane of cells is made of two layers of phospholipid molecules (lipid bilayer) structured such that the phosphate heads (hydrophilic) are towards the inside and outside of the cell and the lipid tails (hydrophobic) are towards each other (Fig. 2.9a). This structure is impermeable to charged and polar molecules. Cells regulate the transport of water-soluble substances across the membrane actively or passively using variety of proteins available in or on the surface of the membrane. Electroporation disturbs the structure of the lipid bilayer transiently (in reversible cases) and creates some pores with hydrophilic walls in the membrane (Fig. 2.9c). Pores are initially formed with hydrophobic

walls (pre-pore), Fig 2.9b, and then transform to more stable hydrophilic ones [2], [82]–[85]. The dynamic of pore creation, expansion, and contraction is determined by the pore energy (such that it is minimized) and is dependent on the transmembrane potential. Fig. 2.10 shows the energy of a pore versus pore radius for different values of transmembrane potential, $\Delta\varphi_{membrane}$. With $\Delta\varphi_{membrane}$=0, hydrophilic pores with radius smaller or larger than r_* can be generated. The pores with radius smaller than r_* are believed to be unstable and rapidly destroyed. However, the ones greater than r_* transform to the hydrophilic form and expand to r_{min} which is energetically more favorable. It should be noted that with increase in the transmembrane voltage the energy minimum disappears and the pores expand to much larger radii [85]. As the transmembrane voltage increases new pores are created and the existent ones expand resulting in an increase in the membrane conductance (since the pores are substantially more conductive that the lipid parts) which in turn lowers the transmembrane voltage. In this self-regulated manner the transmembrane potential tends to control the creation and expansion of pores. At the end of the pulse, as the electric field is removed, pores start to contract to r_{min} and remain at this minimum energy until they eventually overcome the energy barrier $W_* - W_m$ and destroyed completely [86].

Transport of ions in and out of cells occurs during the pulse application by electrodiffusion and after the pulse by diffusion until the pores are fully closed. The transport of larger molecules (e.g. propidium iodide and other similar fluorescent dyes) may stop shortly after the pores contraction since the size of their molecules is larger than r_{min}. However, ions, due to their very small size, can continue diffusing through the pores until they are completely destroyed.

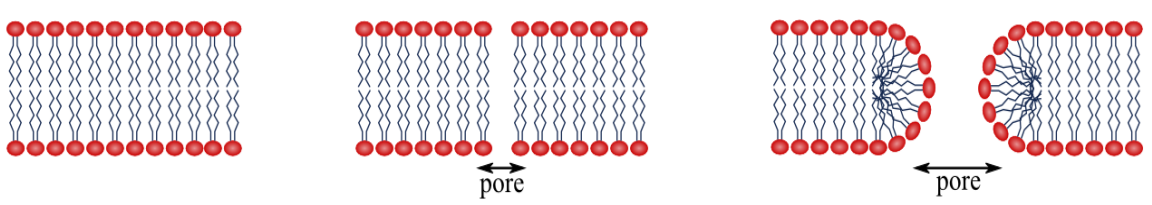

Figure 2.9: *(a) Lipid bilayer structure of an intact membrane. (b) A hydrophobic pore (c) A hydrophilic pore.*

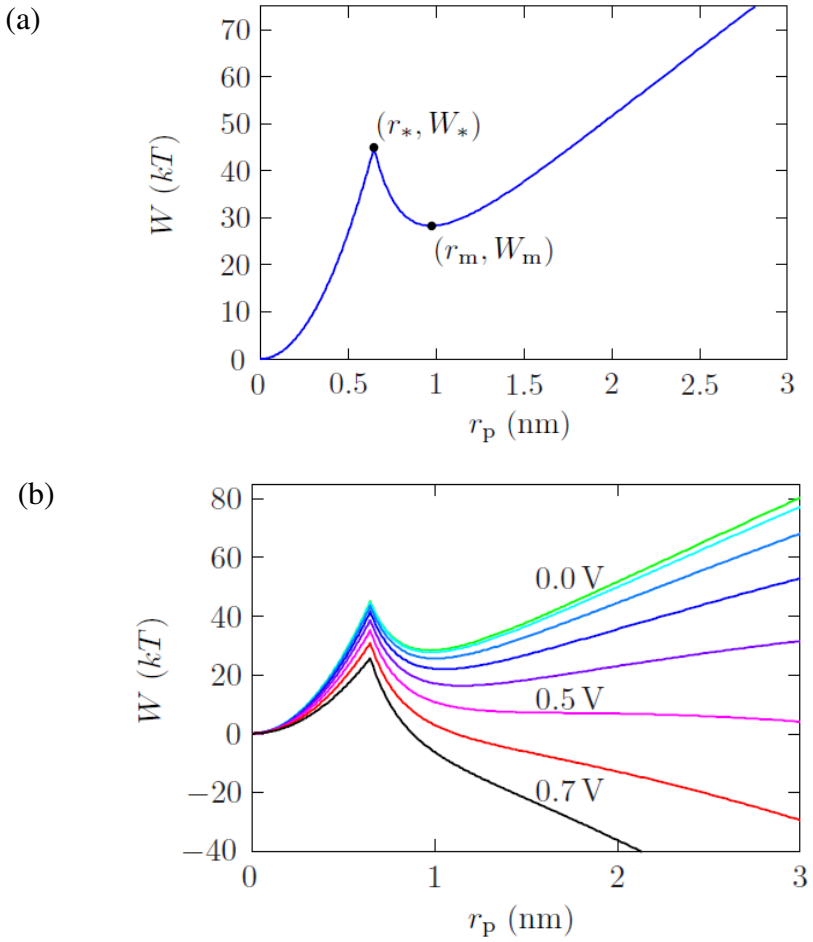

Figure 2.10: *(a) Energy of a pore versus its radius at zero transmembrane voltage. W_* and r_* are the energy and radius of minimum size hydrophilic pores. W_m and r_m are the energy and radius of hydrophilic pores with minimum energy. (b) Energy of a pore versus its radius at different transmembrane voltages. As the transmembrane voltage increases the minimum point disappears. Adapted with permission from* [85]. *Copyright (2011) Massachusetts Institute of Technology.*

In this study we use 100 μs duration pulsed electric fields with amplitude ranging from 0.7 to 2.4 kV/cm to electroporate cells. Previous studies in literature show the uptake of large molecules such as Trypan blue (cylindrical shape with radius 0.59 nm and length 3.16 nm), FD-4 (hydrodynamic radius 1.86 nm), and FD-2000 (hydrodynamic radius 26 nm) for cells electroporated with similar pulses [32], [58]. This suggests that the created pores can expand sufficiently large (or merge with each other) to allow the transport of such large molecules. Simulation results from modeling the electroporation of cells using a 100 μs duration pulse with amplitude 1.5 kV/cm demonstrate that two population of pores with radii 1.5 nm and 12 nm are created after the pulse application [48].

In our studies we measure changes in the cytoplasm conductivity of cells (due to transport of ions through the pores) as an indication of electroporation. Since the radius of ions (primarily Na^+, K^+, and Cl^-) is smaller than 0.5 nm, they can pass through the pores during the pulse as well as after the pulse when most of the pores shrink to their minimum size. In chapters 5 and 6 we demonstrate the temporal changes in the cytoplasm conductivity of single cells after exposure to electroporating pulses.

Chapter 3. DEP Cytometry Apparatus and Measurement Technique

A microfluidic device with coplanar electrodes incorporated in the microfluidic channel, as shown in the inset in Fig. 3.1, is used to sense single cells in the flowing channel as well as to electroporate them with a high intensity electric field or actuate them by a DEP force. Fig. 3.1 represents the schematic of the interferometer-microfluidic system with a set of actuation electrodes, labeled as A, and two sets of sensing electrodes, labeled as S_1 and S_2. Electroporating pulses are applied to a single cell using the actuation electrodes. The same electrodes are employed to generate the non-uniform electric field required for DEP actuation. The sensing electrodes, S_1 and S_2, measure the cells altitude in the channel before and after the DEP actuation.

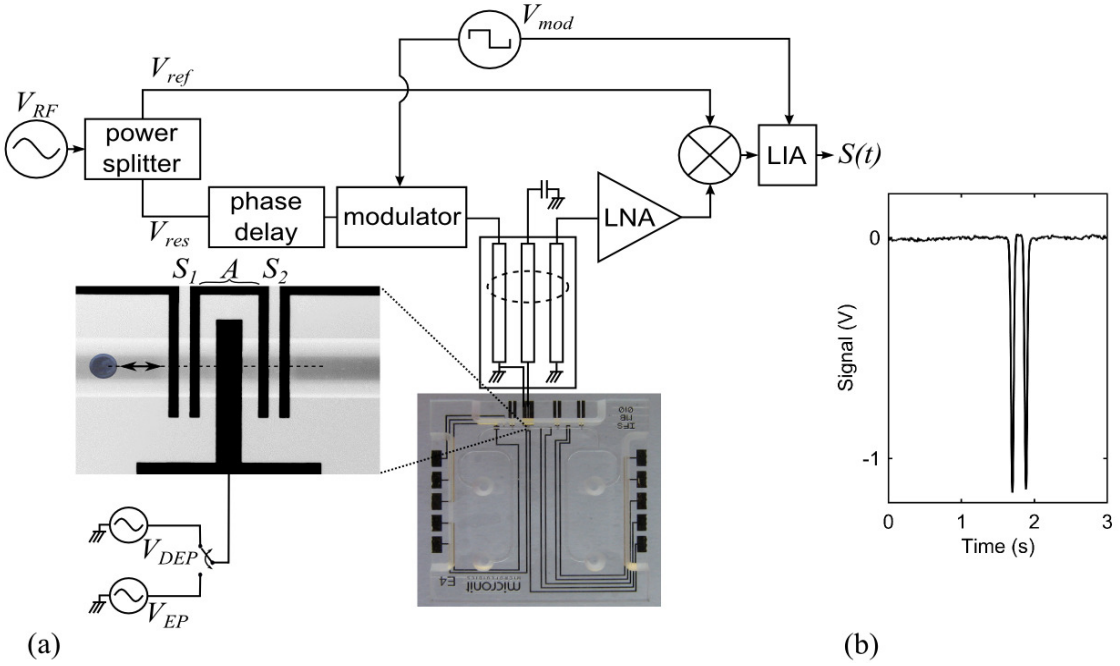

Figure 3.1: *(a) Schematic of the resonator-enhanced microwave interferometer employed to capacitively sense the presence of single cells in the microfluidic channel and estimate their altitude. (b) A typical measured signal for a CHO cell at an altitude of approximately 16 μm above the sensing electrodes. Reproduced from* [94]*, with the permission of AIP Publishing.*

3.1 MICROFLUIDIC SYSTEM

Our microfluidic chip was fabricated by Micronit Microfluidics using their Sensonit Glass-Based Microfluidic Technology with Metallization process. The 15×15 mm chip consists of two layers of borosilicate glass with 1.1 and 0.7 mm thickness as the top and bottom layers. A 20 nm thick Ta adhesion layer and 180 nm thick Au layer are deposited in 200nm depth etched trenches in the bottom layer to form the electrodes. A 40 μm high and 100 μm wide microfluidic channel is etched in the top layer and heat bonded to the bottom layer. The electrodes are 25 μm wide and extend entirely across the microfluidic channel. The spacing between the sensing pairs and the DEP gaps are 25 and 35 μm, respectively. Fluid is pumped through the microfluidic channel via powder-blasted access ports using a

Fluigent MFCS-4C Microfluidic Flow Control System. The throughput of the system is related to the flow velocity and cell suspension concentration. Typical experimental throughput of 30-50 cells per minute is obtained for cell concentration of 2×10^5 cells per milliliter and flow velocity of 1500-2500 μm/s. Substantially higher throughput can be achieved using a larger cell concentration, however, it increases the chance of having more than one cell over the sensing and actuation region.

3.2 DETECTION OF CELLS IN THE MICROFLUIDIC CHANNEL

The detection technique is based on measuring the impedance change (capacitance dominated) of coplanar pairs S_1 and S_2 due to a cell [87]. As a cell passes over the sensing electrode pairs, S_1 or S_2, it displaces the media and results in a slight change in the capacitance of the electrodes. Evaluating the change in the stored energy, with and without the cell assuming that the cell is sufficiently small so that changes in the electric field is negligible over its volume, yields an expression for the capacitance change due to a cell as [88]

$$\Delta C = 3\varepsilon_e V_{cell} Re\{K_{CM}\}\frac{E^2}{U^2}, \tag{3.1}$$

with V_{cell}, the cell volume and U the voltage applied to the sensing electrodes. Since the field generated by coplanar electrodes is a non-uniform electric field the capacitance change due to a cell (given by Eq.(3.1)) is dependent on the intensity of the electric field at the position of the cell. Therefore, the higher the cell in the channel the lower the field intensity and the smaller the capacitance change.

A microwave interferometer, as shown in the block diagram in Fig. 3.1, is used to sense small capacitance changes. A signal generated by the RF source (gigahertz range) is split

between two paths. One is the reference signal, V_{ref}, and the other one passes through the sensing path, V_{res}. The sensing path contains a quarter-wavelength coupled microstrip resonator connected to the sensing electrodes in the microfluidic channel. The presence of cells in the microfluidic channel changes the capacitance of sensing electrodes and causes a slight shift in the resonant frequency, and thus the insertion phase, of the resonator. A sensing signal, S, is generated by combining V_{ref} and V_{res} using a mixer and detecting their phase difference. To improve the signal-to-noise ratio a lock-in amplifier (LIA) technique is used which enables narrow-band detection of the mixer's output. In the absence of cells the frequency of the RF signal is set near the resonant frequency of the resonator, f_0, and the phase delay is adjusted so that V_{ref} and V_{res} are 90° out of phase. In the presence of a cell the sensing signal from the interferometer is

$$S = G|V_{ref}||V_{res}|sin(\Delta\theta)\,, \tag{3.2}$$

where G is the gain of the mixer and LIA and $\Delta\theta$ is the phase change due to the presence of a cell. When operating near the resonant frequency and for very small changes in capacitance, such that the change in the resonant frequency is much less than the resonator bandwidth, the sensing signal will be dominated by ΔC rather than amplitude changes. For small $\Delta\theta$, Eq.(3.2) can then be written as

$$S = G|V_{ref}||V_{res}|\Big|_{f_0}\left(\frac{d\theta}{dC}\right)\Big|_{f_0}\Delta C\,. \tag{3.3}$$

In Eq.(3.3) ΔC is the capacitance change of the sensing electrodes due to the presence of a cell and $(d\theta/dC)_{f_0}$ is the rate of change of phase shift of the resonator with capacitance at the resonant frequency. For a quarter-wavelength short-circuit resonator terminated in a capacitive load, [89], [90]

$$\left.\frac{d\theta}{dC}\right|_{f_0} = -2Qf_0Z_0\,, \tag{3.4}$$

with Q and Z_0 the quality factor and the characteristic impedance of the resonator, respectively. Sensing of cells is performed with a low amplitude (about 500 mV_{pp}) and high frequency (about 1.5 GHz) signal to avoid microwave DEP actuation of cells and minimize variation due to interfacial dispersion (variation among cells in a culture affects $Re\{K_{CM}\}$ to lesser extent at higher frequencies). The signal obtained for a CHO cell at an elevation approximately 16 µm above the sensing electrodes is shown in Fig. 3.2. It features two peaks corresponding to the maximum field regions of the two sensing electrodes. In this result the LIA time constant is 3 ms, equivalent to a measurement bandwidth of about 42 Hz. The signal amplitude is 1.1 V and the rms noise is 5.4 mV (calculated over a window of 1 s, as shown in the Fig. 3.2) providing a measured signal-to-noise ratio 23 dB. Using Eq.(3.1) the induced capacitance change for a CHO cell passing over the sensing electrodes at an altitude of 16 µm is approximately 30 aF and thus the system detection sensitivity is 0.15 aF for a 42 Hz bandwidth.

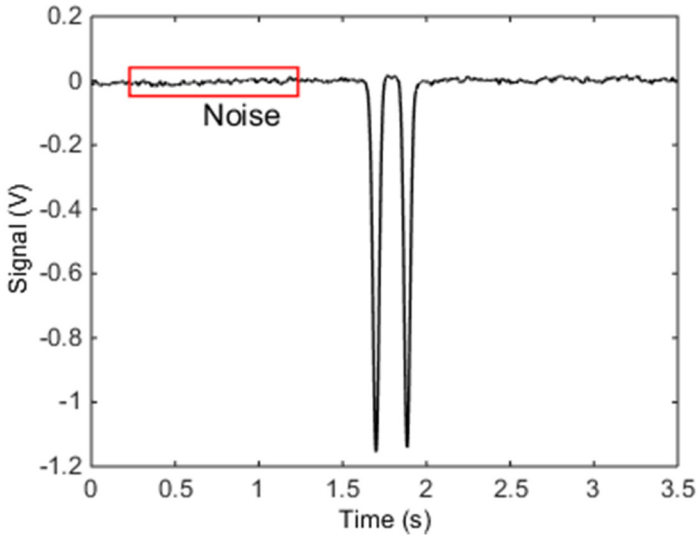

Figure 3.2: *The sensing signal for a CHO cell using the microfluidic-interferometer system. A window of 1s is used to calculate the rms noise highlighted by the red box.*

3.3 MEASUREMENT OF THE DEP FORCE ACTING ON A CELL

As a cell passes in the microfluidic channel, it experiences a DEP force generated by actuation electrodes, A in the inset of Fig. 3.1. The two sets of sensing electrodes, S_1 and S_2, on each side of the DEP actuation electrode are used to measure the altitude of a cell in the channel before and after the DEP actuation. Example trajectories and corresponding signals for cells passing over the electrodes are shown in Fig. 3.3. The DEP actuation electrode, A, applies a DEP force on a passing cell which causes it to approach S_2 at a higher (when experiencing nDEP) or lower altitude (when experiencing pDEP). As a result, the amplitude of the peak P_2 registered by S_2 differs from the peak P_1 registered at S_1 depending on the strength and direction of the DEP force applied to the cell (Eq.(2.2)). We define a parameter, force index, $\varphi = (P_2 - P_1)/P_1$ to quantify the change in the electrical signal due to a DEP actuation. The force index is a measure of the DEP force acting on the cell and hence the Clausius-Mossotti factor of the cell in its suspending medium.

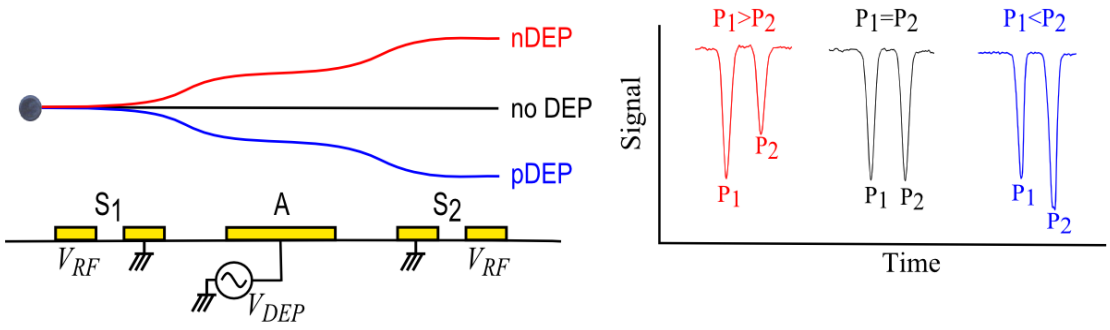

Figure 3.3: *Schematic of the sensing (S_1 and S_2) and actuation (A) electrodes in the microfluidic channel and illustrative trajectory of a cell subjected to nDEP ($P_1>P_2$), no DEP ($P_1=P_2$), or pDEP ($P_1<P_2$). Examples of sensing signals recorded for single CHO cells experiencing nDEP, no DEP, and pDEP ar shown on the right.*

In order to calculate $Re\{K_{CM}\}$ from the measured force indices, fluid dynamics simulation is employed. Here the movement of a homogenous particle with various dielectric constants (resulting in $Re\{K_{CM}\}$ ranging from -0.4 to +0.4) is simulated using *COMSOL Multiphysics 4.3b Particle Tracking for Fluid Flow* and *Electric Currents* modules. With the particle entering at a given altitude, h_1, and subjected to DEP and hydrodynamic forces, we obtain its exit altitude, h_2, at the location of the second pair of sensing electrodes, for different values of $Re\{K_{CM}\}$ (Fig. 3.4a). The capacitance change of the two pairs of sensing electrodes due to the particle is then calculated using Eq. (3.1) with $|\bar{E}^{RF}|^2$ obtained from solving the Laplace equation using *COMSOL Multiphysics*. Fig. 3.4b shows the profile of $|\bar{E}^{RF}|^2$ for several exit altitudes when V^{RF}=*0.5* V_{pp}. The capacitance change of the sensing electrodes due to a particle versus the particle's altitude is shown in Fig. 3.4c. Since the amplitude of the signals associated with sensing electrodes S_1 and S_2 are proportional to their capacitance change, the force index corresponding to each $Re\{K_{CM}\}$ is estimated from $\varphi = \frac{\Delta C|_{h_2} - \Delta C|_{h_1}}{\Delta C|_{h_1}}$.

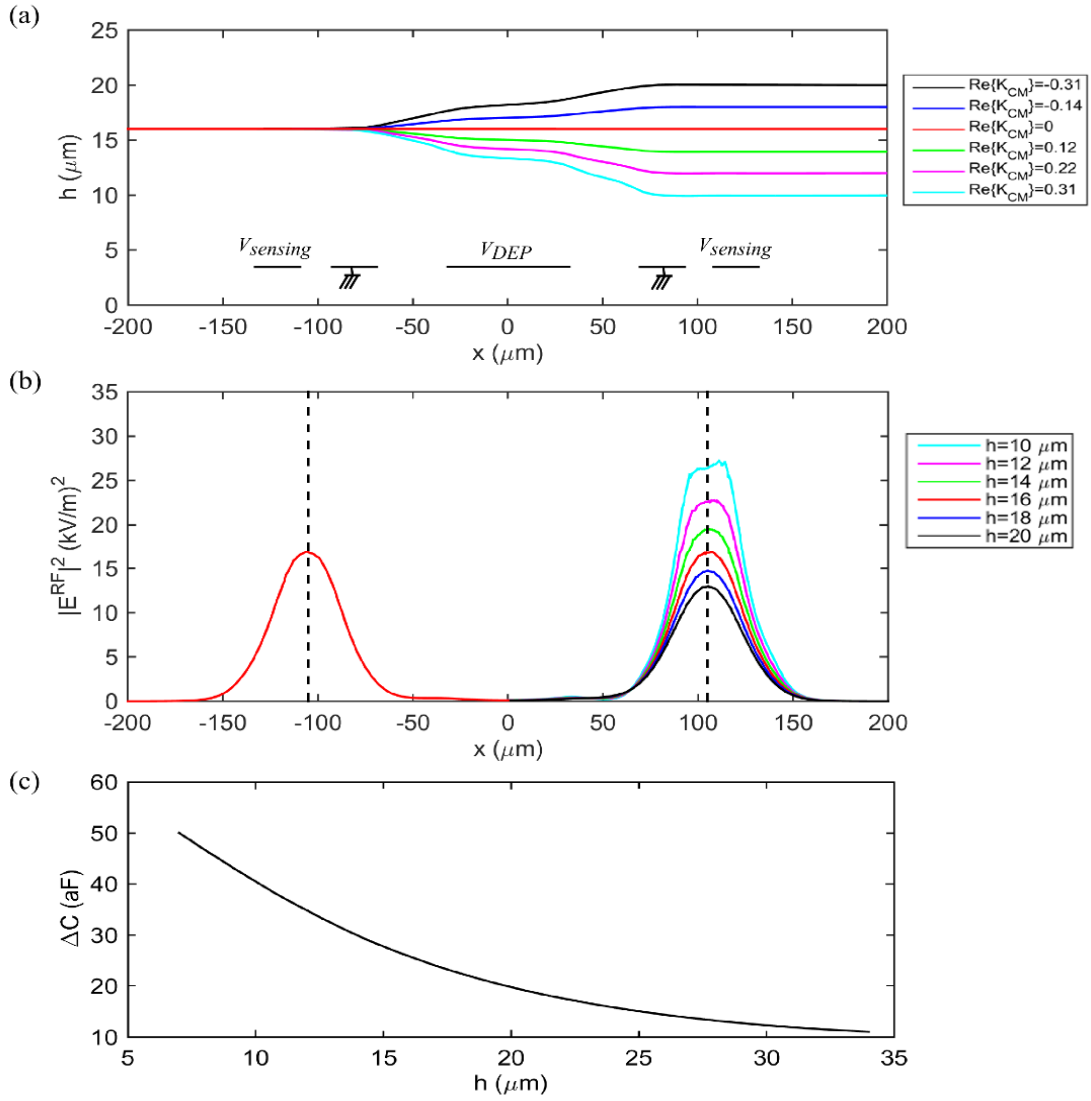

Figure 3.4: *(a) Trajectories of a 6 μm radius particle with variable Re{K_{CM}} and an entrance altitude 16 μm subjected to DEP and hydrodynamic forces as obtained from COMSOL simulations. The trajectories are used to estimate the altitude of the particle after DEP actuation for different values of Re{K_{CM}} ranging from -0.4 to +0.4. (b) Simulation results of the amplitude of the square of the electric field over the sensing electrodes for different exit altitudes. The capacitance change of a pair of sensing electrodes due to a particle is directly proportional to $|E^{RF}|^2$ at its center. (c) Capacitance change of the second sensing electrode pair (after DEP actuation) versus altitude as obtained from Eq. (3.1). This curve is used to calculate the force index corresponding to different values of Re{K_{CM}}. Reproduced from* [94]*, with the permission of AIP Publishing.*

3.4 SIMULATION OF DEP AND HYDRODYNAMIC FORCES

Fluid flow in a microfluidic channel can be assumed laminar since the Reynolds number is much less than one [91]. Given that in our experiments the fluid is viscous and incompressible and there is no fluid acceleration, a Poiseuille flow is established in the microfluidic channel which is characterized by a parabolic velocity profile (zero at walls and maximum at the center of the channel). The fluid velocity at any altitude, *h*, from the bottom of the channel is given by [91]

$$v_m = 6\langle v_m \rangle \frac{h}{H}\left(1 - \frac{h}{H}\right), \tag{3.5}$$

where $\langle v_m \rangle$ is the mean flow velocity and *H* is the height of the channel. The majority of cells flowing in the microfluidic channel sediment and acquire an equilibrium altitude before entering the DEP actuation region. Forces which govern the vertical movement of a cell outside the DEP actuation region are gravity, buoyancy, and hydrodynamic lift force given by [92]

$$\vec{F}_{grav-bouy} = \frac{4\pi}{3} r^3 g(\rho_c - \rho_m)(-\hat{y}), \tag{3.6}$$

$$\vec{F}_{lift} = C\frac{6\eta\langle v_m \rangle r^3}{H(h-r)}\, sgn(\frac{H}{2} - h)\hat{y}\,, \tag{3.7}$$

where g= 9.81 m/s^2 is the gravitational acceleration, ρ_c and ρ_m are densities of the cell and suspension medium, *r* is the cell radius, η is the viscosity of the medium, *h* is the distance from the cell centre to the bottom of the channel. Here *C* is a coefficient which is obtained experimentally using standard dielectric particles (section 4.2.1). The equilibrium altitude, h_{eq}, of a cell is the elevation at which gravity, buoyancy, and lift forces are in balance. We use h_{eq} obtained from Eq. (3.5)-(3.7) (with the velocity and size matching the average of

our measured data for single cells) as the initial altitude in our simulations. During DEP actuation the gravity and buoyancy forces are negligible as compared with other forces and the cell movement is mostly impacted by the DEP, drag and hydrodynamic lift forces (in the case that the cell is close to a wall). The DEP and lift force are expressed in Eq. (2.2) and Eq. (3.7) and the fluid drag force is given by [93]

$$\vec{F}_{drag} = 6\pi\eta r(\vec{v}_m - \vec{v}_c)\lambda\,, \tag{3.8}$$

Where $\vec{v}_m$ and $\vec{v}_c$ are the fluid and particle velocities, respectively, and λ represents the ratio of the force experienced by a particle between two confining walls to the force in an unbounded fluid. λ is a function of the cell altitude in the channel and varies as the cell moves in response to the DEP force. Given the channel geometry we obtain the altitude dependent λ for our system from the data provided in literature [93].

In our simulations the channel, particle, and medium parameters are set according to our experiments and are listed in Table 3.1. Fig. 3.5 is an example plot of force index versus $Re\{K_{CM}\}$ for a 6 μm (radius) particle moving with initial velocity of 2200 μm/s at an equilibrium altitude of h_{eq}=16.5 μm and experiencing a DEP force generated by a sinusoidal voltage of 8 V_{pp} applied to the actuation electrodes.

Table 3.1: *Channel, particle, and medium parameters employed in simulations. Reproduced from* [94]*, with the permission of AIP Publishing.*

Parameter	Symbol	Value	Ref.
Channel height	H	40 μm	
Channel width	W	100 μm	
PSS density	ρ_c	1050 kg/m^3	Datasheet [95]
Cell density	ρ_c	1050 kg/m^3 [a]	[96]
PSS radius	r	5.5 μm	Datasheet [95]
Cell radius	r	5.9 - 6.2 μm	Measured
Particle initial velocity	v_{c0}	2000 – 2500 μm/s	Measured
Medium density	ρ_m	1019 – 1027 kg/m^3	Calculated[b]

Medium viscosity	η	0.001 Pa.s	[97]
Medium conductivity	σ_m	0.17 – 0.5 S/m	Measured
Medium Permittivity	ε_e	$78\varepsilon_0$	[98]

[a] This is an average value reported in litrature for CHO cells. It should be noted that not all cells have the same density.
[b] Cells are measured in media with different conductivities. The density of the medium is calculated considering its glucose and sucrose content [97].

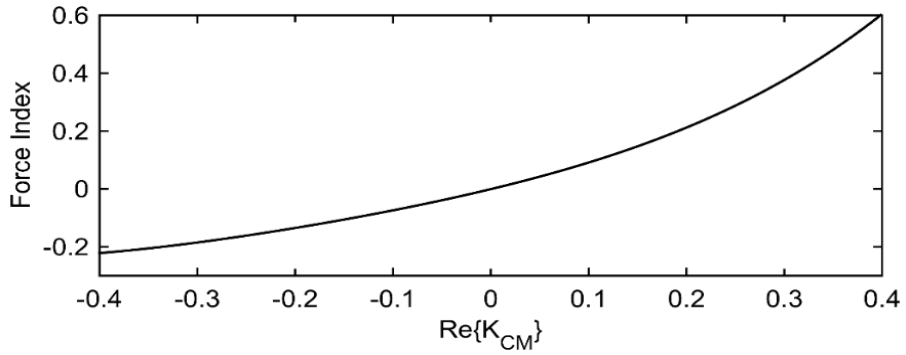

Figure 3.5: *Force index versus Re{K_{CM}} obtained from simulation for a 6 μm particle moving with an initial velocity 2200 μm/s and an altitude 16.5 in the microfluidic channel subjected to DEP and hydrodynamic forces. The DEP force is generated by applying a 8 V_{pp} sinusoidal voltage to the actuation electrodes. Channel, particle and medium parameters are listed in Table 3.1. Reproduced from* [94]*, with the permission of AIP Publishing.*

3.5 ELECTROPORATION AND DEP STUDY OF SINGLE CELLS

The actuation electrodes employed for DEP application are also used to apply electroporating pulses (EP) to cells, Fig. 3.6.

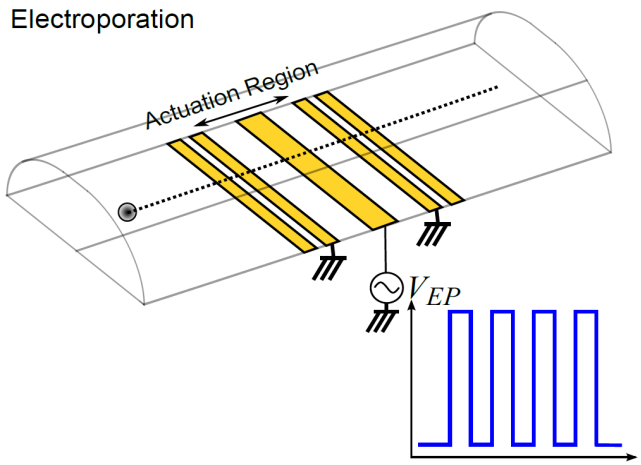

Figure 3.6: *Electroporation of single cells by applying pulses to actuation electrodes.*

In order to study the temporal response of individual cells to electroporating pulses, we continuously shuttle a single cell back and forth over the electrodes in the microfluidic channel (by proper adjustment of inlets and outlets pressures) and measure its response to a DEP force over a period of time. Fig. 3.7 shows the procedure used for continuous DEP and EP application to a single cell and the simulated electric field profile in the channel. First, we measure the cell's DEP response for several passes at a specific frequency (such that it is sensitive to the cell's internal conductivity) before electroporation. Then, as the cell passes over the actuation region, we expose it to several electroporating pulses by applying a pulsed electric voltage with desirable duration and intensity to the actuation electrodes. We measure the temporal changes in the DEP response of the cell immediately after electroporation for a period of a few minutes as the cell continues moving back and forth in the channel.

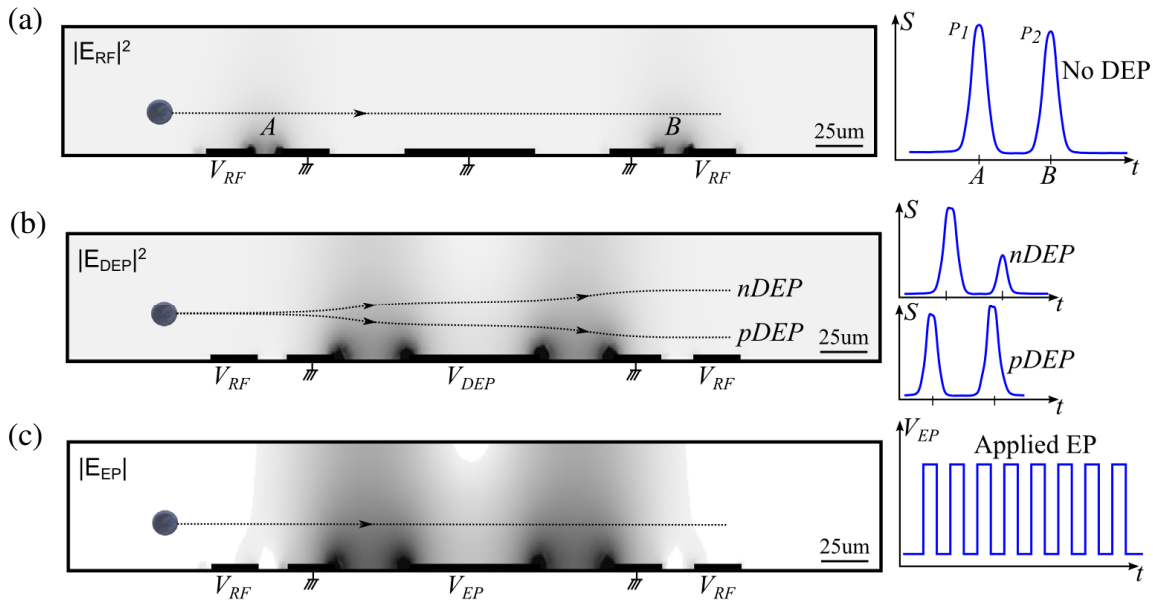

Figure 3.7: *Profiles of the electric field in the sensing and actuation regions of the microfluidic channel (panels on the left). (a) The sensing signal, S, (right) as the cell traverse the electrodes is proportional to the amplitude of the sensing electric field squared. (b) The DEP force applied to a cell is proportional to the amplitude of the DEP electric field squared. (c) The pulsed voltage applied to the actuation electrode (right) generates the electroporation electric field over two gap regions through which the cell traverse.*

3.6 CONCLUSIONS

In this chapter we described the DEP measurement apparatus and the microwave interferometry technique we employ to detect and actuate single cells. We introduced a dielectrophoresis based measurement technique to simultaneously electroporate a single cell and measure the induced changes in its DEP response. By shuttling a single cell back and forth in a microfluidic channel and studying its DEP response before and after applying electroporation, we are able to measure the induced changes in the cell's response within seconds after pulse exposures. We also developed a simulation model to relate the measured DEP response of cells to their $Re\{K_{CM}\}$. This will be employed in chapter 4 to

obtain a dielectric model for CHO cells and in chapters 5 and 6 to relate changes in the DEP response of cells after electroporation to their internal conductivity.

Chapter 4. Dielectric Model for CHO Cells

Chinese hamster ovary (CHO) cells have widespread biopharmaceutical and biomedical applications. Adaptability and ease of genetic manipulation have made CHO cells the industries' primary mammalian host for commercial production of therapeutic protein [99]. CHO cells have been used in numerous biological and biomedical research studies such as, cell cycle, toxicology, cancer biology, and DNA damage and repair studies [100]–[103]. Despite the extensive applications of CHO cells, their dielectric properties are not well established. In studies where an electrical model of CHO cells is required, a model with its parameters taken from other mammalian cell lines or yeast is often adopted [56], [104]–[106]. With growing interest in dielectrically probing the metabolic status of CHO cells in biopharmaceutical reactors [107], [108] or employing CHO cells in dielectric study of biological phenomena (e.g. apoptosis or electroporation), a complete model of CHO which includes the cell and its internal organelles and their dielectric parameters is essential to make accurate conclusions and predictions. In this chapter we employ a double-shell

dielectric model and present the dielectric parameters for the membrane, cytoplasm, nuclear envelope, and nucleoplasm as measured using a dielectrophoresis technique.

Impedance spectroscopy and AC electrokinetic techniques are the two main label-free dielectric study methods. Both are based on the polarization of cells in an applied electric field. In impedance spectroscopy the frequency dependent electrical properties of a cell suspension is measured and the cells' dielectric parameters are extracted using theoretical models to remove the effect of the suspension medium [109], [110]. This technique has been implemented in both time-domain and frequency-domain to obtain the dielectric parameters of a population of normal and malignant white blood cells [111]–[113], electroporated and non-electroporated Jurkat cells [41], [53], and mouse lymphocytes and erythrocytes [79], for example. In AC electrokinetic techniques the frequency dependent motion of cells induced by electrorotation or dielectrophoresis (DEP) is measured. Theoretical or numerical analysis is then employed to relate the motion to the cells' dielectric parameters. Electrorotation and dielectrophoresis have been employed to study the dielectric properties of drug-treated and non-drug-treated Friend murine erythroleukemia cells [66], [67], apoptotic human leukemia cells[114], and MDR human leukemia cells [68]. AC electrokinetic techniques can measure the response of single cells. This allows measurement of individual cells without the influence of neighboring cells and aggregation effects.

In this chapter we employ the DEP cytometry technique, explained in chapter 3, to determine the dielectric properties of CHO cells based on a double-shell model. Using our microfluidic device the DEP induced translation of many individual CHO cells are measured as they flow through the channel. Cells are suspended in media with different

conductivities and their response is measured over the frequency range 0.6 – 10 MHz. Performing numerical simulations and curve-fitting to measured data, we obtain the membrane permittivity, cytoplasm conductivity, nuclear envelope permittivity, nucleoplasm conductivity, and plasma membrane thickness of CHO cells. We report the values of the double-shell model parameters for CHO cells and compare them with three other mammalian cells.

4.1 MATERIALS AND METHODS

We use a double-shell model for CHO cells and determine its parameters using the dielectrophoresis based technique explained in chapter 3. The approach we take is to obtain $Re\{K_{CM}\}$ from the DEP response of many single cells over a specified frequency range. $Re\{K_{CM}\}$ is a function of the dielectric properties of the cell internal structure and the double-shell model parameters are extracted by curve-fitting to the measured data.

4.1.1 Extracting Cell Model Parameters from $Re\{K_{CM}\}$

A Chinese Hamster Ovary cell is a eukaryote with a nucleus much larger than other organelles and approximately half the cell's radius (Fig. 4.1a). In this study we employ a double-shell model for CHO cells consisting of the cell nucleus, nuclear envelope, cytoplasm, and plasma membrane, as shown in Fig. 4.1b. With this model there are eight dielectric parameters (permittivity and conductivity of each compartment) and four geometric parameters (radius of the cell and nucleus and the thickness of the membrane and nuclear envelope). The parameters are obtained by curve fitting to the measured data ($Re\{K_{CM}\}$ vs. frequency). Reliably extracting all parameters is challenging due to interdependency of some parameters and insensitivity of some parameters over the

frequency range of measured data. To overcome this we perform a sensitivity analysis to determine the parameters that predominantly effect the $Re\{K_{CM}\}$ spectrum over the frequency range of measurements. We also obtain the size of the cells and their nuclei by optical microscopy.

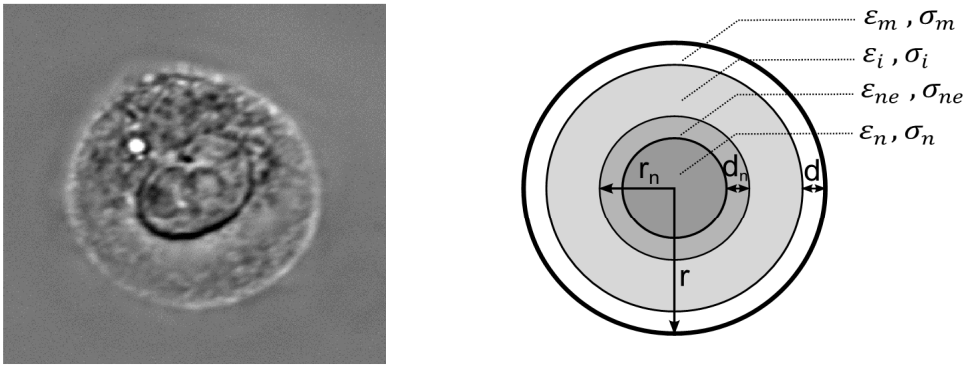

(a) (b)

Figure 4.1: *(a) Image of a typical CHO cell in our experiment obtained using an inverted DIC microscope. (b) Double-shell model of a cell consisting of the cell nucleus, nuclear envelope, cytoplasm, and plasma membrane. The dielectric and geometric parameters of the model are indicated. Reproduced from* [94]*, with the permission of AIP Publishing.*

A. Sensitivity Analysis

The sensitivity of the $Re\{K_{CM}\}$ spectrum to a parameter x_i is defined as the relative root-mean-square change in the entire spectrum of $Re\{K_{CM}\}$ due to a small change in x_i over the relative change of x_i. The sensitivity function at x_i=x_{i0} is described as [115]

$$u(x_i)|_{x_{i0}} = \frac{\sqrt{\frac{\int_{f_{min}}^{f_{max}}[K(f,x_1,\dots,x_{i0}+dx_i,\dots,x_n)-K(f,x_1,\dots,x_{i0},\dots,x_n)]^2 df}{\int_{f_{min}}^{f_{max}} K^2(f,x_1,\dots,x_{i0},\dots,x_n)df}}}{dx_i/_{x_{i0}}}, \tag{4.1}$$

where $K(f,x_1,\dots,x_i,\dots,x_n)$ is the function $Re\{K_{CM}\}$, f_{min} and f_{max} denote the frequency range of measurement, and x_i represent the dielectric and geometric parameters. For calculating

the sensitivity to each parameter x_i we vary its value over a selected range (chosen for mammalian cells) while keeping other parameters constant. Therefore, $u(x_i)|_{x_{i0}}$ is dependent on the value of all parameters and are initially selected to be that of typical values reported for mammalian cells [79], [111]. Larger $u(x_i)$ implies greater effect on the spectrum of $Re\{K_{CM}\}$ over the measured frequency range. Based on the sensitivity analysis a subset of the most sensitive parameters are chosen for curve-fitting to the measured $Re\{K_{CM}\}$ spectra. Insensitive parameters are identified and their values are kept as the typical reported values.

B. Obtaining Parameters by Curve Fitting

The value of the parameters which are selected for optimization (based on the sensitivity analysis) are obtained by curve fitting to the measured $Re\{K_{CM}\}$ spectra. The Nelder-Mead simplex optimization technique (MATLAB R2014b Optimization Toolbox) is employed to minimize the error function

$$E = \sqrt{\int_{f_{min}}^{f_{max}} \left[K_{meas}(f, x_1, \dots, x_n) - K_{opt}(f, x_1, \dots, x_n)\right]^2 df}\,, \tag{4.2}$$

where $K_{meas}(f,x_1,\dots,x_n)$ and $K_{opt}(f,x_1,\dots,x_n)$ are the measured and fitted $Re\{K_{CM}\}$ spectra, respectively.

4.1.2 Cell Preparation

The Chinese hamster ovary cells (CHODG44-EG2-hFc/clone 1A7), kindly provided by Yves Durocher of the National Research Council, are grown in 250 mL shaker flasks and incubated at 37°C with a 10% CO_2 overlay on a shaker platform (120 rpm). The cells are passaged every 2 – 3 days with a seeding density of 2×10^5 cells/mL in BioGro-CHO

serum-free medium (BioGro Technologies, Winnipeg, MB) supplemented with 0.5 g/L yeast extract (BD, Sparks, MD), 1 mM glutamine (Sigma, St. Louis, MO), and 4 mM GlutaMax I (Invitrogen, Grand Island, NY). On the day of the experiment the cell suspension is prepared by centrifuging and resuspending day 2 cells in a mix of low conductivity [22.9 mM sucrose (Sigma), 16 mM glucose (Fisher), 1 mM $CaCl_2$ (Fisher), 16 mM Na_2HPO_4 (Fisher)] and BioGro CHO medium to a concentration of 2×10^5 cells/mL. The ratio of low conductivity to BioGro CHO medium is based on the desired sample conductivity: 0.17 S/m (30:2), 0.30 S/m (26.8:5.2), 0.40 S/m (24.4:7.6), 0.50 S/m (22:10). All media are isotonic and their osmotic pressure, as measured with an osmometer (Advanced® Model 3300 Micro-Osmometer, Advanced Instruments Inc., Norwood, USA), is 291, 303, 298, and 305 mOsm/kg for conductivities 0.17, 0.3, 0.4, and 0.5, respectively.

4.2 RESULTS AND DISCUSSION

4.2.1 System Calibration

In order to determine the lift coefficient, C, and verify our COMSOL simulations, experiments are performed on 11 μm diameter (close to CHO cell diameter and density) polystyrene spheres (PSS) suspended in a medium with the same density and viscosity as the one used for cells. While applying a 10MHz, 8 V_{pp} DEP voltage to the actuating electrode, force indices are recorded for 800 individual beads flowing at different velocities which causes them to settle at different equilibrium altitudes. Given that a PSS acts like a lossless dielectric sphere with ε_r=2.5 in the MHz range, we simulate the DEP response of a bead at a specific initial altitude. The lift coefficient, C=0.31, is obtained by adjusting it such that the force index predicted by the simulation matches the average of force indices

measured for beads with the same altitude in the channel. To verify the result we use the obtained value of C to simulate beads at other initial altitudes (ranging from 11 to 27 µm) and compare the results with the measured data. The results depicted in Fig. 4.2 show a good agreement between the simulation and measured data.

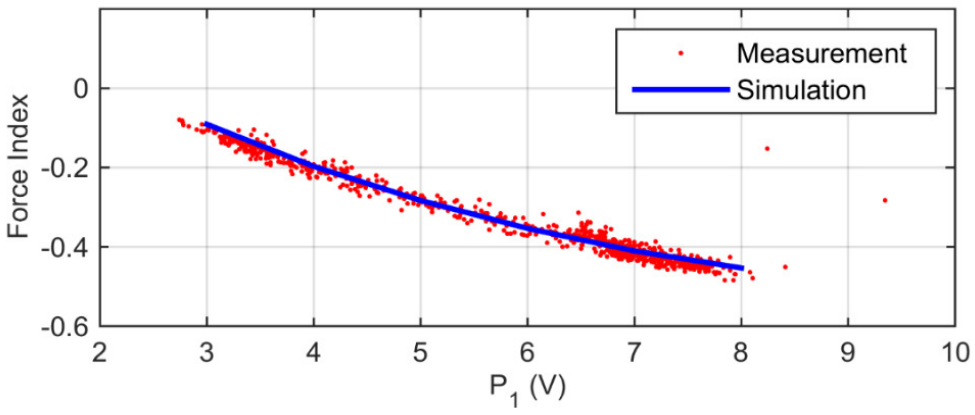

Figure 4.2: *Measured and simulated force indices for 11 µm polystyrene spheres. The x-axis is the amplitude of the peak registered by the sensing electrodes, S_1, before the DEP actuation, which is a measure of particles altitude in the channel (See Fig. 3.4b). Good agreement between the measured and simulation results verifies the lift coefficient value, C=0.031. Reproduced from* [94]*, with the permission of AIP Publishing.*

4.2.2 Measurement of the DEP Response of CHO cells

CHO cells are suspended in media with conductivities of 0.17, 0.3, 0.4, and 0.5 S/m and the DEP response of individual cells are measured at frequencies 0.6, 1, 6, and 10 MHz in each media. The measurement frequency range is selected to include the part of $Re\{K_{CM}\}$ spectrum which exhibits the dispersion effects of the cells internal structure (see Fig.2.2). Measurements at very low and very high frequencies are limited by our measurement setup. Cells in the medium with the lowest ionic concentration, 0.17 S/m, were tested beforehand to ensure their viability were not affected over the course of an experiment (approximately an hour). The average measured force indices versus frequency for each medium is

depicted in Fig. 4.3a with error bars representing the standard error of the mean. Each data point is the average of force indices of approximately 400 individual cells. In this experiment the system throughput is approximately 40 cells per minute. The values of $Re\{K_{CM}\}$ corresponding to average measured force indices, obtained using COMSOL simulations as described in sections 3.3 and 3.4, yields the result shown in Fig. 4.3b. Error bars represent the deviation in simulation results when the particle velocity (which has influence on the determination of the particle initial altitude) is set to one standard deviation above and below the average velocity of measured cells.

4.2.3 Measurement of Cell and Nucleus size

The average diameter of cells is determined by optical imaging using a Cedex XS cell analyzer (Innovatice, Germany) which provide the average diameter based on approximately 150 viable cells. The average radius of CHO cells suspended in 0.17, 0.3. 0.4, and 0.5 S/m media was measured to be 5.9, 6.1, 6.0, and 6.2, respectively. In order to determine the nucleus diameter, CHO cells were imaged in suspension using an inverted differential interference contrast (DIC) microscope (Observer.Z1, Zeiss, Germany). A typical cell image is shown in Fig. 4.1a. After analyzing the images of 40 cells (using the ImagJ image processing program) the ratio of nucleus radius (average of major and minor axes, major /minor=1.25) to cell radius is obtained as r_n/r = 0.55. This is consistent with other reported results [116].

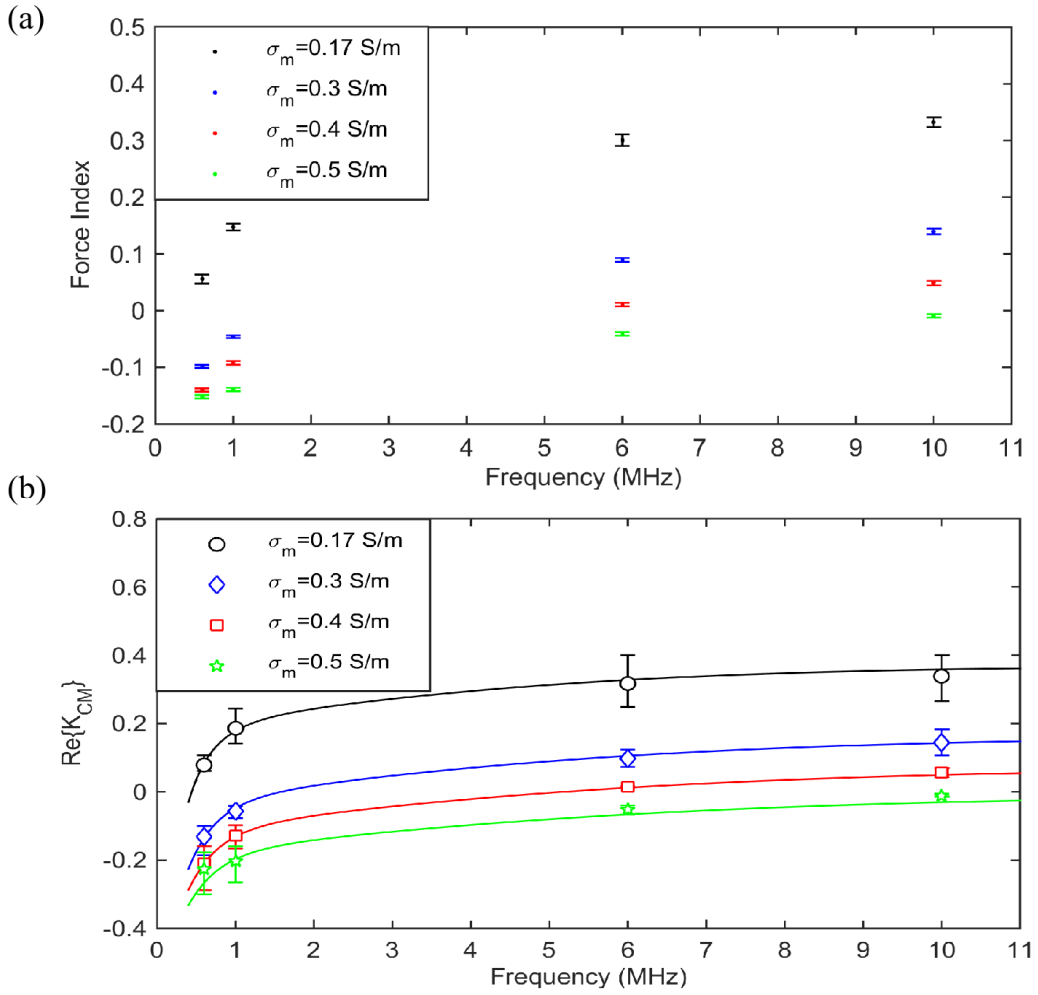

Figure 4.3: *Average measured force indices for CHO cells suspended in media with various conductivities. Each data point is the average of approximately 400 individual cells. Error bars represent the standard error of the mean. (b) Re{K_{CM}} corresponding to the measured force indices as obtained from simulations. Error bars represent the deviation in simulation results when the particle velocity is set to one standard deviation above and below the average velocity of measured cells. Data points correspond to the measured values in Fig. 4.3a. Solid lines show the calculated Re{K_{CM}} spectrum using the curve-fitted CHO double-shell model dielectric parameters as determined later (see Table 4.1). Reproduced from* [94]*, with the permission of AIP Publishing.*

4.2.4 Cell Model Parameter Sensitivity Analysis

The double-shell model parameters of a CHO cell are extracted by curve fitting to the measured spectrum for $Re\{K_{CM}\}$ employing an optimization method as described in section 4.1.1.B. The double-shell model requires optimization of ten parameters, assuming that the

cell and nucleus radii are obtained by optical methods. An initial evaluation of the number of parameters that can be reliably optimised is determined by sensitivity analysis while testing the optimization process with sets of synthetic data. Due to interdependency and insensitivity of some parameters for the frequency range and conductivities chosen in the experiments the optimization algorithm is able to recover five parameters with less than 0.2% error. Fig. 4.4 shows the sensitivity factor for different cell parameters calculated using Eq. (4.1) as their values vary over the following ranges: $10^{-7} < \sigma_{mem} < 10^{-5}$ S/m , $3\varepsilon_0 < \varepsilon_{mem} < 20\varepsilon_0$ F/m, $0.1 < \sigma_{cyt} < 1.2$ S/m , $50\varepsilon_0 < \varepsilon_{cyt} < 90\varepsilon_0$ F/m, $10^{-5} < \sigma_{ne} < 10^{-2}$ S/m, $15\varepsilon_0 < \varepsilon_{ne} < 90\varepsilon_0$ F/m, $0.1 < \sigma_n < 4.8$ S/m (which makes $1 < \sigma_n/\sigma_{cyt} < 4$), $50\varepsilon_0 < \varepsilon_n < 130\varepsilon_0$ F/m, $5 < d < 8$ nm, $10 < d_n < 40$ nm. The range of variation for each parameter is chosen such that it encompasses the values previously reported in literature for other mammalian cells [67], [79], [111], [117]–[122]. Sensitivity of each parameter is calculated with respect to the nominal values: $\sigma_{mem}=1\times10^{-6}$ S/m, $\varepsilon_{mem}=11\varepsilon_0$ F/m, $\sigma_{cyt}= 0.4$ S/m, $\varepsilon_{cyt}= 60\varepsilon_0$ F/m, $\sigma_{ne}= 1\times10^{-3}$ S/m, $\varepsilon_{ne}= 86\varepsilon_0$ F/m, $\sigma_n/\sigma_i = 2$, $\varepsilon_n= 120\varepsilon_0$ F/m, d=7 nm, d_{ne}= 40 nm which are the values obtained for normal lymphocyte cells [79], [111]. Since the medium conductivity has a substantial influence, the sensitivities are presented for five media conductivities (0.17, 0.3, 0.4, and 0.5 S/m media as employed in our measurements and a very low conductivity medium, 0.01 S/m, which has been used in many other dielectric parameter studies [67], [68], [114], [118], [122], [123]).

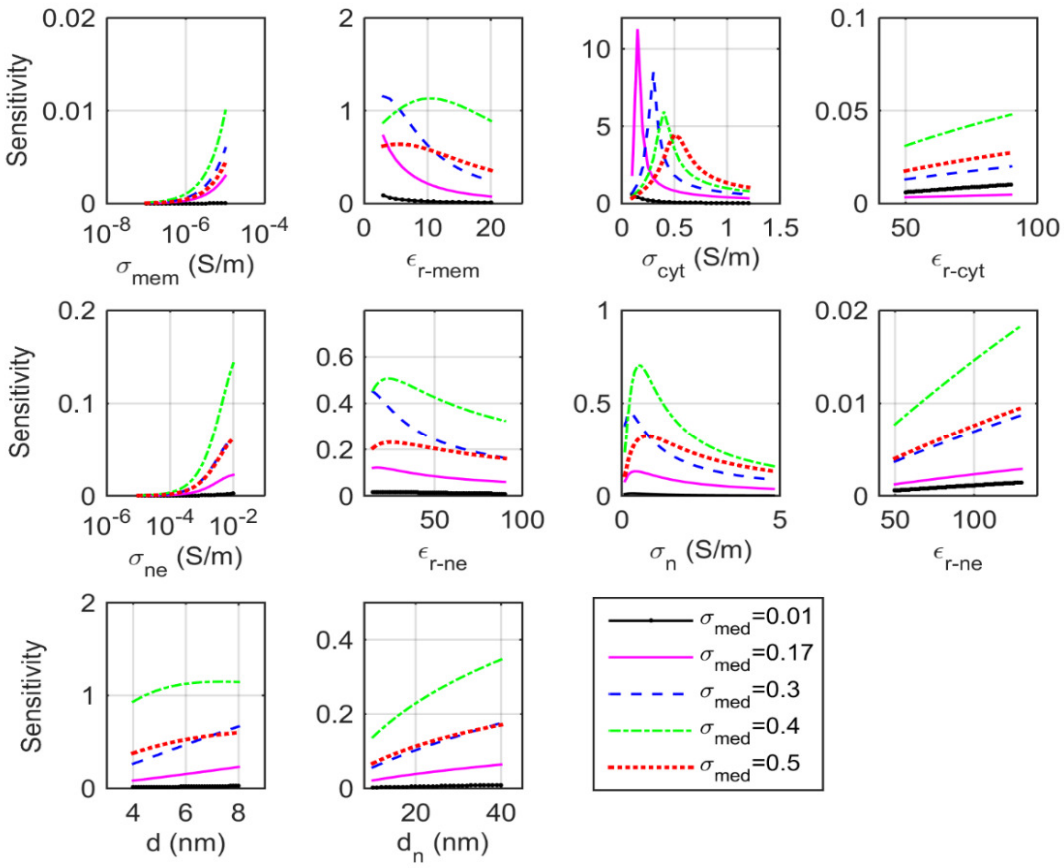

Figure 4.4: *Sensitivity factors of ten electrical and geometrical parameters for a double-shell cell model as their values vary over specified ranges. The sensitivity of each parameter is calculated with respect to the nominal values:* σ_{mem}*=* 1×10^{-6} *S/m,* $\varepsilon_{mem}=11\varepsilon_0$ *F/m, d =7 nm,* $\sigma_{cyt}=0.4$ *S/m,* $\varepsilon_{cyt}=60\varepsilon_0$ *F/m,* $\sigma_{ne}=1\times10^{-3}$ *S/m,* $\varepsilon_{ne}=86\varepsilon_0$ *F/m,* $d_{ne}=40$ *nm,* $\sigma_n/\sigma_i=2$, $\varepsilon_n=120\varepsilon_0$ *F/m* [79], [111]. *Sensitivities are presented for five media conductivities (0.17, 0.3, 0.4, and 0.5 S/m, as employed in our measurements and one very low conductivity medium, 0.01 S/m). Reproduced from* [94]*, with the permission of AIP Publishing.*

As our measurements are in the 0.6 – 10 MHz frequency range, the sensitivity to the membrane conductivity is low as this parameter predominantly affects the low frequency part of the $Re\{K_{CM}\}$ spectrum (less than 200 kHz). Similarly, the cytoplasm and nucleoplasm permittivities predominantly affect the high frequency part of the $Re\{K_{CM}\}$ spectrum (greater than 50 MHz). Based on the sensitivity results in Fig. 4.4, membrane permittivity, cytoplasm conductivity, nuclear envelope permittivity, nucleoplasm

conductivity, and plasma membrane thickness are selected as parameters for optimization. Among these parameters, cytoplasm conductivity is the most sensitive parameter for our measured frequency range. In general the membrane thickness and permittivity have an interdependency and in many cases is modeled as a membrane capacitance. In this work we maintain them as separate parameters. The nuclear envelope thickness has a slight effect on the $Re\{K_{CM}\}$ spectrum over our measured frequency range. We chose to fix the nuclear envelope thickness to 40 nm, $d_n = 40$ nm, which is the value reported in literature by optical measurement of single nuclear pore permeability [124] and electron microscopy [117]. It should be noted that the sensitivity to cell parameters (especially the nucleus and nuclear envelope) is substantially lower for media with very low ionic concentration (less than 0.1 S/m). Therefore, parameters of a double-shell model extracted from measurements in a very low conductivity medium may have lower accuracy.

4.2.5 CHO Double-shell Model Parameters

The final double-shell model parameters of CHO cells are given in Table 4.1. Seven parameters are obtained by curve fitting to the measured data and optical measurements (cell and nucleus sizes). Five remaining parameters, which our measurements are most insensitive to, σ_{mem}, ε_{cyt}, σ_{ne}, ε_n, and d_{ne}, are set to the values obtained for normal lymphocyte cells [79], [111]. The reported parameters of three other mammalian cells (leukocytes) obtained by time domain dielectric spectroscopy [111], frequency domain dielectric spectroscopy [79], and electrorotation technique [121] are also presented in Table 4.1 for comparison.

Table 4.1: *Double shell-model parameters for CHO cells (and three other mammalian cells). Reproduced from* [94]*, with the permission of AIP Publishing.*

Parameters	CHO	T lymphocytes[a]	Lymphocytes[b]	Monocytes[c]
Membrane permittivity (F/m)	8.5 ε_0	11.1ε_0	6.8ε_0	8.6ε_0 [d]
cytoplasm conductivity (S/m)	0.42	0.65	0.32	0.56
Nuclear envelope permittivity (F/m)	23.2 ε_0	85.6 ε_0	28 ε_0	N/A
Nucleoplasm conductivity (S/m)	1.50	1.26	1.35	N/A
Membrane thickness (nm)	5	7	7	N/A
Average cell radius (μm)	6.0	3.4	2.9	4.6
Nucleus radius / Cell radius	0.55	0.84	0.86	N/A
Membrane conductivity (S/m)	1×10^{-6}	27.4×10^{-6}	$<10^{-5}\sigma_{cyt}$	1×10^{-4} [d]
Cytoplasm permittivity (F/m)	60 ε_0	60 ε_0	60 ε_0	126.8 ε_0
Nuclear envelope conductivity (S/m)	1×10^{-3}	8.8×10^{-3}	6×10^{-3}	N/A
Nucleoplasm permittivity (F/m)	120 ε_0	120 ε_0	52 ε_0	N/A
Nuclear envelope thickness (nm)	40	40	40	N/A

[a] *Measured using time domain dielectric spectroscopy* [111].
[b] *Measured using frequency domain dielectric spectroscopy* [79].
[c] *Measured using electrorotation technique employing a single-shell model* [121].
[d] *Assuming a membrane thickness of 5 nm.*

Our values of membrane permittivity and cytoplasm conductivity of CHO cells is close to the values reported for other mammalian cells. Parameters for the nuclei of cells have been investigated to a lesser extent and the reported values are scattered over a broader range. Our obtained value for the nuclear envelope permittivity is close to references [79] and [117]. We found that the nucleoplasm conductivity is substantially higher than the cytoplasm conductivity. This is consistent with the findings in [41], [111] which describe the nuclear envelope as a dynamic ion-selective membrane capable of maintaining ion gradients across. A plot of $Re\{K_{CM}\}$ based on the extracted CHO model (Table 4.1) is given in Fig. 4.3b showing the fit to the measured data.

CHO cells have a much smaller nucleus (less than 20 percent of the cell volume) as compared with leukocytes. Nevertheless, measurements in moderately conductive media (which increases the sensitivity to nucleus parameters) enable us to accurately determine the dielectric properties of the nucleus. Fig. 4.5 shows the simulated spectrum of $Re\{K_{CM}\}$ for a CHO cell with parameters given in Table 4.1 and medium conductivity of 0.01 and 0.17 S/m (close to medium conductivities used in several pervious works [42], [54], [67], [73], [74], [114], [122]). It demonstrates that changing the radius of the nucleus by 25 percent (while keeping all other parameters the same) causes a noticeable change in the spectrum for medium conductivity 0.17 S/m. The effect on the spectrum for medium conductivity 0.01 S/m is not discernible at frequencies less than 10 MHz and less pronounced at higher frequencies. The single-shell model (membrane and cytoplasm with no nucleus) spectrum is also shown in Fig. 4.5.

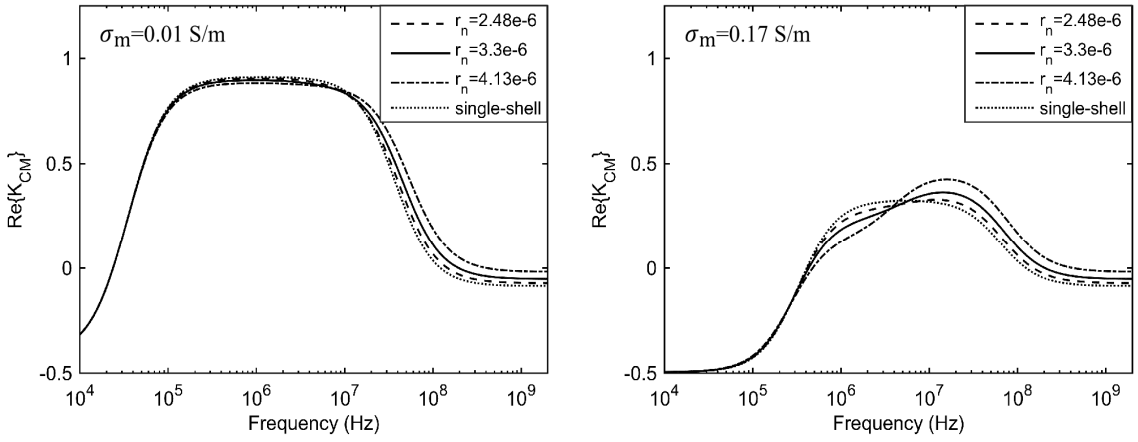

(a) (b)

Figure 4.5: *Simulated spectrum of $Re\{K_{CM}\}$ for a CHO cell with parameters from Table 4.1 in a medium with conductivity (a) 0.01 S/m and (b) 0.17 S/m (solid line). The effect of changing the nucleus radius by 25 percent smaller (dashed line) and larger (dash-dot line) on the spectrum as well as modeling the cell with a single-shell structure, including only the membrane and cytoplasm, (dotted line) is demonstrated. Reproduced from* [94]*, with the permission of AIP Publishing.*

4.3 CONCLUSIONS

In this chapter we showed how the dielectric properties of CHO cells could be represented accurately by a double-shell model. By measuring the DEP response of single CHO cells along with optical measurements we reported values for CHO cells' membrane permittivity, membrane thickness, cytoplasm conductivity, nuclear envelope permittivity, nucleoplasm conductivity, cell size, and nucleus size. The parameters reported are the most sensitive ones over the frequency range of our experiments (0.6 – 10 MHz). Despite the small size of CHO cell's nucleus, it causes a discernable dispersion over our measured frequency range for the chosen media conductivities. This enabled us to determine the nucleus and nuclear envelope dielectric parameters fairly accurately.

The dielectric model developed for CHO cells in this chapter is used in chapters 5 and 6 to obtain quantified results on how the cytoplasm conductivity of cells changes after electroporation with pulses with various intensities.

Chapter 5. Single Cell Cytoplasm Conductivity Change Induced by Electroporation

In this chapter we present the results for measuring changes in the cytoplasm conductivity of several individual cells subjected to pulses with various intensities using our DEP cytometry technique. Individual cells are exposed to electroporating pulses and their DEP response is measured before and after the pulse exposure. The electroporation induced changes in the cells' DEP response is then translated to changes in their cytoplasm conductivity using numerical simulations.

5.1 MATERIALS AND METHODS

5.1.1 Cell Preparation

The Chinese Hamster Ovary (CHO) cell line (CHODG44-EG2-hFc/clone 1A7) used for this study is kindly provided by Yves Durocher of the NRC, Canada (Bell et al., 2010). The cells are maintained by passaging them every 2 – 3 days and growing them in 250 mL baffled shaker flasks (VWR International, Radnor, PA) at 120 rpm in an incubator at 37°C

with a 10% CO_2 overlay. The culture medium used is BioGro-CHO serum-free (BioGro Technologies, Winnipeg, MB) supplemented with 0.5 g/L yeast extract (BD, Sparks, MD), 4 mM GlutaMax I (Invitrogen, Grand Island, NY), and 1 mM glutamine (Sigma, St. Louis, MO). For this study a sample of cells is taken from the shaker flask and centrifuged at 377xg for 1 min. The cell pellet is then re-suspended in fresh growth and low conductivity (~0.067 S/m) medium [22.9 mM sucrose (Sigma), 16 mM glucose (Fisher), 1 mM $CaCl_2$ (Fisher), 16 mM Na_2HPO_4 (Fisher)] (Polevaya et al., 1999) at a ratio of 1:15 to reach a final conductivity of ~0.17 S/m as determined using a conductivity meter (Orion 3-Star Plus, Thermo Scientific, Waltham, MA). While re-suspending the cell pellet, the sample is diluted to a final concentration of $5x10^4$ cells/mL.

5.1.2 Pulsed Electric Field Exposure

In our experiments a single cell is identified and then continuously shuttled back and forth over the electrodes in the microfluidic channel. We first measure the cell's DEP response for several passes at 10 MHz (sensitive to cell's internal conductivity) before electroporation. Then, as the cell passes over the actuation region, we apply several 200 ns rise-time and 100 µs duration trapezoidal pulses with an intensity in the range 0.7 to 2.4 kV/cm to the cell. The repetition rate of pulses is set to 100 or 200 Hz and the number of applied pulses is dependent on the cell's velocity as it passes over the actuation electrodes. The total number of applied pulses is obtained by time analysis of the recorded sensing and the pulse generator signals. In order to generate pulses with intensity in the range 0.7 to 2.4 kV/cm, pulsed voltages of amplitude 5 V to 15 V are applied to actuation electrodes. Fig. 5.1 shows simulation results of the amplitude profile of the electric field in the actuation region at three different altitudes from the electrodes. For a specific pulse amplitude the

intensity of the field applied to the cell is a function of its altitude in the channel and it is determined by post analysis of the signal from the sensing electrodes. Immediately after electroporation the DEP response of the cell is measured over a period of time as it continues moving back and forth in the channel.

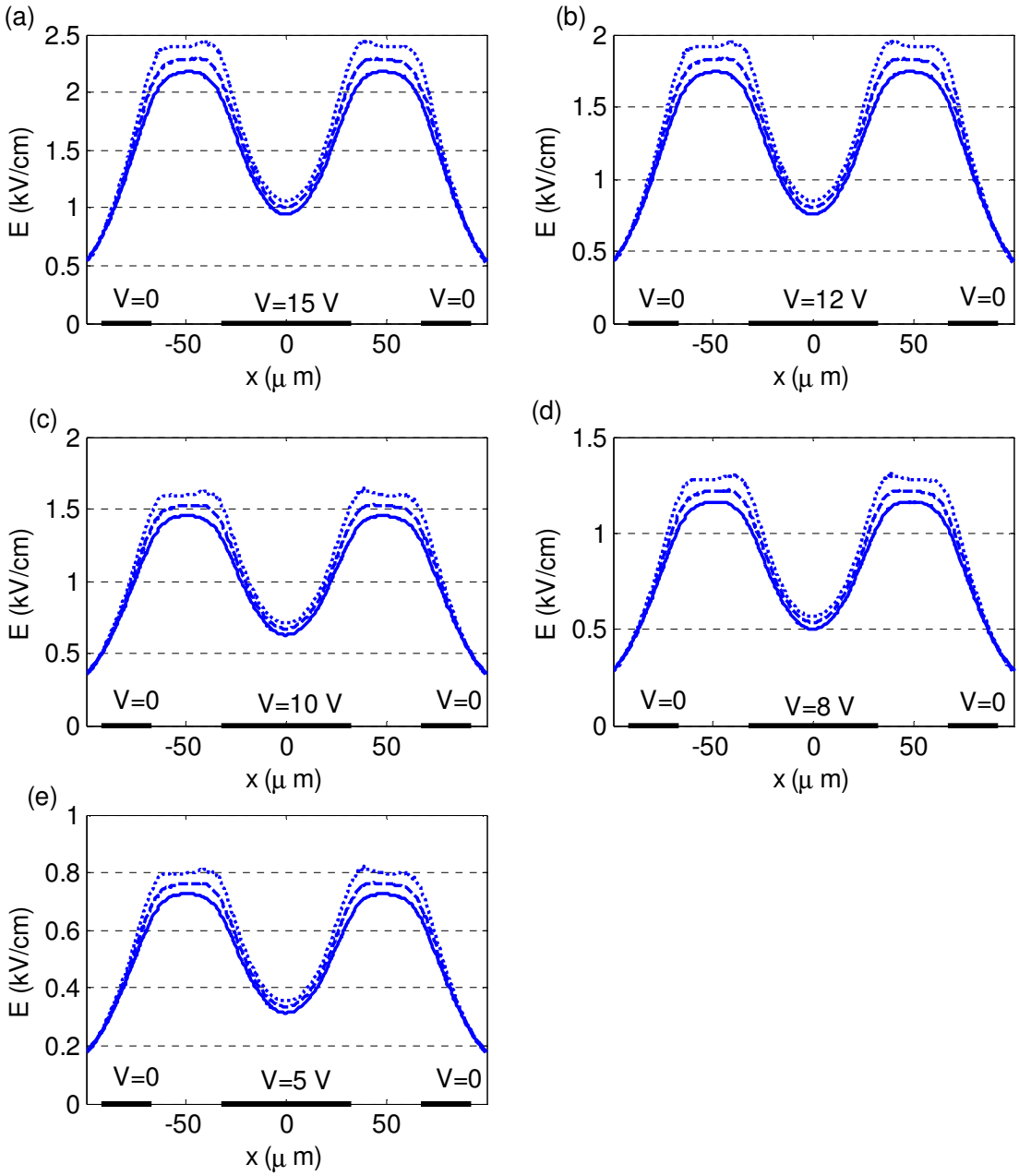

Figure 5.1: *Amplitude profile of the electric field in the actuation region at altitudes 16 μm (solid line), 14 μm (dashed line), and 12 μm (dotted line) from electrodes for applied voltages of (a) 15 V, (b) 12 V, (c) 10 V, (d) 8 V, and. (e) 5 V.*

5.1.3 Calculation of Changes in Cells, Cytoplasm Conductivity

The measured force indices before and after electroporation for an individual cell are related to the DEP force and hence $Re\{K_{CM}\}$ (Eq. (2.2)). Numerical simulation in *COMSOL Multiphysics 4.3 b Particle Tracking for Fluid Flow* and *Electric Currents* modules is performed to obtain $Re\{K_{CM}\}$ from the measured average force indices before and after electroporation. Through simulation of the DEP and hydrodynamic forces (drag, lift, and buoyancy) acting on a spherical cell with variable $Re\{K_{CM}\}$ (within the range -0.4 to 0.4) in the microfluidic channel, we find the exit altitude (at the location of the second sensing electrode, S_2) of the cell. For each altitude change we estimate the corresponding capacitance change of the sensing electrodes and hence the sensing signal and expected force index. The cell's $Re\{K_{CM}\}$ is determined by selecting among the simulated force indices the one that is closest to the measured force index for the cell and finding its corresponding $Re\{K_{CM}\}$. The size, initial height, and initial velocity of the particle is selected to match the measured values for each cell. Details of the numerical simulation is provided in Chapter 3 sections 3.3 and 3.4.

With the DEP actuation at 10 MHz, $Re\{K_{CM}\}$ is mostly affected by the cell internal conductivity. Employing the CHO dielectric model developed in Chapter 4, the percentage change in $Re\{K_{CM}\}$ at 10 MHz for 10 percent change in different cell dielectric parameters is summarized in Table 5.1. It is evident that the cytoplasm conductivity has the dominant effect on $Re\{K_{CM}\}$ at the selected DEP frequency. It should be noted that the membrane conductivity can be significantly affected by electroporation, however, its impact on $Re\{K_{CM}\}$ at 10 MHz is insignificant. The cell and nucleus size have substantial effects on $Re\{K_{CM}\}$ at our measurement frequency (10 MHz). Noticeable changes in the size of cells'

nucleus induced by microsecond duration pulses have not been primarily observed in previous studies and, therefore, we consider it invariable. Increase in the cell's size may occur because of electroporation. Using the information obtained from the sensing signal, we consider its effect in our simulations (more details in the results section).

In order to determine the cells' cytoplasm conductivity, σ_{cyt}, before and after electroporation, we vary the value of σ_{cyt} in the double-shell dielectric model of CHO (with other parameters remaining the same) such that the resulting $Re\{K_{CM}\}$, calculated at 10 MHz, is close to the one obtained from our measurement.

Table 5.1: *Relative change of $Re\{K_{CM}\}$ at 10 MHz for ten percent change in various cell dielectric parameters. Dielectric model for a CHO cell from* [94]

Parameter	Symbol	Nominal Value	Change of $Re\{K_{CM}\}$ at 10 MHz (%) [(a)]
Membrane permittivity	ε_{mem}	8.5 ε_0 (F/m)	0.3
Membrane conductivity	σ_{mem}	1×10^{-6} (S/m)	0.0002
Cytoplasm permittivity	ε_{cyt}	60 ε_0 (F/m)	0.005
Cytoplasm conductivity	σ_{cyt}	0.42 (S/m)	12
Nuclear envelope permittivity	ε_{n-env}	23.2 ε_0 (F/m)	1.65
Nuclear envelope conductivity	σ_{n-env}	1×10^{-3} (S/m)	0.058
Nucleoplasm permittivity	ε_n	120 ε_0 (F/m)	0.028
Nucleoplasm conductivity	σ_n	1.50 (S/m)	0.89
Nuclear envelope thickness	d_{n-env}	40 (nm)	1.24
Nucleus radius	R_n	3.3 (nm)	4.6
Membrane thickness	d_{mem}	5 (nm)	0.22
Cell radius	R_{cell}	6 (nm)	3.2

[(a)] Medium conductivity, σ_e, and permittivity, ε_e, are set to .017 (S/m) and 78 ε_0 (F/m), respectively.

5.2 RESULTS AND DISCUSSION

5.2.1 DEP Measurement of Electroporated Cells

Several individual cells are captured and continuously shuttled back and forth in the microfluidic channel and their DEP response to 100 μs duration pulsed electric fields (PEF)

with intensity 0.7 – 2.4 kV/cm is measured. Six to eight pulses (depending on the cell velocity) with repetition rate 100 Hz is applied to each cell. For two cases with the highest intensity (2.2 kV/cm) 15 pulses with repetition rate 200 Hz is employed. For each cell measurement the DEP signal is recorded for every pass of the cell over the electrodes. At first no DEP is applied to the cell which results in force indices close to zero (Fig. 5.2a). Then a 10 MHz and 7 V_{pp} sinusoidal DEP voltage is applied to the actuation electrodes to measure the cell's average force index before the electroporation. The cell's DEP response before pulse exposure is measured for approximately one minute. Then, a multiple pulse voltage with desired amplitude is applied to the actuation electrodes and the cell experiences the PEFs as it passes once over the actuation region. The amplitude of the applied electric field is obtained from simulation of the field intensity in the channel after finding the altitude of the cell during the pulse exposure pass. After pulse application the actuation electrode voltage is set back to a 10 MHz and 7 V_{pp} sinusoidal signal and the cell's average force index after electroporation is measured. The first measurement is a few seconds after the pulse exposure (the time required for the cell to return in the channel and reach the electrodes). Fig. 5.2 shows an example measurement result for a cell subjected to seven pulses with amplitude 1.5 kV/cm over a time period of six minutes. Each bar in Fig. 5.2a corresponds to one pass of the cell over the electrodes. Red lines represent the average of force indices with error bars being the standard deviation. With no DEP application (initial 30 seconds) the average force index is close to zero. During the DEP application (next 100 seconds) the cell experiences a pDEP force resulting in positive force indices. After the pulse exposure the cell still experiences a pDEP force, however, the average force index is significantly smaller. The raw data showing example signatures of the cell as it is

cycled over the electrodes right before electroporation, during the pulse application, and after electroporation is presented in Fig. 5.3. There are fluctuations in the measured force indices since the cells are not perfectly spherical and they rotate as they move back and forth [125], they have an inhomogeneous and asymmetric internal structure, and there is a slight variation in the height and velocity of the cell over time. However, the measured change in the average force indices before and after electroporation is considerably larger than the fluctuations. The amplitude of P_1 and the cell's velocity over the measurement period are plotted in Fig 5.2b and c, respectively. We use these plots to obtain the height and velocity information required for post processing simulations. The sensing signal recorded during no DEP actuation is used to estimate the initial average velocity of the cell and hence its initial equilibrium altitude in the channel. During the DEP application, the cell is forced out of its equilibrium altitude and as it is shuttled back in the channel toward the electrodes it may not reach the equilibrium due to the short travel distance. Therefore, the equilibrium altitude calculated for the no DEP actuation case is not valid to be used in simulations with DEP actuation. During the time period that the DEP is applied, we estimate the average (over several passes) entrance altitude (h_1) of the cell using the information in the peak amplitude from the first sensing electrodes, P_1 (using the plot of ΔC versus altitude since P_1 is proportional with ΔC).

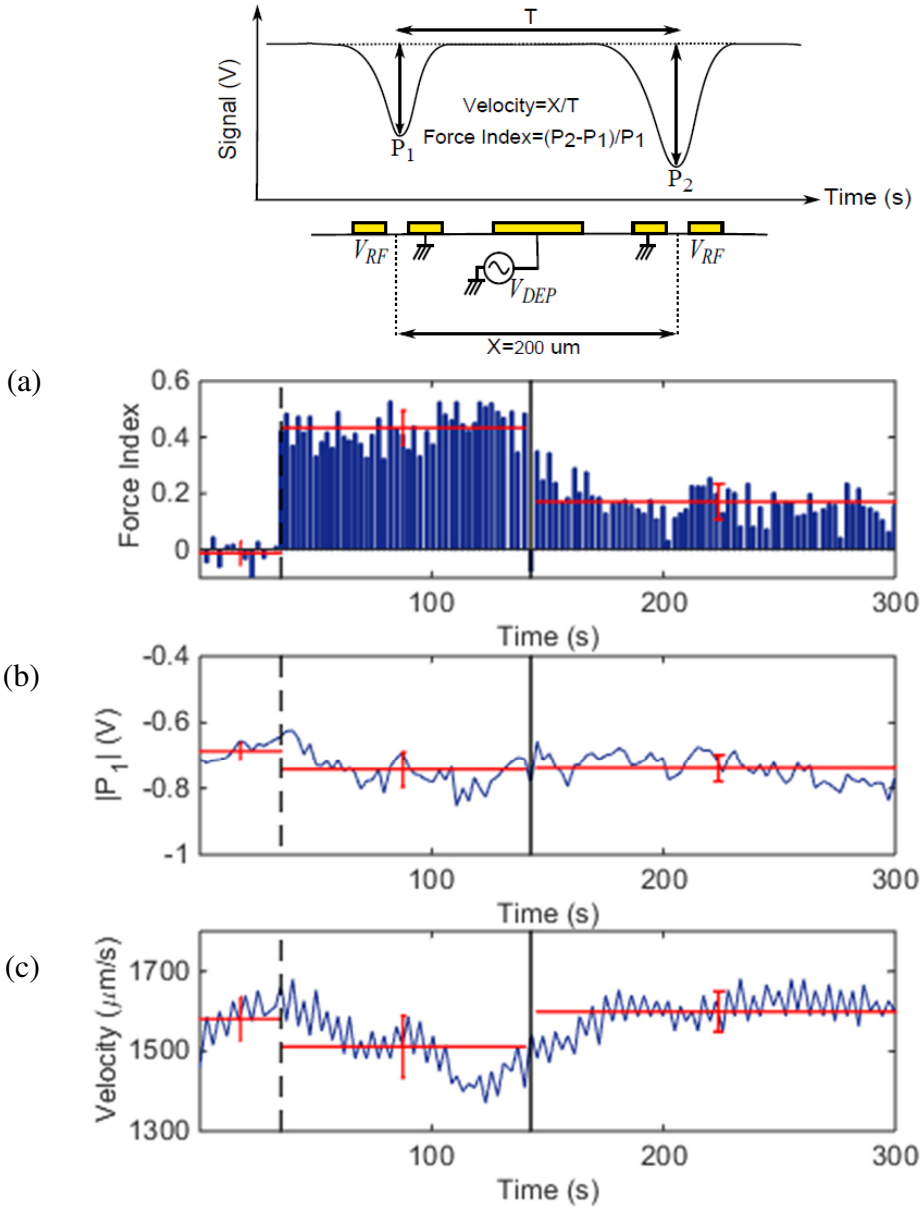

Figure 5.2: *Example of measured results for a single CHO cell shuttled back and forth over the electrodes array in the microfluidic channel with σ_e=0.17 S/m and subjected to seven 100 μs pulses with amplitude 1.5 kV/cm and repetition rate 100 Hz. (a) Measured force indices before and after electroporation. Each bar represents one pass of the cell over the electrodes. The red lines indicate the average with the error bars being the standard deviation. Before the DEP application (shown by a dashed black line) the force index is approximately zero. After DEP application (at 10 MHz) the cell experiences a strong pDEP force. After electroporation (shown by a solid black line) the intensity of the pDEP force decreases. (b) Amplitude of the peak, P_1, recorded by the first sensing electrode pair (located before the DEP electrode). This plot is used to estimate the average altitude of the cell in the channel before and after electroporation (required for post-processing simulations). (c) Velocity of the cell as it moves back and forth in the channel. Fluctuations in the velocity causes slight changes in the cell's altitude and amplitude of P_1.*

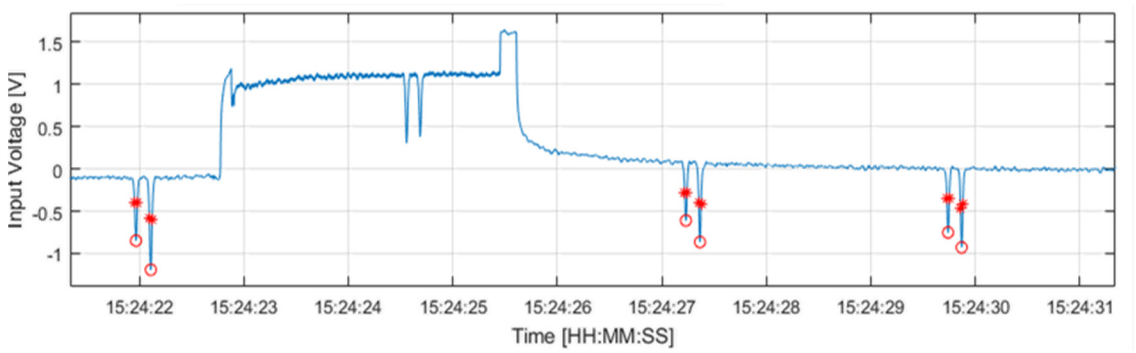

Figure 5.3: *Example signatures of the cell in Fig. 5.2 as it is cycled over the sensing electrodes. The first signature is for the cell actuated by a DEP force before electroporation. The second signature is when electroporation is applied (during this period pulsed electric voltages are applied to the actuation electrodes). The third and fourth signatures are for the cell actuated by a DEP force after electroporation. These signatures are used to obtain the force indices, peak amplitudes, and velocity information plotted in Fig. 5.2.*

Measurements are performed on more than 20 individual cells subjected to PEFs with intensities close to 0.7, 1.2, 1.5, 1.8, and 2.2 kV/cm. Fig. 5.3-5.7 presents the gradual change of force index before and after electroporation for application of pulses with intensities 2.2 kV/cm (Fig. 5.3), 1.8 kV/cm (Fig. 5.4), 1.5 kV/cm (Fig. 5.5), 1.2 kV/cm (Fig. 5.6), and 0.7 kV/cm (Fig. 5.7).

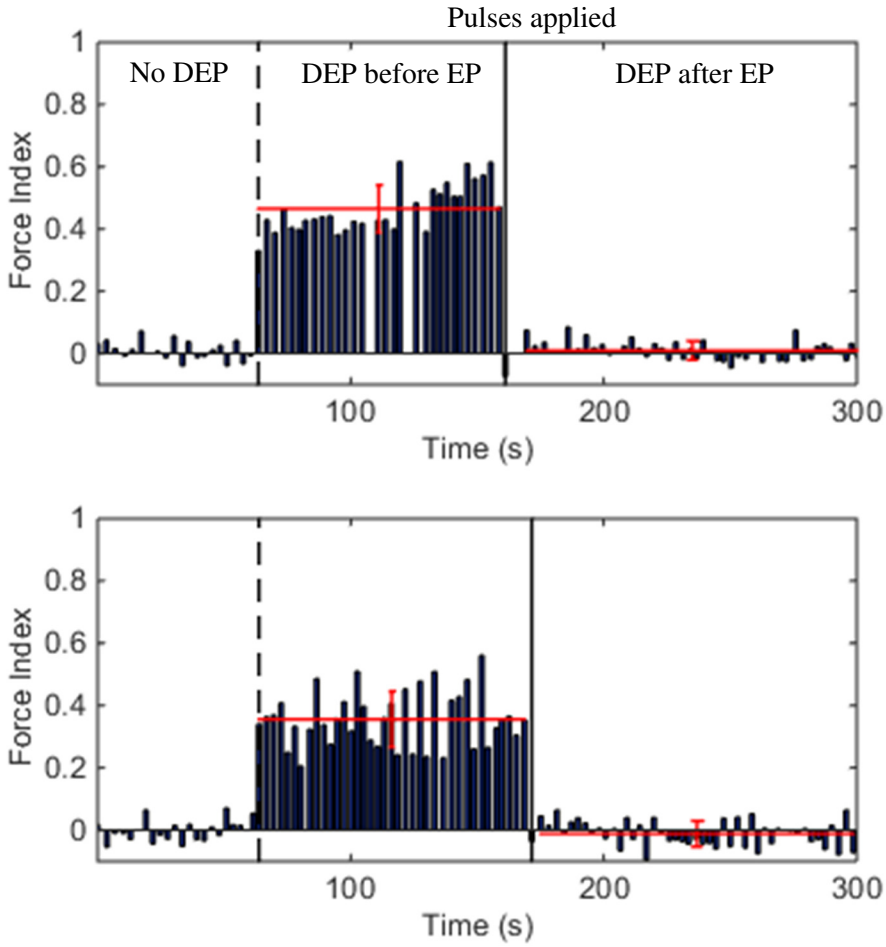

Figure 5.4: *Force index vs. time for two CHO cells (top and bottom) before and after exposure to 100 μs, 2.2 kV/cm pulses. In each case the force index is shown for three states: (i) no DEP actuation (before the dashed black line), (ii) 10 MHz DEP actuation before the application of pulses (between the dashed and solid black lines), and (iii) 10 MHz DEP actuation after application of pulses (after the solid black line). The mean of φ before and after pulse exposures is shown by red lines with the error bar being the standard deviation.*

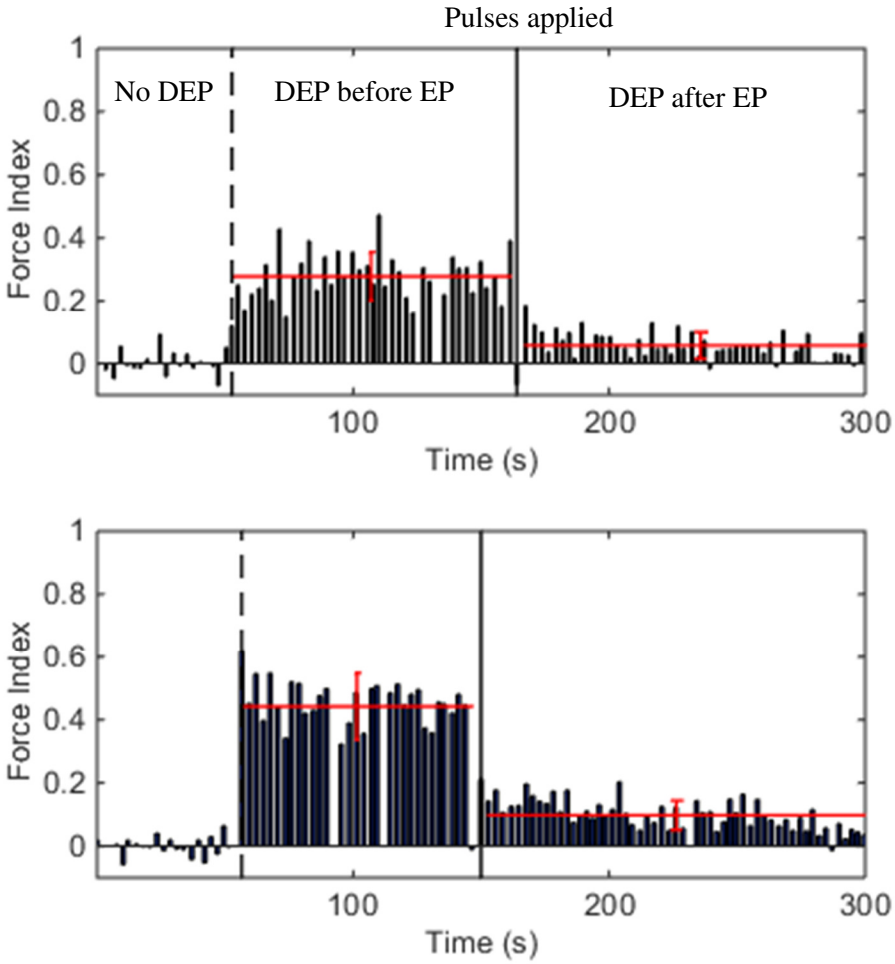

Figure 5.5: *Force index vs. time for two CHO cells (top and bottom) before and after exposure to 100 µs, 1.8 kV/cm pulses. In each case the force index is shown for three states: (i) no DEP actuation (before the dashed black line), (ii) 10 MHz DEP actuation before the application of pulses (between the dashed and solid black lines), and (iii) 10 MHz DEP actuation after application of pulses (after the solid black line). The mean of φ before and after pulse exposures is shown by red lines with the error bar being the standard deviation.*

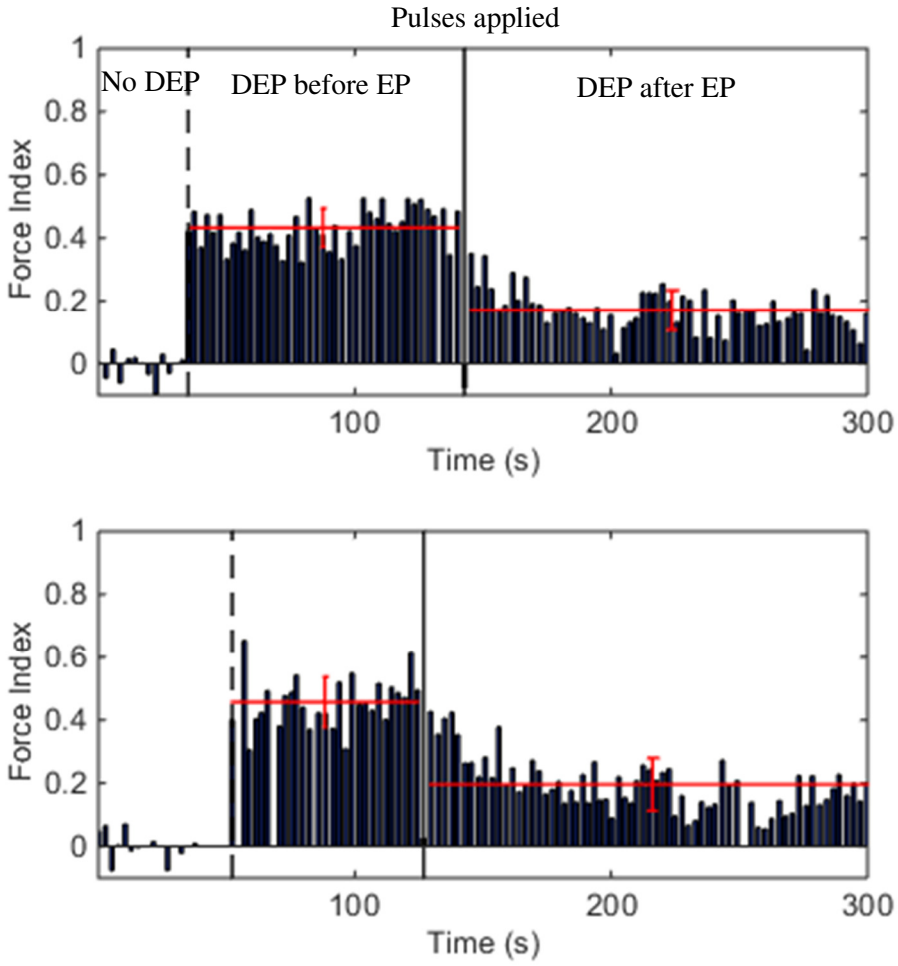

Figure 5.6: *Force index vs. time for two CHO cells (top and bottom) before and after exposure to 100 μs, 1.5 kV/cm pulses. In each case the force index is shown for three states: (i) no DEP actuation (before the dashed black line), (ii) 10 MHz DEP actuation before the application of pulses (between the dashed and solid black lines), and (iii) 10 MHz DEP actuation after application of pulses (after the solid black line). The mean of φ before and after pulse exposures is shown by red lines with the error bar being the standard deviation.*

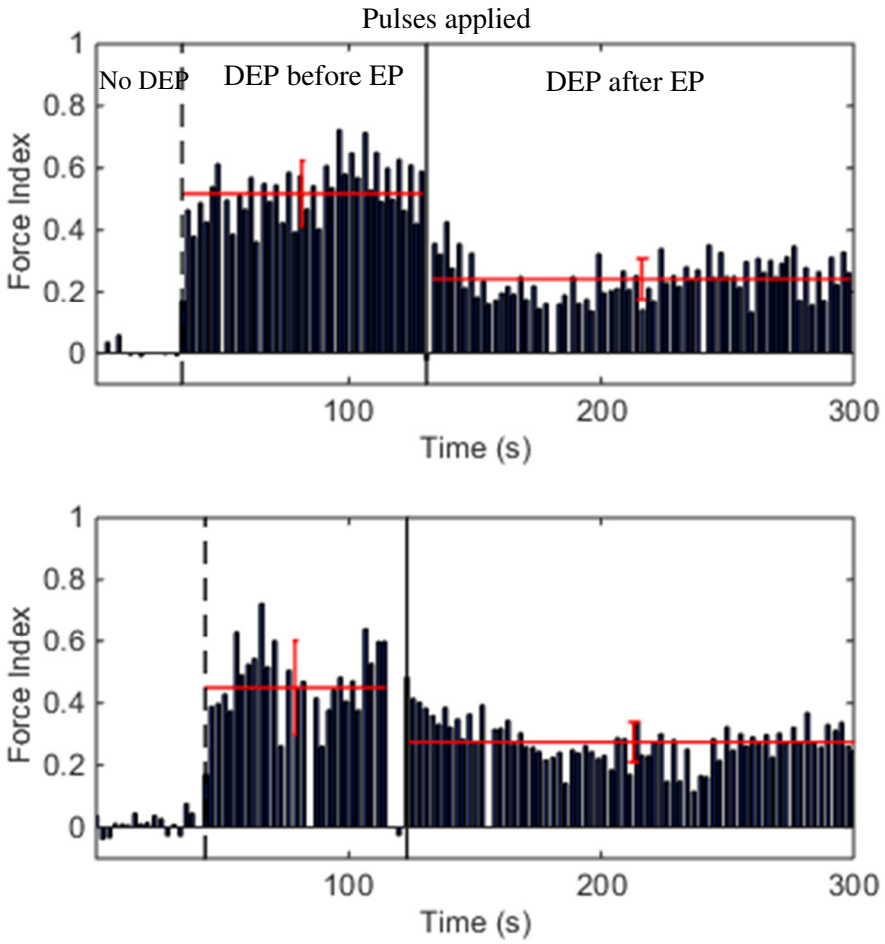

Figure 5.7: *Force index vs. time for two CHO cells (top and bottom) before and after exposure to 100 μs, 1.2 kV/cm pulses. In each case the force index is shown for three states: (i) no DEP actuation (before the dashed black line), (ii) 10 MHz DEP actuation before the application of pulses (between the dashed and solid black lines), and (iii) 10 MHz DEP actuation after application of pulses (after the solid black line). The mean of φ before and after pulse exposures is shown by red lines with the error bar being the standard deviation.*

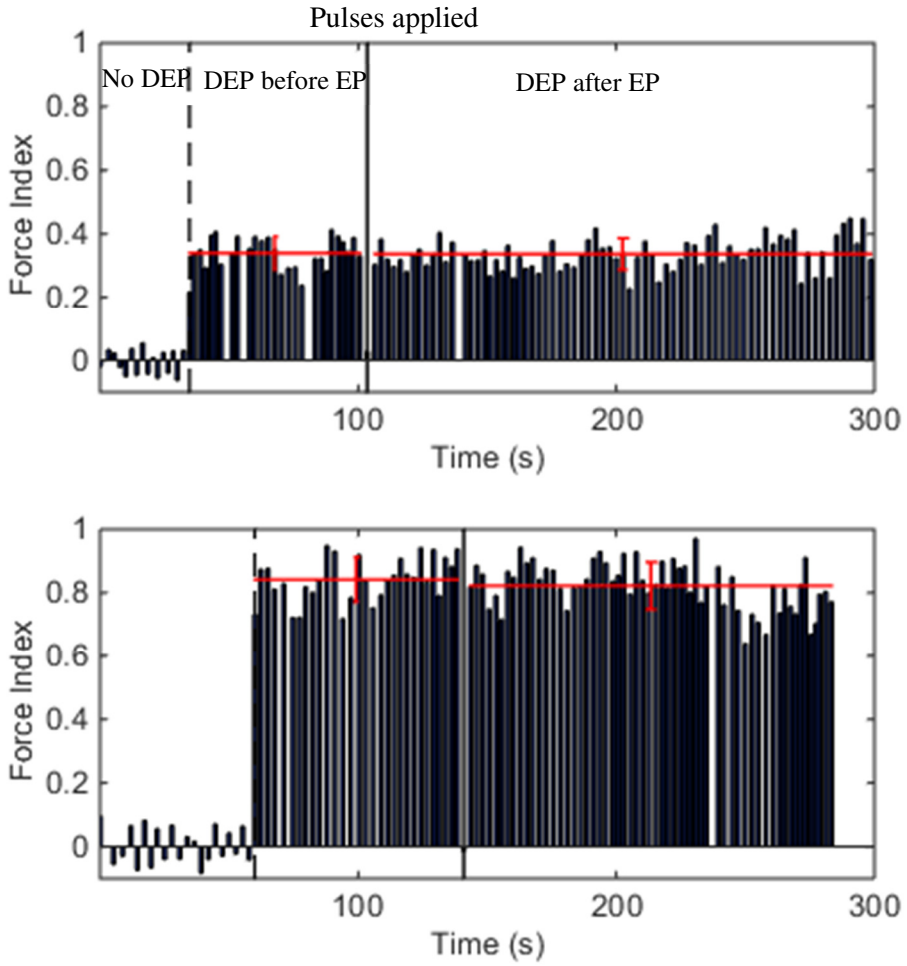

Figure 5.8: *Force index vs. time for two CHO cells (top and bottom) before and after exposure to 100 µs, 0.7 kV/cm pulses. In each case the force index is shown for three states: (i) no DEP actuation (before the dashed black line), (ii) 10 MHz DEP actuation before the application of pulses (between the dashed and solid black lines), and (iii) 10 MHz DEP actuation after application of pulses (after the solid black line). The mean of φ before and after pulse exposures is shown by red lines with the error bar being the standard deviation. In this case the pulse amplitude is not sufficiently strong to affect the cell.*

It is evident that changes in φ after pulse applications is highly dependent on the intensity of applied pulses. The mean and standard deviation of force indices before and after electroporation for each pulse amplitude is listed in Table 5.2.

Table 5.2: *Mean and standard deviation of force indices (φ) before and after electroporation for results of Fig. 5.3-5.7.*

Pulse Amplitude		mean of φ before pulse exposures	std of φ before pulse exposure	mean of φ after pulse exposures	std of φ after pulse exposures
2.2 kV/cm	Cell A1	0.46	0.08	0.01	0.03
	Cell A2	0.36	0.09	-0.01	0.04
1.8 kV/cm	Cell B1	0.28	0.08	0.06	0.04
	Cell B2	0.44	0.11	0.10	0.05
1.5 kV/cm	Cell C1	0.43	0.06	0.17	0.06
	Cell C2	0.46	0.08	0.20	0.08
1.2 kV/cm	Cell D1	051	0.10	0.24	0.07
	Cell D2	0.45	0.15	0.27	0.06
0.7 kV/cm	Cell E1	0.34	0.05	0.34	0.05
	Cell E2	0.84	0.07	0.82	0.07

The results show larger change in φ (and thus $Re\{K_{CM}\}$) for stronger pulses. For comparison, the time evolution of the normalized force indices (4-point moving average) for five cells subjected to these pulses are shown in Fig. 5.8. For pulse amplitudes 0.7 – 1.8 kV/cm the cells are subjected to six or seven pulses with repetition rate 100 Hz. For pulse amplitude 2.2 kV/cm the cell is subjected to fifteen pulses with repetition rate 200 Hz. Comparable behavior is observed for other cells subjected to similar pulse amplitudes. It is noted that while electric fields above 1.2 kV/cm cause measurable change in the force index (and dielectric properties) of cells, a 0.7 kV/cm field intensity is not sufficiently strong to affect the cells. This is consistent with findings in other reports [31], [50], [56], [58]–[60], [126] where similar pulses are employed and optical techniques are used to

measure the permeability of dyes into cells due to electroporation. As an example, in [42] B16F10 cells in a medium with conductivity 0.125 S/m are electroporated using 8, 100 μs duration rectangular pulses with amplitudes 1.2 kV/cm, 1.5 kV/cm, and 1.8 kV/cm. In their study a population of cells is electroporated in an electroporation cuvette and then it is loaded into a DEP chamber where a DEP force is applied to cells and the shift in the first cross-over frequency is monitored approximately five minutes after pulse applications. Their results show an increase in the first cross-over frequency after electroporation. However, they do not correlate the shift in cross-over frequency to the amplitude of applied pulses. In their study the electroporation of cells is confirmed by fluorescent imaging in a flow cytometer. Using PI fluorescent dyes they confirm an increase in the fluorescence intensity of cells electrporated by stronger pulses. They attribute this to higher extent electroporation and more uptake of PI. The temporal response of cells presented in Fig. 5.8 suggests a time constant associated with the conductivity change of cells ranging from 3 to 30 seconds depending on the pulse amplitude. This agrees with the results recently published by Son *et al.* [86] based on the numerical modeling of electroporation which demonstrate that the transport of Calcium ions into a cell continues up to 10 s after application of a single 100 μs duration pulse with amplitude 1 kV/cm. In their simulations the lifetime of pores is assumed to be 4 s, however, after resealing the pores remain (at their minimum size ~1 nm) for a long time (more than 20 s) [86]. Using Thallium ions with fluorescent microscopy (preloading cells with a dye which fluoresces upon entry of Thallium cations into cells after electroporation), *Bowman et al.* have reported a lifetime in the range of 10 minutes for nanopores created by nanosecond duration pulses [33]. The

result presented here can be used to infer information about the density and resealing time of very small size pores and their relation with the intensity of applied pulses.

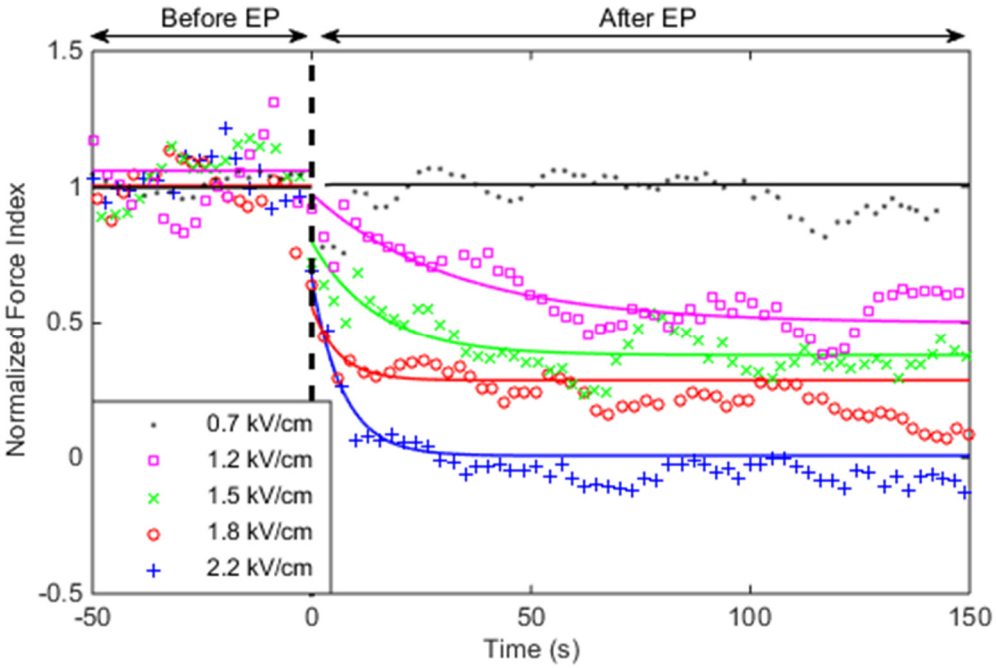

Figure 5.9: *Normalized force indices (4-point moving average) for four cells subjected to six or seven 100 µs duration pulses with amplitude 0.7, 1.2, 1.5, and 1.8 kV/cm and repetition rate 100 Hz and one cell subjected to fifteen 100 µs duration pulses with amplitude 2.2 kV/cm and repetition rate 200 Hz. Solid lines represent an exponential fit to the measured data points. The dashed line indicates when the electroporation pulse is applied. Medium conductivity is 0.17 S/m.*

Cell swelling has been associated with conventional electroporation (pulses in millisecond and microsecond duration range) in several previous studies [42], [80]. While Zhuang *et al.* reported no significant change in cells' size after electroporation with 8, 100 µs, 1.1 kV/cm pulses [53] Moisescu *et al.* observed thirty percent increase in cells' diameter after exposure to 8, 100 µs, 1.8 kV/cm pulses [42]. Golzio *et al.* also reported an increase in cells' diameter by thirty percent caused by 5ms, 0.8 kV/cm pulses [80]. In our experiments expansion in the cells' size is observed for PEFs with amplitude greater than 1.8 kV/cm

and we consider it in our simulations. This observation is based on noticeable increase in the amplitude of P_1 immediately after electroporation without significant decrease in the cells' velocity (due to the parabolic flow velocity profile in the channel lower cell velocity correlates with lower altitude in the channel and hence larger amplitude of P_1). Increase in size of cells after electroporation with strong fields has an impact on their DEP response. The cell's size affects the DEP force acting on it directly (since F_{DEP} is proportional to the cell volume) as well as through $Re\{K_{CM}\}$. Although cell enlargement may occur after electroporation this effect is not sufficient to explain the significant changes observed in our experiments. Cell swelling is observed only for strong field applications (pulses of 1.8 kV/cm or larger) for which our results demonstrate dramatic decrease of force index to $\varphi \approx 0$, corresponding to $Re\{K_{CM}\} \approx 0$.

5.2.2 Cytoplasm conductivity analysis

Electroporation induced changes in the DEP response of cells, presented in Fig. 5.3-5.7 and Table 5.2, are attributed primarily to changes in cells' internal conductivity since the DEP actuation is performed at 10 MHz ($Re\{K_{CM}\}$ is dominantly influenced by the cell cytoplasm conductivity at this frequency). The cytoplasm conductivity of each cell before and after electroporation in a medium with conductivity σ_e=0.17 S/m is obtained by numerical simulation (explained in section 5.1.3) and is plotted in Fig. 5.9. In simulations the nucleoplasm conductivity, σ_n, is chosen such that the ratio σ_n/σ_{cyt} is maintained at the value for untreated CHO cells while other cell parameters are remained at their nominal values given in Table 4.1. This is because previous studies suggest that the nuclear envelope is capable of maintaining the ion concentration gradient between the nucleus and cytoplasm [41], [111]. Square data points indicate cytoplasm conductivities before PEF

application. Solid circle data points represent cells subjected to 6-8 pulses with repetition rate 100 Hz and the empty circle data points represent cells subjected to fifteen pulses with repetition rate 200 Hz. The average cytoplasm conductivity of cells before electroporation is 0.34 S/m with standard deviation 0.04 S/m. There is a slight variation in the initial conductivity of selected cells as they may be at different phases of their growth cycle. In all cases cytoplasm conductivity decreases after electroporation and pulses with higher intensity cause a larger decrease in the cell's internal conductivity. Given that the ion concentration in the suspension medium (σ_e= 0.17 S/m) is less than in the cell's cytoplasm, electrodiffusion during pulse application and diffusion during the pore resealing period result in a large efflux of ions (predominantly potassium, sodium, chloride) from the cell. This happens to a larger extent with higher intensity pulses since they create a larger number of pores in the cell membrane (providing more pathways for ion transport) and cause a larger drift induced current. In our experiments the lowest internal conductivity obtained for cells after electroporation is approximately 0.15 S/m. Increasing the number of pulses to fifteen (empty circle data points in Fig. 5.9) or applying two sets of fifteen pulses with a three second interval (data not shown) does not lead to further decrease in the cytoplasm conductivity. Although the obtained limit for decrease in the cells' internal conductivity, 0.15 S/m, is close to the external medium conductivity, 0.17 S/m, it does not imply equilibrium of ion concentrations inside and outside the cell. Since the mobility of ions inside the cell is significantly lower than the suspension medium (by a factor of 3 to 4) [127], [128] similar ion concentration inside the cell as in the external medium would results in a conductivity approximately 0.05 S/m. One possible explanation for this lower limit is the presence of large and relatively immobile negative ions inside the cell which

attract mobile positive ions (mainly sodium and potassium) to maintain the cell electrical neutrality. The concentration of immobile negative ions inside CHO cells is calculated, using the Goldman equation, osmolality balance, and electrical neutrality [129] to be 69 mM with an average electrical charge 1.07, $[X]^{-1.07}$. The required concentration of Na^+ or K^+ inside a cell to maintain the cell electrically neutral is 74 mM which results in an internal conductivity approximately 0.1 S/m. A decrease in the cytoplasm conductivity to 0.1 S/m is reported in another study [41] where the dielectric parameters of a population of electroporated cells (in a medium with conductivity 0.1 S/m) were measured using time-domain dielectric spectroscopy technique. Although the result is for nanosecond duration pulse applications it is consistent with the finding here.

The measurement results for the cells in Fig. 5.9 is summarized in Table 5.3.

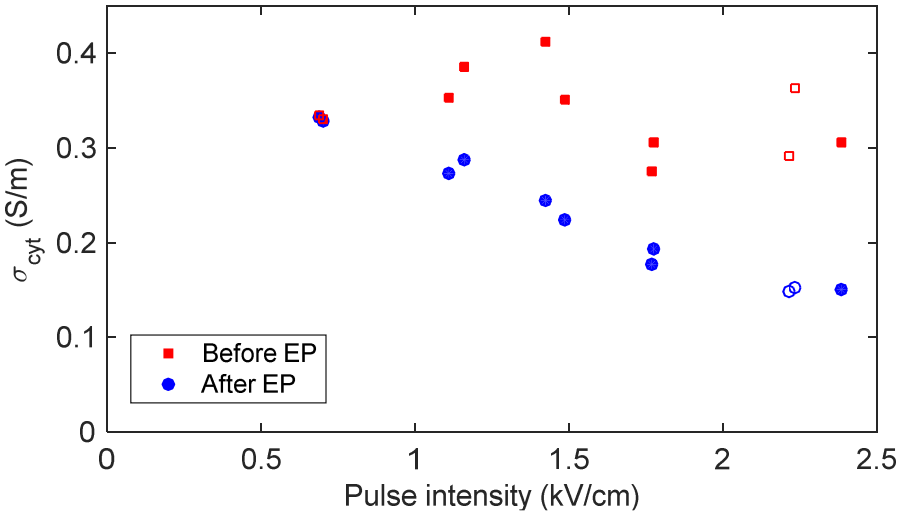

Figure 5.10: *Cytoplasm conductivity of single cells before and after exposure to 100 μs duration pulses with various intensities. Solid markers represent the results for applying six to eight pulses with repetition rate 100 Hz and open markers show the results for fifteen pulses with repetition rate 200 Hz.*

Table 5.3: *Summarized measurement results for the cells in Fig. 5.9.*

Altitude in channel (μm)	Amplitude of pulses (kV/cm)	Number of pulses	Conductivity before EP (S/m)	Conductivity after EP (S/m)
12.1	2.4	8	0.31	0.15
14.9	2.2	15	0.36	0.15
15.3	2.2	15	0.29	0.15
15.2	1.8	7	0.31	0.19
15.3	1.8	6	0.28	0.18
14.2	1.5	7	0.35	0.22
16.1	1.4	7	0.41	0.25
16.1	1.2	6	0.39	0.29
18.1	1.1	6	0.35	0.27
17.5	0.7	6	0.33	0.33
18.5	0.7	6	0.34	0.33

To verify that the obtained limit on the decrease of cells internal conductivity after electroporation, 0.15 S/m, is not related to the employed medium conductivity, we place cells in a lower conductivity medium (σ_e=0.05 S/m) and perform similar experiments. Single cells are exposed to eight 100 μs duration pulses with amplitude 2.2 kV/cm. Fig. 5.10 shows the results for two cells. It is evident that the force indices and subsequently $Re\{K_{CM}\}$ decreases after electroporation. The force index does not reach zero (or close to zero) after electroporation implying that not all the internal ions (the mobile ones that contribute in the internal conductivity) defuse out of the cell to the medium with very low ionic concentration. This confirms that with reversible electroporation there is a limit on the out flow of ions to the external medium. With the cells internal conductivity approximately 0.42 S/m corresponding to $Re\{K_{CM}\}$=0.68 (for medium with conductivity 0.05 S/m) before electroporation, and assuming a linear relationship between force index and $Re\{K_{CM}\}$, we obtain the cell's cytoplasm conductivity after electroporation as approximately 0.13 S/m. This is close to the result obtained for cells in a medium with conductivity 0.17 S/m.

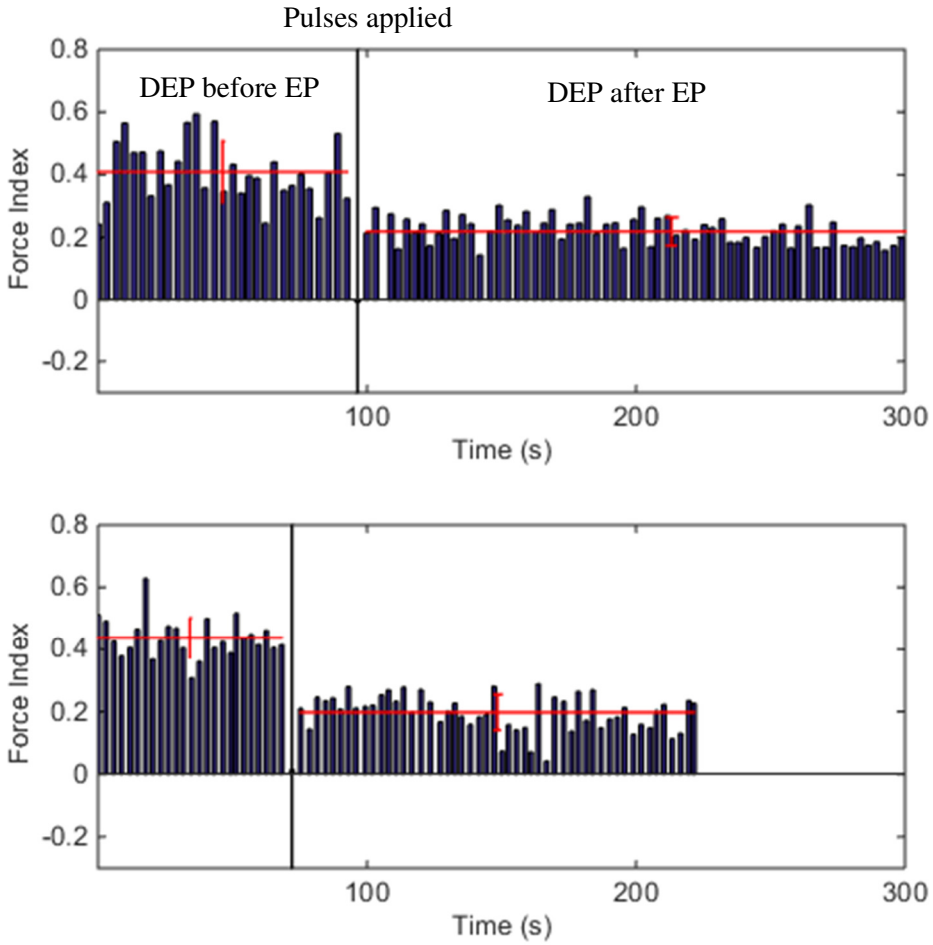

Figure 5.11: *Force index vs. time for two CHO cells (top and bottom) before and after exposure to 100 μs, 2.2 kV/cm pulses in a medium with conductivity 0.05 S/m. In each case the force index is shown for two states: (i) 10 MHz DEP actuation before the application of pulses (before the solid black line), and (ii) 10 MHz DEP actuation after application of pulses (after the solid black line). The mean of φ before and after pulse exposures is shown by red lines with the error bar being the standard deviation.*

5.2.3 Heat Effect of Electroporation

To verify that electroporation pulses do not heat the sample, causing thermal effects, a simulation is performed using *COMSOL Multiphysics Heat Transfer* module. Static fluid in the channel is assumed in our simulation which may lead to an overestimation of temperature increase in the channel (worst case scenario). Fig. 5.11 shows the maximum temperature in the channel during and after applying a 100μs duration, 2.2 kV/cm

amplitude trapezoidal pulse (starting at t=1 μs) with the same rise-time and intensity as the ones in the experiments. A maximum temperature increase of 0.45 K occurring during the pulse application verifies no heat associated effects. Also, the temperature settles to almost its initial value after 10 ms (for a repetition rate of 100 Hz the pulses are applied every 10 ms) assuring a negligible average temperature increase in case of repetitive pulse applications.

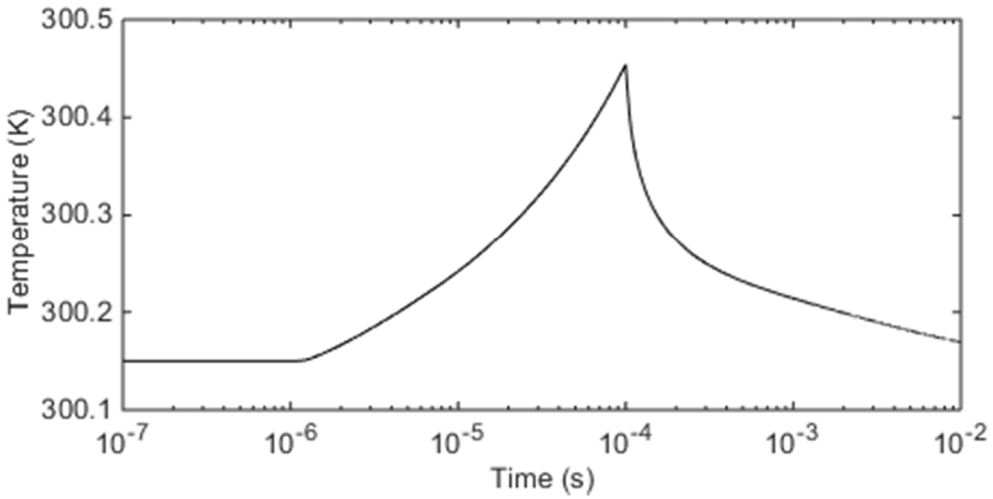

Figure 5.12: *Maximum temperature in the channel during and after applying an EP pulse of 100 μs duration, 2.2 kV/cm intensity, and 200 ns rise-time (the pulse starts at t=1 μs).*

5.3 CONCLUSIONS

In this chapter we presented quantitative results for changes in the cytoplasm conductivity of single cells subjected to pulsed electric fields with various intensities. We observed that when electroporation is performed in a medium with lower ionic concentration than cells cytoplasm, the internal conductivity of cells decreases after electroporation and its value depends on the intensity of applied pulses. We also observed that with reversible electroporation there is a limit on the decrease in the cells' internal conductivity suggesting

that some ions always remain inside the cell independent of the strength and number of applied pulses. We hypothesize the reason for this is the presence of large and relatively immobile negative ions inside the cell which attract mobile positive ions (mainly sodium and potassium) to maintain cell electrical neutrality. We monitored the temporal response of cells after electroporation to measure the time constant of changes due to ion transport and observed it ranges from seconds to tens of seconds depending on the applied pulse intensity. Only minimum-size pores exist during this time period and this observation is based on the transport of appropriately sized ions that can pass through these pores. This result can be used to infer information about the density and resealing time of very small pores (not measurable with conventional marker molecules) and their relationship with the intensity of applied pulses.

Chapter 6. Effect of Medium Conductivity

The results presented in chapter 5 showed how cells' internal conductivity is affected by electroporation when suspended in a medium with conductivity 0.17 S/m (lower than the typical cytoplasm conductivity of cells, 0.42 S/m). In order to study the effect of medium conductivity, we suspend cells in media with conductivities close to cells typical internal conductivity (0.4 S/m) and extremely lower (0.001 S/m) and perform electroporation and DEP studies on them.

6.1 ELECTROPORATION IN MEDIUM WITH CONDUCTIVITY 0.4 S/m

In this section we study the effect of using a high conductivity medium on the electroporation of cells and their final internal conductivity. Although a high conductivity growth media used for cell culturing ($\sigma_e \approx 1.5$ S/m) is ideal to use in this experiment we are limited to a medium with maximum conductivity $\sigma_e = 0.4$ S/m due to the electrolysis of water by the high electric field required for electroporation. This is often why many studies are done at much lower conductivities. The medium conductivity 0.4 S/m is close to the

internal conductivity of a healthy CHO cell. This medium is prepared by mixing fresh growth and low conductivity (~0.067 S/m) medium [22.9 mM sucrose (Sigma), 16 mM glucose (Fisher), 1 mM $CaCl_2$ (Fisher), 16 mM Na_2HPO_4 (Fisher)] (Polevaya et al., 1999), at a ratio of 7.6:24.4.

The measured results for three cells subjected to 100 μs duration pulses with an amplitude approximately 1.5 kV/cm (the highest intensity we could apply without electrolysing the water) is shown in Fig. 6.1 and summarized in Table 6.1. It is observed that the cells experience electroporation and their force indices noticeably decreases after electroporation. The force indices of all three cells obtain negative values eventually after electroporation confirming that the cells internal conductivity can decrease to lower than the medium conductivity. This was not observed in the medium 0.17 S/m because the internal conductivity of CHO cells cannot decrease below 0.15 S/m after a reversible electroporation (as observed and explained in section 5.2.2). The cells electroporated in medium 0.4 S/m have higher internal conductivity after electroporation compared to the ones subjected to similar pulses in a medium 0.17 S/m (see Table 5.3). The reason could be the higher concentration of ions in the medium 0.4 S/m which can transport into the cell through the created pores. Similar to electroporation in medium 0.17 S/m, time-dependent changes in the DEP response of cells after electroporation is evident for all three cells in Fig. 6.1 reflecting the time period that ions transport through minimum-size pores.

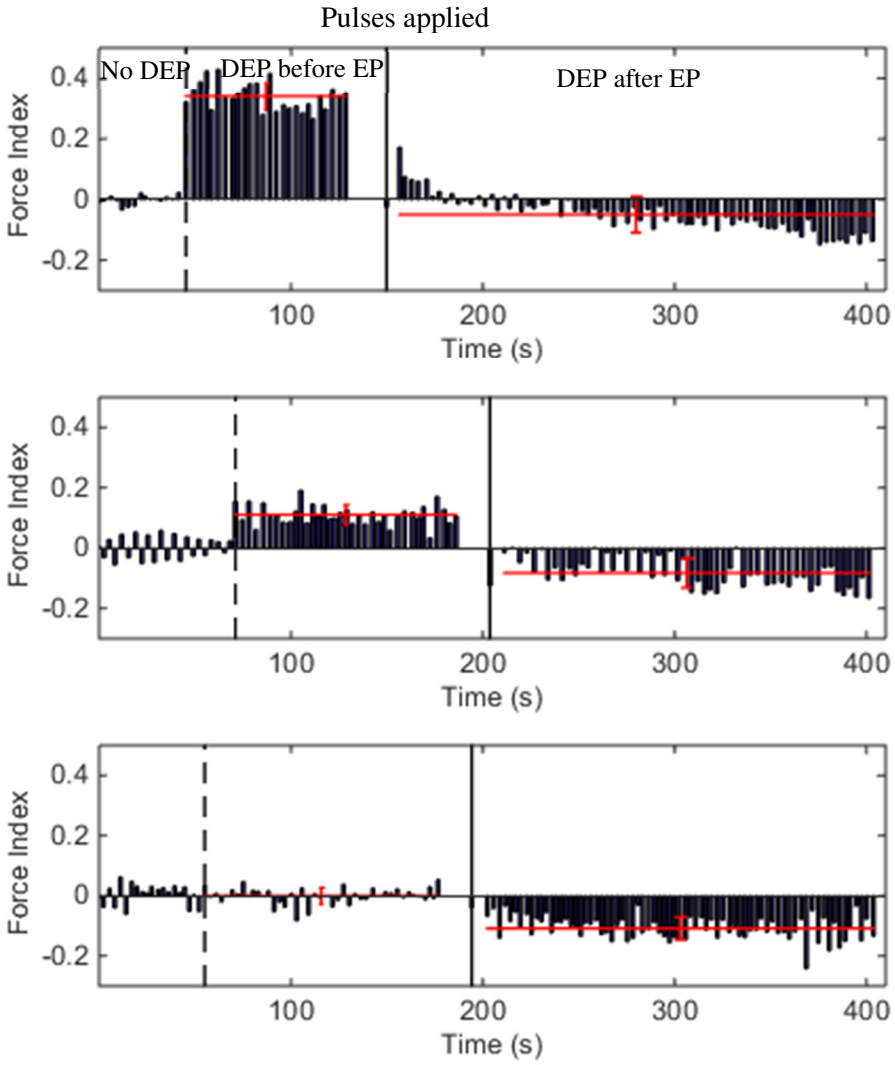

Figure 6.1: *Force index vs. time for three CHO cells (top to bottom) before and after exposure to 100 μs, 1.5 kV/cm pulses in a medium with conductivity 0.4 S/m. In each case the force index is shown for three states: (i) no DEP actuation (before the dashed black line), (ii) 10 MHz DEP actuation before the application of pulses (between the dashed and solid black lines), and (iii) 10 MHz DEP actuation after application of pulses (after the solid black line). The mean of φ before and after pulse exposures is shown by red lines with the error bar being the standard deviation.*

Table 6.1: *Summarized measurement results for the cells in Fig. 6.1.*

Altitude in channel (μm)	Amplitude of pulses (kV/cm)	Number of pulses	Conductivity before EP (S/m)	Conductivity after EP (S/m)
13.0	1.5	10	0.53	0.32
13.6	1.5	10	0.43	0.29
13.8	1.5	9	0.37	0.29

6.2 ELECTROPORATION IN MEDIUM WITH CONDUCTIVITY 0.001 S/m

In dielectric study of biological phenomena (in vitro studies) it is desired to have cells in a very low conductivity medium in order to decrease the electrode polarization effect. This is also the case to avoid electrolysis of water when very high short time-scale PEFs is studied. In this section we study electroporation of cells suspended in a medium with conductivity 0.001 S/m.

6.2.1 Cell Preparation

The cell preparation procedure is slightly different than that described in sections 5.11 and 6.1. The Chinese Hamster Ovary (CHO) cell line (CHODG44-EG2-hFc/clone 1A7) used for this study is kindly provided by Yves Durocher of the NRC, Canada (Bell et al., 2010). The cells are maintained by passaging them every 2 – 3 days and growing them in 250 mL baffled shaker flasks (VWR International, Radnor, PA) at 120 rpm in an incubator at 37°C with a 10% CO_2 overlay. The culture medium used is BioGro-CHO serum-free (BioGro Technologies, Winnipeg, MB) supplemented with 0.5 g/L yeast extract (BD, Sparks, MD), 4 mM GlutaMax I (Invitrogen, Grand Island, NY), and 1 mM glutamine (Sigma, St. Louis, MO). For this study a cell sample is taken from the shaker and centrifuged at 377xg for 1 min. The cell pellet is then washed two times with a very low conductive medium [229 mM sucrose (Sigma), 16 mM glucose (Fisher)] and re-suspended in the same medium adjusted to a conductivity of ~0.001 S/m with 6 µL 1X PBS (Gibco) and 9.5 µL 0.1 M NaOH (Fisher) as determined using a conductivity meter (Orion 3-Star Plus, Thermo Scientific, Waltham, MA). While re-suspending the cell pellet, the sample is diluted to a final concentration of 10^5 cells/mL for single cell studies and $2x10^6$ cells/ml for bulk studies. The viability of cells suspended in medium 0.001 S/m over time is tested by Trypan

blue staining method using a Cedex XS cell analyzer (Innovatice, Germany) and it is verified to remain above 92% for at least 60 minutes. In all measurement results presented in the next sections cells do not remain in the 0.001 S/m medium for longer than 45 minutes.

6.2.2 Single Cell Electroporation Measured by DEP Study

Several single CHO cells are shuttled back and force in the microfluidic channel and their DEP response is studied before and after electroporation with 8-10 pulses with 100 μs duration and 3 kV/cm intensity. In this case the DEP study is performed at 20 MHz since our simulations show that at very low conductivity media (0.001 S/m) $Re\{K_{CM}\}$ is more sensitive to the cytoplasm conductivity at 20 MHz. The measured force indices versus time is shown in Fig. 6.2. It is observed that, unlike electroporation in 0.05, 0.17, and 0.4 S/m media, no significant change in the DEP response of cells is observed in this medium for the measured time (approximately one minute) after pulse applications. Despite the very strong pulses employed, electroporation effects cells to a very low extent in this case since the high medium resistance (due to its very low conductivity) increases the charging time constant of the membrane and does not allow it to reach the required voltage of electroporation. Similar observations are reported in [130]–[132] showing that in very low conductivity media larger electric fields are required to achieve a similar extent of electroporation as compared with electroporation in high or moderately high conductivity media. In the case of a spherical cell in a uniform electric field, the time dependent response of the transmembrane potential to a PEF can be calculated theoretically [133] and is plotted in Fig. 6.3 for four different suspending medium conductivities. It is evident that the transmembrane potential reaches the required threshold of electroporation (approximately

1 V) quickly after the start of the pulse (the pulse starts at time zero) in media 0.05, 0.17, and 0.4 S/m while in medium 0.001 S/m it occurs almost at the end of the pulse. Our observation is in agreement with this theoretical prediction.

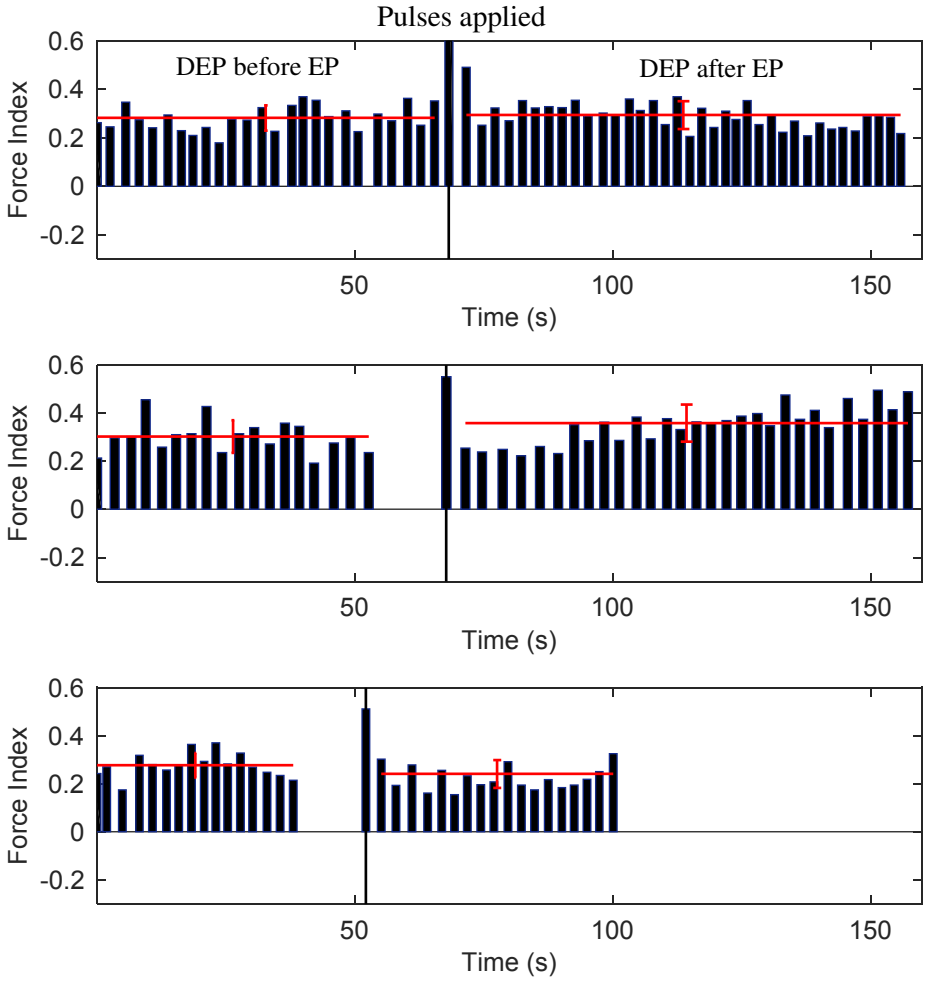

Figure 6.2: *Force index vs. time for three CHO cells before and after exposure to ten, nine, and eight (from top to bottom) 100 μs, 3 kV/cm pulses in a medium with conductivity 0.001 S/m. In each case the force index is shown for two states: (i) 20 MHz DEP actuation before the application of pulses (before the solid black line), and (ii) 20 MHz DEP actuation after application of pulses (after the solid black line). The mean of φ before and after pulse exposures is shown by red lines with the error bar being the standard deviation.*

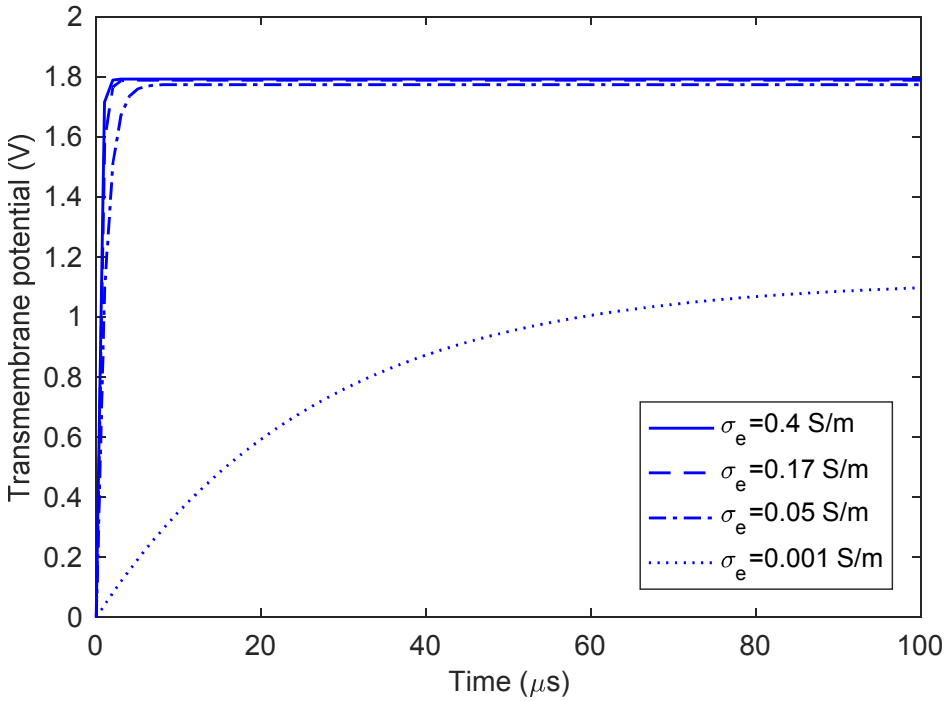

Figure 6.3: *Time dependent response of the transmembrane potential to a pulsed electric field for a spherical cell in a uniform electric field for four different suspending medium conductivities. The pulse starts at time zero and continues for 100 μs. The transmembrane potential reaches the required voltage of electroporation (~1 V) within a few microseconds for media 0.4, 0.17, and 0.05 S/m while in medium 0.001 S/m, this occurs at the end of the pulse.*

6.2.3 Bulk Electroporation Measured by Dye Exclusion and DEP Cytometry

In order to verify our results with a standard biological technique we build a microfluidic device to perform bulk electroporation and study the sample using a dye exclusion technique. The microfluidic device is fabricated by cutting a 3 mm wide serpentine channel from a polymer sheet with adhesive coating on both sides and sandwiching it between two gold coated glass slides. The height of the channel is measured approximately 160 μm. Access to the channel is provided by drilling inlet and outlet holes in the top glass slide and cells are introduced to the channel using a syringe pump. Cells in the channel are subjected to eight PEFs with 100 μs duration and various intensities generated by an Agilent function

generator and amplified by a high-voltage amplifier (Model 9400, Tabor Electronics). Experiments are performed only on cells in a medium with conductivity 0.001 S/m due to a limitation on the output current of the amplifier. After electroporation, cells are pumped out of the channel and collected for dye exclusion and DEP studies. Collected cells remain in the 0.001 S/m medium at room temperature for all subsequent Trypan blue tests. At times 1, 2, 5, and 10 minutes after pulse application, 20 µl of the sample is taken and mixed with the staining dye in a 1:1 ratio and the number of stained cells is counted using a Cedex XS cell analyzer (Innovatice, Germany). In DEP studies, cells are diluted with 0.001 S/m to a concentration 10^5 cells/ml and loaded to the DEP cytometry apparatus within a minute after pulse application. Approximately 300 single cells are analysed over a period of 18 minutes. Control studies follow similar procedures except that no pulses are applied to cells. Fig. 6.4 shows the results of dye exclusion and DEP studies for pulse amplitudes 0.6, 0.9, 1.5, and 1.8 kV/cm. DEP studies are performed continuously for 18 minutes, however, in order to make it comparable with the Trypan blue exclusion tests we take the average of periods $t<3.5$, $3.5<t<8.5$, $8.5<t<13.5$, $13.5<t<18.5$ to represent time points 1, 6, 11, and 16 minutes after electroporation, respectively.

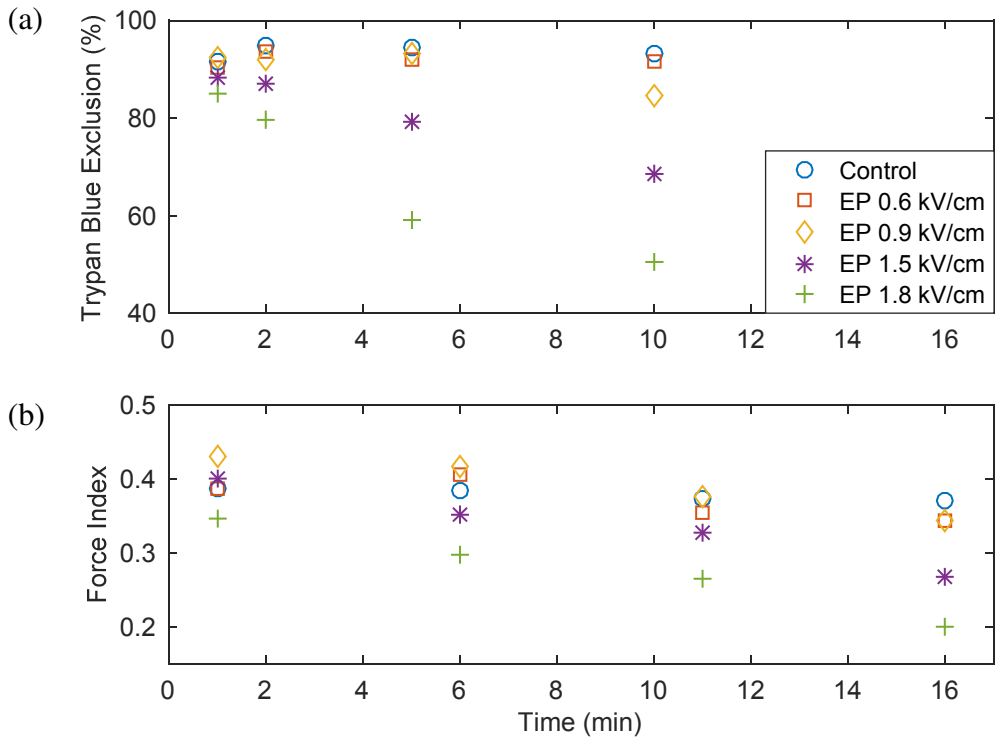

Figure 6.4: *(a) Percentage of cells not stained by Trypan blue after exposure to eight 100 µs duration pulses with various amplitudes. Cells are suspended in a medium with conductivity 0.001 S/m. (b) Force index versus time for single cells subjected to a DEP force at 10 MHz after electroporation with eight 100 µs duration pulses with various amplitudes. Each data point is the average of approximately 70 single cells. DEP studies are performed continuously for 18 minutes (starting at 1 minute after pulse application) and the average of periods t<3.5, 3.5<t<8.5, 8.5<t<13.5, 13.5<t<18.5 is taken to represent time points 1, 6, 11, and 16 minutes after electroporation, respectively.*

The results of the Trypan blue test show no significant difference between the control and electroporated cells one minute after electroporation. This could be due to either reversible electroporation or no significant electroporation. Cells subjected to 1.5 and 1.8 kV/cm start to take up Trypan blue after 2 minutes while the control and low amplitude pulsed cells remain impermeable to the dye. The control cells and those subjected to 0.6 kV/cm remain more than 90% impermeable to Trypan blue during the ten-minute measurement period. Similar results is obtained from the DEP cytometer. While the control and low amplitude

pulsed cells show no significant change in their DEP response (cytoplasm conductivity) the ones subjected to 1.5 and 1.8 kV/cm show decrease in the measured force indices. This is due to efflux of ions through the membrane and, hence, lower internal conductivity.

From these observations and the result of single cell electroporation presented in Fig. 6.2, we conclude that in a medium with very low conductivity (0.001 S/m) the pulses employed in our experiments create a small number of pores in cells' membrane which is not sufficient for quick uptake of Trypan blue. As an explanation for the uptake of trypan blue after few minutes, we hypothesize the reason is that the pores fail to reseal and they expand to larger radii since the low conductivity medium does not have the essential ions to maintain the cells functionality. This results in the gradual increase in the permeability of the staining dye into cells as observed by the Cedex cell analyzer as well as leakage of ions out of cells (by diffusion) as observed by the DEP cytometer. This hypothesis was verified by electroporating cells using pulses of 1.5 kV/cm and then immediately resuspend them in a regular growth medium. Trypan blue tests show that the resuspended cells remain impermeable to the staining dye over ten-minute measurement period confirming no damage to the cells' membrane.

6.3 CONCLUSIONS

In this chapter we studied the electroporation of cells and its effect on their internal conductivity when cells were subjected to PEF in media with conductivities 0.4 S/m (close to internal conductivity of healthy CHO cells) and 0.001 S/m (extremely lower than cells' internal conductivity). In the case of electroporation in medium 0.4 S/m, we observed a decrease in the internal conductivity of cells after electroporation and a time dependent

behavior similar to the results presented in the previous chapter for electroporation in a medium with conductivity 0.17 S/m. We also observed that the internal conductivity of cells decreased to lower than the external medium conductivity. In the case of electroporation in medium 0.001 S/m, we observed no significant changes in the internal conductivity of cells immediately after electroporation with pulse intensities similar to the ones employed in electroporation in higher medium conductivities. We conclude that electroporation in very low conductivity media requires stronger pulses to achieve a similar poration extent as compared with electroporation in moderately high conductivity media.

Chapter7. Conclusions and Future Work

7.1 CONCLUSIONS

Increasing the permeability of a biological cell's membrane using intense pulsed electric fields, electroporation, has found extensive medical and biological applications. Despite the research and numerous studies on electroporation and its applications the dynamic process of formation and resealing of pores is not well understood. Besides the conventional methods of studying electroporation such as dye exclusion techniques, fluorescent cytometry, and patch-clamp techniques dielectric based methods are attracting interest as a new label-free and non-invasive modality to investigate the phenomenon. The dielectric properties of a cell exposed to electroporating pulses are affected during and after the pulse exposure due to changes in the membrane structure and ions/molecules that transport through the created pores. As such, electroporation and its subsequent physiological effects on a cell can be studied by monitoring changes in the cell dielectric properties. In this work we introduce a DEP cytometry technique to study changes in the

cytoplasm conductivity of single Chinese hamster ovary cells induced by electroporation with various pulse intensities. The main contributions of this study are as follow:

1. We introduced a dielectric model based on the double-shell structure for Chinese hamster ovary (CHO) cells. This was achieved by measuring the DEP response of CHO cells and curve-fitting to the measured data. Explained in Chapter 4 and published in the journal Biomicrofluidics, a set of dielectric parameters measured for CHO cells was presented. This model is used in subsequent chapters to analyze and interpret the electroporation data. It should be mentioned that in previous literatures where an electrical model of CHO cells is required, a model with its parameters taken from other mammalian cell lines or yeast has often been adopted.
2. We introduced a technique to simultaneously electroporate single cells in a microfluidic device and study the induced changes in its dielectric properties. By shuttling a single cell back and forth in the microfluidic channel and studying its DEP response before and after applying electroporating pulses, we measured changes in cell's response within seconds after pulse exposures. Proper selection of the DEP actuation frequency allowed us to specifically monitor changes in the cells internal conductivity due to electroporation.
3. We developed a simulation model to relate the displacement of a cell in the microfluidic channel to its Clausius-Mossotti factor and then to its internal conductivity. This allowed us to obtain quantitative results on how electroporation effects a cell's internal conductivity.
4. We presented quantitative results for changes in the cytoplasm conductivity of single cells subjected to pulsed electric fields with various intensities. We observed

that when electroporation is performed in media with lower ionic concentration than cells cytoplasm, their internal conductivity decreases after electroporation depending on the intensity of applied pulses. We also observe that with reversible electroporation there is a limit on the decrease in the cells internal conductivity. We hypothesize the reason is the presence of large and relatively immobile negative ions inside the cell which attract mobile positive ions (mainly sodium and potassium) to maintain cell electrical neutrality.

5. We presented the temporal change in the cytoplasm conductivity of several individual cells subjected to pulsed electric fields with various intensities. We observed that there is a time constant associated with the cells' internal conductivity change which ranges from seconds to tens of seconds depending on the applied pulse intensity. This result can be used to infer the density and resealing time constant of minimum-size pores (within milliseconds after the end of pulses pores shrink to very small pores, approximately 1 nm radius, and then eventually reseal completely). Measurements using large markers (larger than the pore size) cannot obtain accurate information about small size pores.
6. Using our DEP measurement technique, we showed that electroporation in very low conductivity media requires stronger pulses to achieve a similar poration extent as compared with electroporation in moderately high conductivity media. We noted that even though the cells immediate response suggests a very low electroporation extent, in later times (minutes after pulse exposure) they may experience membrane damage if left in the very low conductivity medium. We hypothesize this is because

the medium does not have the essential ions for cells to reseal the pores and retain their membrane integrity.

7.2 FUTURE WORK

In this work we presented a measurement technique to dielectrically study the electroporation of single cells. We showed quantified results and discussed the observations for CHO cells subjected to 100 μs duration pulses with various intensities. As follow-ups for this work, our suggestions are as follow:

1. We showed that the medium conductivity affects the extent of electroporation as well as the cells ability to reseal. An interesting study is to suspend cells in high conductivity culture medium and measure changes in the internal conductivity of cells due to electroporation. In this case both influx and efflux of ions affect the internal conductivity. In the case of reversible electroporation the time required for cells to reach their original equilibrium can be measured.
2. In nanosecond electroporation of cells, nanopores with radius approximately 1 nm are created in the cells membrane. Using conventional dye molecules to study these pores may result in inaccurate conclusions since the size of the dye molecules is generally larger than the nanopores. Ions are ideal markers for studying nanopores and we showed that our measurement technique and apparatus can measure changes in ionic content of cells. Measuring changes in the conductivity of single cells induced by nanosecond duration pulses and comparing the results with microsecond ones (presented here) can provide insight on the mechanism of electroporation in these two different regimes.

3. In nanosecond electroporation, it has been shown that the electric field penetrates into cells and electroporate the internal organelles' membrane. Here, we showed that the cytoplasm conductivity of cells is affected by electroporation. This changes the charging time constant of cells internal membranes and may affect the process of electroporation in multiple pulse applications. Incorporating changes in the cytoplasm conductivity of cells after each pulse into the model of electroporation can make more accurate predictions and help with optimizing the pulse parameters for specific applications.
4. Changes in the cytoplasm conductivity after electroporation can be explained by electrodiffusion (during pulse application) and diffusion (after the pulse) of ions in and out of the cell through the created pores. In a recent published study [85], [86] the numerical model of electroporation (based on the Smoluchowski equation) is integrated with diffusion and electrodiffusion equations to estimate the transport of ions through pores under the condition that the effect of the solutes transport on the ionic current of pores is negligible. This assumption holds for fluorescent marker molecules and low concentration ions such as Ca^{2+}. An interesting research study is to modify the numerical model developed in [85], [86] to predict the transport of Na^{+}, K^{+}, and Cl^{-} (available inside and outside of the cell in a high concentration) and compare the results with the experimental results presented here.

References

[1] D. S. Dimitrov, “Electric field-induced breakdown of lipid bilayers and cell membranes: a thin viscoelastic film model.,” *J. Membr. Biol.*, vol. 78, no. 1, pp. 53–60, 1984.

[2] R. W. Glaser, S. L. Leikin, L. V Chernomordik, V. F. Pastushenko, and A. I. Sokirko, “Formation and Evolution of Pores,” *Biochim. Biophys. Acta*, vol. 940, pp. 275–287, 1988.

[3] J. C. Weaver and Y. a. Chizmadzhev, “Theory of electroporation: A review,” *Bioelectrochemistry Bioenerg.*, vol. 41, no. 2, pp. 135–160, 1996.

[4] S. Somiari, J. Glasspool-Malone, J. J. Drabick, R. a Gilbert, R. Heller, M. J. Jaroszeski, and R. W. Malone, “Theory and in vivo application of electroporative gene delivery.,” *Mol. Ther.*, vol. 2, no. 3, pp. 178–187, 2000.

[5] A. I. Daud, R. C. DeConti, S. Andrews, P. Urbas, A. I. Riker, V. K. Sondak, P. N. Munster, D. M. Sullivan, K. E. Ugen, J. L. Messina, and R. Heller, “Phase I trial of interleukin-12 plasmid electroporation in patients with metastatic melanoma,” *J. Clin. Oncol.*, vol. 26, no. 36, pp. 5896–5903, 2008.

[6] L. M. Mir, “Nucleic acids electrotransfer-based gene therapy (electrogenetherapy): past, current, and future.,” *Mol. Biotechnol.*, vol. 43, no. 2, pp. 167–76, Oct. 2009.

[7] D. Miklavčič, B. Mali, B. Kos, R. Heller, and G. Serša, “Electrochemotherapy: from the drawing board into medical practice.,” *Biomed. Eng. Online*, vol. 13, no. 1, p. 29, Jan. 2014.

[8] M. L. Yarmush, A. Golberg, G. Serša, T. Kotnik, and D. Miklavčič, "Electroporation-based technologies for medicine: principles, applications, and challenges.," *Annu. Rev. Biomed. Eng.*, vol. 16, pp. 295–320, Jul. 2014.

[9] I. Edhemovic, E. M. Gadzijev, E. Brecelj, D. Miklavcic, B. Kos, A. Zupanic, B. Mali, T. Jarm, D. Pavliha, M. Marcan, G. Gasljevic, V. Gorjup, M. Music, T. P. Vavpotic, M. Cemazar, M. Snoj, and G. Sersa, "Electrochemotherapy: A New Technological Approach in Treatment of Metastases in the Liver," *Technol. Cancer Res. Treat.*, vol. 10, no. 5, pp. 475–485, Oct. 2011.

[10] M. Marty, G. Sersa, J. R. Garbay, J. Gehl, C. G. Collins, M. Snoj, V. Billard, P. F. Geertsen, J. O. Larkin, D. Miklavcic, I. Pavlovic, S. M. Paulin-Kosir, M. Cemazar, N. Morsli, D. M. Soden, Z. Rudolf, C. Robert, G. C. O'Sullivan, and L. M. Mir, "Electrochemotherapy - An easy, highly effective and safe treatment of cutaneous and subcutaneous metastases: Results of ESOPE (European Standard Operating Procedures of Electrochemotherapy) study," *Eur. J. Cancer, Suppl.*, vol. 4, no. 11, pp. 3–13, 2006.

[11] L. M. Mir and S. Orlowski, "Mechanisms of electrochemotherapy," *Adv. Drug Deliv. Rev.*, vol. 35, no. 1, pp. 107–118, Jan. 1999.

[12] R. Heller, M. Jaroszeski, L. Glass, J. Messina, D. Rapaport, R. DeConti, N. Fenske, R. Gilbert, L. Mir, and D. Reintgen, "Phase I/II trial for the treatment of cutaneous and subcutaneous tumors using electrochemotherapy," *Cancer*, vol. 77, no. 5, pp. 964–971, Mar. 1996.

[13] K. H. Schoenbach, R. P. Joshi, R. H. Stark, F. C. Dobbs, and S. J. Beebe, "Bacterial

decontamination of liquids with pulsed electric fields," *IEEE Trans. Dielectr. Electr. Insul.*, vol. 7, no. 5, pp. 637–645, 2000.

[14] C. Gusbeth, W. Frey, H. Volkmann, T. Schwartz, and H. Bluhm, "Pulsed electric field treatment for bacteria reduction and its impact on hospital wastewater," *Chemosphere*, vol. 75, no. 2, pp. 228–233, Apr. 2009.

[15] H. J. Scheffer, K. Nielsen, M. C. de Jong, A. A. J. M. van Tilborg, J. M. Vieveen, A. R. A. Bouwman, S. Meijer, C. van Kuijk, P. M. P. van den Tol, and M. R. Meijerink, "Irreversible electroporation for nonthermal tumor ablation in the clinical setting: a systematic review of safety and efficacy.," *J. Vasc. Interv. Radiol.*, vol. 25, no. 7, p. 997–1011; quiz 1011, Jul. 2014.

[16] C. Jiang, R. V Davalos, and J. C. Bischof, "A review of basic to clinical studies of irreversible electroporation therapy.," *IEEE Trans. Biomed. Eng.*, vol. 62, no. 1, pp. 4–20, Jan. 2015.

[17] A. Golberg and M. L. Yarmush, "Nonthermal irreversible electroporation: fundamentals, applications, and challenges.," *IEEE Trans. Biomed. Eng.*, vol. 60, no. 3, pp. 707–14, Mar. 2013.

[18] M. Breton and L. M. Mir, "Microsecond and nanosecond electric pulses in cancer treatments.," *Bioelectromagnetics*, vol. 33, no. 2, pp. 106–23, Feb. 2012.

[19] J. C. Weaver, K. C. Smith, A. T. Esser, R. S. Son, and T. R. Gowrishankar, "A brief overview of electroporation pulse strength-duration space: A region where additional intracellular effects are expected," *Bioelectrochemistry*, vol. 87, pp. 236–243, 2012.

[20] S. J. Beebe, P. M. Fox, L. J. Rec, E. L. K. Willis, and K. H. Schoenbach, "Nanosecond, high-intensity pulsed electric fields induce apoptosis in human cells.," *FASEB J.*, vol. 17, no. 11, pp. 1493–5, Aug. 2003.

[21] P. T. Vernier, L. Marcu, C. M. Craft, and M. A. Gundersen, "Ultrashort pulsed electric fields induce membrane phospholipid translocation and caspase activation: differential sensitivities of Jurkat T lymphoblasts and rat Glioma C6 cells," *IEEE Trans. Dielectr. Electr. Insul.*, vol. 10, no. 5, pp. 795–809, Oct. 2003.

[22] P. T. Vernier, Y. Sun, L. Marcu, S. Salemi, C. M. Craft, and M. a. Gundersen, "Calcium bursts induced by nanosecond electric pulses," *Biochem. Biophys. Res. Commun.*, vol. 310, no. 2, pp. 286–295, 2003.

[23] S. J. Beebe, P. F. Blackmore, J. White, R. P. Joshi, and K. H. Schoenbach, "Nanosecond pulsed electric fields modulate cell function through intracellular signal transduction mechanisms," *Physiol. Meas.*, vol. 25, no. 4, pp. 1077–1093, Aug. 2004.

[24] K. H. Schoenbach, R. P. Joshi, J. F. Kolb, N. Chen, M. Stacey, P. F. Blackmore, E. S. Buescher, and S. J. Beebe, "Ultrashort electrical pulses open a new gateway into biological cells," *Proc. IEEE*, vol. 92, no. 7, pp. 1122–1136, 2004.

[25] K. H. Schoenbach, B. Hargrave, R. P. Joshi, J. F. Kolb, R. Nuccitelli, C. Osgood, A. Pakhomov, M. Stacey, R. J. Swanson, J. a. White, S. Xiao, J. Zhang, S. J. Beebe, P. F. Blackmore, and E. S. Buescher, "Bioelectric effects of intense nanosecond pulses," *IEEE Trans. Dielectr. Electr. Insul.*, vol. 14, no. 5, pp. 1088–1107, 2007.

[26] R. Nuccitelli, K. Tran, S. Sheikh, B. Athos, M. Kreis, and P. Nuccitelli, "Optimized

nanosecond pulsed electric field therapy can cause murine malignant melanomas to self-destruct with a single treatment.," *Int. J. cancer*, vol. 127, no. 7, pp. 1727–36, Oct. 2010.

[27] A. T. Esser, K. C. Smith, T. R. Gowrishankar, Z. Vasilkoskl, and J. C. Weaver, "Mechanisms for the intracellular manipulation of organelles by conventional electroporation," *Biophys. J.*, vol. 98, no. 11, pp. 2506–2514, 2010.

[28] W. Ren, N. M. Sain, and S. J. Beebe, "Nanosecond pulsed electric fields (nsPEFs) activate intrinsic caspase-dependent and caspase-independent cell death in Jurkat cells.," *Biochem. Biophys. Res. Commun.*, vol. 421, no. 4, pp. 808–12, May 2012.

[29] C. S. Djuzenova, U. Zimmermann, H. Frank, V. L. Sukhorukov, E. Richter, and G. Fuhr, "Effect of medium conductivity and composition on the uptake of propidium iodide into electropermeabilized myeloma cells," *Biochim. Biophys. Acta - Biomembr.*, vol. 1284, no. 2, pp. 143–152, 1996.

[30] B. Gabriel and J. Teissié, "Time courses of mammalian cell electropermeabilization observed by millisecond imaging of membrane property changes during the pulse.," *Biophys. J.*, vol. 76, no. 4, pp. 2158–2165, 1999.

[31] Z. Ji, S. Member, S. M. Kennedy, J. H. Booske, S. Member, and S. C. Hagness, "Experimental Studies of Persistent Poration Dynamics of Cell Membranes Induced by Electric Pulses," *IEEE Trans. Plasma Sci.*, vol. 34, no. 4, pp. 1416–1424, 2006.

[32] D. a Zaharoff, J. W. Henshaw, B. Mossop, and F. Yuan, "Mechanistic analysis of electroporation-induced cellular uptake of macromolecules.," *Exp. Biol. Med. (Maywood).*, vol. 233, no. 1, pp. 94–105, 2008.

[33] A. M. Bowman, O. M. Nesin, O. N. Pakhomova, and A. G. Pakhomov, "Analysis of plasma membrane integrity by fluorescent detection of Tl(+) uptake.," *J. Membr. Biol.*, vol. 236, no. 1, pp. 15–26, 2010.

[34] A. G. Pakhomov, R. Shevin, J. a. White, J. F. Kolb, O. N. Pakhomova, R. P. Joshi, and K. H. Schoenbach, "Membrane permeabilization and cell damage by ultrashort electric field shocks," *Arch. Biochem. Biophys.*, vol. 465, no. 1, pp. 109–118, 2007.

[35] A. G. Pakhomov, J. F. Kolb, J. a. White, R. P. Joshi, S. Xiao, and K. H. Schoenbach, "Long-lasting plasma membrane permeabilization in mammalian cells by nanosecond Pulsed Electric Field (nsPEF)," *Bioelectromagnetics*, vol. 28, no. 8, pp. 655–663, 2007.

[36] B. L. Ibey, S. Xiao, K. H. Schoenbach, M. R. Murphy, and A. G. Pakhomov, "Plasma membrane permeabilization by 60- and 600-ns electric pulses is determined by the absorbed dose," *Bioelectromagnetics*, vol. 30, no. 2, pp. 92–99, 2009.

[37] V. Nesin, A. M. Bowman, S. Xiao, and A. G. Pakhomov, "Cell permeabilization and inhibition of voltage-gated Ca 2+ and Na + channel currents by nanosecond pulsed electric field," *Bioelectromagnetics*, vol. 33, no. 5, pp. 394–404, 2012.

[38] M. Hibino, M. Shigemori, H. Itoh, K. Nagayama, and K. Kinosita, "Membrane conductance of an electroporated cell analyzed by submicrosecond imaging of transmembrane potential.," *Biophys. J.*, vol. 59, no. 1, pp. 209–220, 1991.

[39] M. Hibino, H. Itoh, and K. Kinosita, "Time courses of cell electroporation as revealed by submicrosecond imaging of transmembrane potential.," *Biophys. J.*, vol. 64, no. 6, pp. 1789–1800, 1993.

[40] M. Schmeer, T. Seipp, U. Pliquett, S. Kakorin, and E. Neumann, “Mechanism for the conductivity changes caused by membrane electroporation of CHO cell-pellets,” *Phys. Chem. Chem. Phys.*, vol. 6, no. 24, p. 5564, 2004.

[41] A. L. Garner, G. Chen, N. Chen, V. Sridhara, J. F. Kolb, R. J. Swanson, S. J. Beebe, R. P. Joshi, and K. H. Schoenbach, “Ultrashort electric pulse induced changes in cellular dielectric properties,” *Biochem. Biophys. Res. Commun.*, vol. 362, no. 1, pp. 139–144, 2007.

[42] M. G. Moisescu, M. Radu, E. Kovacs, L. M. Mir, and T. Savopol, “Changes of cell electrical parameters induced by electroporation. A dielectrophoresis study,” *Biochim. Biophys. Acta - Biomembr.*, vol. 1828, no. 2, pp. 365–372, 2013.

[43] K. a DeBruin and W. Krassowska, “Modeling electroporation in a single cell. I. Effects Of field strength and rest potential.,” *Biophys. J.*, vol. 77, no. 3, pp. 1213–1224, 1999.

[44] K. a DeBruin and W. Krassowska, “Modeling electroporation in a single cell. II. Effects Of ionic concentrations.,” *Biophys. J.*, vol. 77, no. 3, pp. 1225–1233, 1999.

[45] R. P. Joshi, Q. Hu, and K. H. Schoenbach, “Dynamical Modeling of Cellular Response to Short-Duration, High-Intensity Electric Fields,” *IEEE Trans. Dielectr. Electr. Insul.*, vol. 10, no. 5, pp. 778–787, 2003.

[46] K. C. Smith and J. C. Weaver, “Active mechanisms are needed to describe cell responses to submicrosecond, megavolt-per-meter pulses: cell models for ultrashort pulses.,” *Biophys. J.*, vol. 95, no. 4, pp. 1547–1563, 2008.

[47] G. Pucihar, D. Miklavčič, and T. Kotnik, "A time-dependent numerical model of transmembrane voltage inducement and electroporation of irregularly shaped cells," *IEEE Trans. Biomed. Eng.*, vol. 56, no. 5, pp. 1491–1501, 2009.

[48] R. S. Son, K. C. Smith, T. R. Gowrishankar, P. T. Vernier, and J. C. Weaver, "Basic features of a cell electroporation model: illustrative behavior for two very different pulses.," *J. Membr. Biol.*, vol. 247, no. 12, pp. 1209–28, Dec. 2014.

[49] I. G. Abidor, L. H. Li, and S. W. Hui, "Studies of cell pellets: I. Electrical properties and porosity.," *Biophys. J.*, vol. 67, no. 1, pp. 418–426, 1994.

[50] M. Pavlin, M. Kanduser, M. Rebersek, G. Pucihar, F. X. Hart, R. Magjarevic, and D. Miklavcic, "Effect of cell electroporation on the conductivity of a cell suspension.," *Biophys. J.*, vol. 88, no. 6, pp. 4378–4390, 2005.

[51] A. L. Garner, N. Chen, J. Yang, J. Kolb, R. J. Swanson, K. C. Loftin, S. J. Beebe, R. P. Joshi, and K. H. Schoenbach, "Time domain dielectric spectroscopy measurements of HL-60 cell suspensions after microsecond and nanosecond electrical pulses," *IEEE Trans. Plasma Sci.*, vol. 32, no. 5 II, pp. 2073–2084, 2004.

[52] U. Pliquett, R. P. Joshi, V. Sridhara, and K. H. Schoenbach, "High electrical field effects on cell membranes," *Bioelectrochemistry*, vol. 70, no. 2, pp. 275–282, 2007.

[53] J. Zhuang, W. Ren, Y. Jing, and J. F. Kolb, "Dielectric evolution of mammalian cell membranes after exposure to pulsed electric fields," *IEEE Trans. Dielectr. Electr. Insul.*, vol. 19, no. 2, pp. 609–622, 2012.

[54] J. Oblak, D. Križaj, S. Amon, A. Maček-Lebar, and D. Miklavčič, "Feasibility study

for cell electroporation detection and separation by means of dielectrophoresis," *Bioelectrochemistry*, vol. 71, no. 2, pp. 164–171, 2007.

[55] Q. Hu, R. P. Joshi, and a. Beskok, "Model study of electroporation effects on the dielectrophoretic response of spheroidal cells," *J. Appl. Phys.*, vol. 106, no. 2, 2009.

[56] J. Cemažar and T. Kotnik, "Dielectrophoretic field-flow fractionation of electroporated cells.," *Electrophoresis*, vol. 33, no. 18, pp. 2867–74, Sep. 2012.

[57] S. C. Bürgel, C. Escobedo, N. Haandbæk, and A. Hierlemann, "On-chip electroporation and impedance spectroscopy of single-cells," *Sensors Actuators B Chem.*, vol. 210, pp. 82–90, 2015.

[58] B. Gabriel and J. Teissié, "Control by electrical parameters of short- and long-term cell death resulting from electropermeabilization of Chinese hamster ovary cells," *Biochim. Biophys. Acta - Mol. Cell Res.*, vol. 1266, no. 2, pp. 171–178, Apr. 1995.

[59] M. P. Rols and J. Teissié, "Electropermeabilization of mammalian cells to macromolecules: Control by pulse duration," *Biophys. J.*, vol. 75, no. 3, pp. 1415–1423, 1998.

[60] M. Pavlin and D. Miklavčič, "Theoretical and experimental analysis of conductivity, ion diffusion and molecular transport during cell electroporation - Relation between short-lived and long-lived pores," *Bioelectrochemistry*, vol. 74, no. 1, pp. 38–46, 2008.

[61] L. a Flanagan, J. Lu, L. Wang, S. a Marchenko, N. L. Jeon, A. P. Lee, and E. S. Monuki, "Unique dielectric properties distinguish stem cells and their differentiated

progeny.," *Stem Cells*, vol. 26, no. 3, pp. 656–665, 2008.

[62] M. Toner and D. Irimia, "Blood-on-a-chip.," *Annu. Rev. Biomed. Eng.*, vol. 7, pp. 77–103, 2005.

[63] M. Hashimoto, H. Kaji, and M. Nishizawa, "Selective capture of a specific cell type from mixed leucocytes in an electrode-integrated microfluidic device," *Biosens. Bioelectron.*, vol. 24, pp. 2892–2897, 2009.

[64] C. L. Asbury, A. H. Diercks, and G. van den Engh, "Trapping of DNA by dielectrophoresis," *Electrophoresis*, vol. 23, no. 16, pp. 2658–2666, Aug. 2002.

[65] J. Regtmeier, T. T. Duong, R. Eichhorn, D. Anselmetti, and A. Ros, "Dielectrophoretic Manipulation of DNA: Separation and Polarizability," *Anal. Chem.*, vol. 79, no. 10, pp. 3925–3932, May 2007.

[66] J. P. Burt, R. Pethig, P. R. Gascoyne, and F. F. Becker, "Dielectrophoretic characterisation of Friend murine erythroleukaemic cells as a measure of induced differentiation.," *Biochim. Biophys. Acta*, vol. 1034, no. 1, pp. 93–101, 1990.

[67] P. R. Gascoyne, R. Pethig, J. P. Burt, and F. F. Becker, "Membrane changes accompanying the induced differentiation of Friend murine erythroleukemia cells studied by dielectrophoresis.," *Biochim. Biophys. Acta*, vol. 1149, no. 1, pp. 119–126, 1993.

[68] F. H. Labeed, H. M. Coley, H. Thomas, and M. P. Hughes, "Assessment of multidrug resistance reversal using dielectrophoresis and flow cytometry.," *Biophys. J.*, vol. 85, no. 3, pp. 2028–2034, 2003.

[69] Y. Huang, R. Hölzel, R. Pethig, and X. B. Wang, "Differences in the AC electrodynamics of viable and non-viable yeast cells determined through combined dielectrophoresis and electrorotation studies.," *Phys. Med. Biol.*, vol. 37, no. 7, pp. 1499–1517, 1992.

[70] I. Doh and Y.-H. Cho, "A continuous cell separation chip using hydrodynamic dielectrophoresis (DEP) process," *Sensors Actuators A Phys.*, vol. 121, no. 1, pp. 59–65, May 2005.

[71] G. H. Markx, M. S. Talary, and R. Pethig, "Separation of viable and non-viable yeast using dielectrophoresis," *J. Biotechnol.*, vol. 32, pp. 29–37, 1994.

[72] P. R. C. Gascoyne, J. Noshari, T. J. Anderson, and F. F. Becker, "Isolation of rare cells from cell mixtures by dielectrophoresis," *Electrophoresis*, vol. 30, no. 8, pp. 1388–1398, 2009.

[73] M. Nikolic-Jaric, T. Cabel, E. Salimi, A. Bhide, K. Braasch, M. Butler, G. E. Bridges, and D. J. Thomson, "Differential electronic detector to monitor apoptosis using dielectrophoresis-induced translation of flowing cells (dielectrophoresis cytometry)," *Biomicrofluidics*, vol. 7, no. 2, pp. 1–15, 2013.

[74] K. Braasch, M. Nikolic-Jaric, T. Cabel, E. Salimi, G. E. Bridges, D. J. Thomson, and M. Butler, "The changing dielectric properties of CHO cells can be used to determine early apoptotic events in a bioprocess," *Biotechnol. Bioeng.*, vol. 110, no. 11, pp. 2902–2914, 2013.

[75] R. Pethig, "Review article-dielectrophoresis: status of the theory, technology, and applications.," *Biomicrofluidics*, vol. 4, no. 2, Jan. 2010.

[76] Z. R. Gagnon, "Cellular dielectrophoresis: Applications to the characterization, manipulation, separation and patterning of cells," *Electrophoresis*, vol. 32, no. 18, pp. 2466–2487, 2011.

[77] T. B. Jones, *Electromechanics of Particles*, 1st ed. Cambridge University Press, 1995.

[78] a Irimajiri, T. Hanai, and a Inouye, "A dielectric theory of 'multi-stratified shell' model with its application to a lymphoma cell.," *J. Theor. Biol.*, vol. 78, no. 2, pp. 251–269, 1979.

[79] K. Asami, Y. Takahashi, and S. Takashima, "Dielectric properties of mouse lymphocytes and erythrocytes," *Biochim. Biophys. Acta - Mol. Cell Res.*, vol. 1010, no. 1, pp. 49–55, Jan. 1989.

[80] M. Golzio, M. P. Mora, C. Raynaud, C. Delteil, J. Teissié, and M. P. Rols, "Control by osmotic pressure of voltage-induced permeabilization and gene transfer in mammalian cells.," *Biophys. J.*, vol. 74, no. 6, pp. 3015–3022, 1998.

[81] H.-Y. Wang and C. Lu, "High-throughput and real-time study of single cell electroporation using microfluidics: effects of medium osmolarity.," *Biotechnol. Bioeng.*, vol. 95, no. 6, pp. 1116–25, Dec. 2006.

[82] I. G. Abidor, V. B. Arakelyan, L. V. Chernomordik, Y. A. Chizmadzhev, V. F. Pastushenko, and M. R. Tarasevich, "246 - Electric breakdown of bilayer lipid membranes I. The main experimental facts and their qualitative discussion," *Bioelectrochemistry Bioenerg.*, vol. 6, no. 1, pp. 37–52, 1979.

[83] R. a Böckmann, B. L. de Groot, S. Kakorin, E. Neumann, and H. Grubmüller, "Kinetics, statistics, and energetics of lipid membrane electroporation studied by molecular dynamics simulations.," *Biophys. J.*, vol. 95, no. 4, pp. 1837–1850, 2008.

[84] Z. a. Levine and P. T. Vernier, "Life cycle of an electropore: Field-dependent and field-independent steps in pore creation and annihilation," *J. Membr. Biol.*, vol. 236, no. 1, pp. 27–36, 2010.

[85] K. C. Smith, "A Unified Model of Electroporation and Molecular Transport," Massachusetts institute of Technology, 2011.

[86] R. S. Son, T. R. Gowrishankar, K. C. Smith, and J. C. Weaver, "Modeling a Conventional Electroporation Pulse Train: Decreased Pore Number, Cumulative Calcium Transport and an Example of Electrosensitization.," *IEEE Trans. Biomed. Eng.*, vol. 63, no. 3, pp. 571–80, Mar. 2016.

[87] G. A. Ferrier, S. F. Romanuik, D. J. Thomson, G. E. Bridges, and M. R. Freeman, "A microwave interferometric system for simultaneous actuation and detection of single biological cells.," *Lab Chip*, vol. 9, no. 23, pp. 3406–3412, 2009.

[88] J. A. Stratton, *Electromagnetic Theory*. Wiley-IEEE Press, 2007.

[89] D. M. Pozar, *Microwave Engineering*. 2005.

[90] M. Nikolic-Jaric, S. F. Romanuik, G. A. Ferrier, G. E. Bridges, M. Butler, K. Sunley, D. J. Thomson, and M. R. Freeman, "Microwave frequency sensor for detection of biological cells in microfluidic channels," *Biomicrofluidics*, vol. 3, no. 3, pp. 1–16, 2009.

[91] I. H. Shames, *Mechanics of Fluids*, 4th ed. Boston: McGraw-Hill, 2003.

[92] S. P. Williams, T. Koch, and J. Calvin Giddings, "Characterization of near-wall hydrodynamic lift forces using sedimentation field-flow fractionation," *Chem. Eng. Commun.*, vol. 111, no. 1, pp. 121–147, Jan. 1992.

[93] P. Ganatos, S. Weinbaum, and R. Pfeffer, "A strong interaction theory for the creeping motion of a sphere between plane parallel boundaries. Part 1. Perpendicular motion.," *J. Fluid Mech.*, vol. 99, no. 4, NaN, 1980. pp. 739–753, 1980.

[94] E. Salimi, K. Braasch, M. Butler, D. J. Thomson, and G. E. Bridges, "Dielectric model for Chinese hamster ovary cells obtained by dielectrophoresis cytometry," *Biomicrofluidics*, vol. 10, p. 14111, 2016.

[95] Polysciences Inc., "Polybead Polystyrene Microspheres Technical Datasheet," 2013.

[96] E. C. Anderson, D. F. Petersen, and R. A. Tobey, "Density invariance of cultured Chinese hamster cells with stage of the mitotic cycle.," *Biophys. J.*, vol. 10, no. 7, pp. 630–45, Jul. 1970.

[97] Gunter Hofmann, *Iscotables: A Handbook of Data for Biological and Physical Scientists*. Lincoln, Nebraska : Instrumentation Specialties Company, 1977.

[98] W. J. Ellison, K. Lamkaouchi, and J. M. Moreau, "Water: A dielectric reference," *J. Mol. Liq.*, vol. 68, no. 2–3, pp. 171–279, 1996.

[99] K. Jayapal, K. Wlaschin, W. Hu, and G. Yap, "Recombinant protein therapeutics from CHO cells-20 years and counting," *Chem. Eng. Prog.*, vol. 103, no. 10, pp. 40–

47, 2007.

[100] M. Fiore, R. Zanier, and F. Degrassi, “Reversible G(1) arrest by dimethyl sulfoxide as a new method to synchronize Chinese hamster cells.,” *Mutagenesis*, vol. 17, no. 5, pp. 419–24, Sep. 2002.

[101] M. J. Fernández, A. López, and A. Santa-Maria, “Apoptosis induced by different doses of caffeine on Chinese hamster ovary cells.,” *J. Appl. Toxicol.*, vol. 23, no. 4, pp. 221–4, Jan. 2003.

[102] Q. Zeng, J.-M. Dong, K. Guo, J. Li, H.-X. Tan, V. Koh, C. J. Pallen, E. Manser, and W. Hong, “PRL-3 and PRL-1 promote cell migration, invasion, and metastasis,” *Cancer Res.*, vol. 63, no. 11, pp. 2716–22, Jun. 2003.

[103] L. F. Z. Batista, V. Chiganças, G. Brumatti, G. P. Amarante-Mendes, and C. F. M. Menck, “Involvement of DNA replication in ultraviolet-induced apoptosis of mammalian cells.,” *Apoptosis*, vol. 11, no. 7, pp. 1139–48, Jul. 2006.

[104] S. Yan, J. Zhang, Y. Yuan, G. Lovrecz, G. Alici, H. Du, Y. Zhu, and W. Li, “A hybrid dielectrophoretic and hydrophoretic microchip for particle sorting using integrated prefocusing and sorting steps.,” *Electrophoresis*, vol. 36, no. 2, pp. 284–91, Jan. 2015.

[105] G. Mernier, S. Majocchi, N. Mermod, and P. Renaud, “In situ evaluation of single-cell lysis by cytosol extraction observation through fluorescence decay and dielectrophoretic trapping time,” *Sensors Actuators B Chem.*, vol. 166–167, pp. 907–912, May 2012.

[106] J. Čemažar, D. Vrtačnik, S. Amon, and T. Kotnik, "Dielectrophoretic field-flow microchamber for separation of biological cells based on their electrical properties.," *IEEE Trans. Nanobioscience*, vol. 10, no. 1, pp. 36–43, Mar. 2011.

[107] C. Justice, A. Brix, D. Freimark, M. Kraume, P. Pfromm, B. Eichenmueller, and P. Czermak, "Process control in cell culture technology using dielectric spectroscopy.," *Biotechnol. Adv.*, vol. 29, no. 4, pp. 391–401, Jan. 2011.

[108] C. F. Opel, J. Li, and A. Amanullah, "Quantitative modeling of viable cell density, cell size, intracellular conductivity, and membrane capacitance in batch and fed-batch CHO processes using dielectric spectroscopy.," *Biotechnol. Prog.*, vol. 26, no. 4, pp. 1187–99, Jan. 2010.

[109] K. Asami, "Characterization of heterogeneous systems by dielectric spectroscopy," *Prog. Polym. Sci.*, vol. 27, no. 8, pp. 1617–1659, Oct. 2002.

[110] S. Gawad, K. Cheung, U. Seger, A. Bertsch, and P. Renaud, "Dielectric spectroscopy in a micromachined flow cytometer: theoretical and practical considerations.," *Lab Chip*, vol. 4, no. 3, pp. 241–251, 2004.

[111] Y. Polevaya, I. Ermolina, M. Schlesinger, B. Z. Ginzburg, and Y. Feldman, "Time domain dielectric spectroscopy study of human cells. II. Normal and malignant white blood cells.," *Biochim. Biophys. Acta*, vol. 1419, no. 2, pp. 257–271, 1999.

[112] I. Ermolina, Y. Polevaya, Y. Feldman, B. Z. Ginzburg, and M. Schlesinger, "Study of normal and malignant white blood cells by time domain dielectric spectroscopy," *IEEE Trans. Dielectr. Electr. Insul.*, vol. 8, no. 2, pp. 253–261, Apr. 2001.

[113] A. Surowiec, S. S. Stuchly, and C. Izaguirre, “Dielectric properties of human B and T lymphocytes at frequencies from 20 kHz to 100 MHz.,” *Phys. Med. Biol.*, vol. 31, no. 1, pp. 43–53, 1986.

[114] F. H. Labeed, H. M. Coley, and M. P. Hughes, “Differences in the biophysical properties of membrane and cytoplasm of apoptotic cells revealed using dielectrophoresis.,” *Biochim. Biophys. Acta*, vol. 1760, no. 6, pp. 922–9, Jun. 2006.

[115] P. R. C. Gascoyne, F. F. Becker, and X.-B. Wang, “Numerical analysis of the influence of experimental conditions on the accuracy of dielectric parameters derived from electrorotation measurements,” *Bioelectrochemistry Bioenerg.*, vol. 36, no. 2, pp. 115–125, 1995.

[116] A. Han, R. Abuhabsah, J. P. Blue, S. Sarwate, and W. D. O’Brien, “Ultrasonic backscatter coefficient quantitative estimates from high-concentration Chinese Hamster Ovary cell pellet biophantoms.,” *J. Acoust. Soc. Am.*, vol. 130, no. 6, pp. 4139–47, Dec. 2011.

[117] A. Irimajiri, Y. Doida, T. Hanai, and A. Inouye, “Passive electrical properties of cultured murine lymphoblast (L5178Y) with reference to its cytoplasmic membrane, nuclear envelope, and intracellular phases,” *J. Membr. Biol.*, vol. 38, no. 3, pp. 209–232, Sep. 1978.

[118] L. Duncan, H. Shelmerdine, M. P. Hughes, H. M. Coley, Y. Hübner, and F. H. Labeed, “Dielectrophoretic analysis of changes in cytoplasmic ion levels due to ion channel blocker action reveals underlying differences between drug-sensitive and multidrug-resistant leukaemic cells.,” *Phys. Med. Biol.*, vol. 53, no. 2, pp. N1-7, Jan.

2008.

[119] C. Merla, M. Liberti, F. Apollonio, C. Nervi, and G. D'Inzeo, "A microwave microdosimetric study on blood cells: Estimation of cell membrane permittivity and parametric EM analysis," *IEEE MTT-S Int. Microw. Symp. Dig.*, pp. 1333–1336, 2009.

[120] P. R. C. Gascoyne, S. Shim, J. Noshari, F. F. Becker, and K. Stemke-Hale, "Correlations between the dielectric properties and exterior morphology of cells revealed by dielectrophoretic field-flow fractionation," *Electrophoresis*, vol. 34, no. 7, pp. 1042–1050, 2013.

[121] J. Yang, Y. Huang, X. Wang, X. B. Wang, F. F. Becker, and P. R. Gascoyne, "Dielectric properties of human leukocyte subpopulations determined by electrorotation as a cell separation criterion.," *Biophys. J.*, vol. 76, no. 6, pp. 3307–3314, 1999.

[122] L. Wu, L.-Y. Lanry Yung, and K.-M. Lim, "Dielectrophoretic capture voltage spectrum for measurement of dielectric properties and separation of cancer cells.," *Biomicrofluidics*, vol. 6, no. 1, pp. 14113–1411310, Mar. 2012.

[123] L. M. Broche, F. H. Labeed, and M. P. Hughes, "Extraction of dielectric properties of multiple populations from dielectrophoretic collection spectrum data.," *Phys. Med. Biol.*, vol. 50, no. 10, pp. 2267–74, May 2005.

[124] O. Keminer and R. Peters, "Permeability of single nuclear pores.," *Biophys. J.*, vol. 77, no. 1, pp. 217–228, Jul. 1999.

[125] M. Nikolic-Jaric, G. A. Ferrier, D. J. Thomson, G. E. Bridges, and M. R. Freeman, "Dielectric response of particles in flowing media: The effect of shear-induced rotation on the variation in particle polarizability," *Phys. Rev. E - Stat. Nonlinear, Soft Matter Phys.*, vol. 84, no. 1, pp. 1–11, 2011.

[126] M. Usaj and M. Kanduser, "The systematic study of the electroporation and electrofusion of B16-F1 and CHO cells in isotonic and hypotonic buffer," *J. Membr. Biol.*, vol. 245, no. 9, pp. 583–590, 2012.

[127] H. Pauly and H. Schwan, "Dielectric properties and ion mobility in erythrocytes," *Biophys. J.*, vol. 6, no. 5, pp. 621–639, 1966.

[128] Y. Huang, X.-B. Wang, R. Holzel, F. F. Becker, and P. R. C. Gascoyne, "Electrorotational studies of the cytoplasmic dielectric properties of Friend murine erythroleukaemia cells," *Phys. Med. Biol.*, vol. 40, no. 11, pp. 1789–1806, Nov. 1995.

[129] J. A. Fraser and C. L.-H. Huang, "Quantitative techniques for steady-state calculation and dynamic integrated modelling of membrane potential and intracellular ion concentrations," *Prog. Biophys. Mol. Biol.*, vol. 94, no. 3, pp. 336–372, Jul. 2007.

[130] E. Neumann, "Membrane electroporation and direct gene transfer," *Bioelectrochemistry Bioenerg.*, vol. 28, no. 1–2, pp. 247–267, Aug. 1992.

[131] G. Pucihar, T. Kotnik, M. Kandušer, and D. Miklavčič, "The influence of medium conductivity on electropermeabilization and survival of cells in vitro," *Bioelectrochemistry*, vol. 54, no. 2, pp. 107–115, 2001.

[132] A. Ivorra, J. Villemejane, and L. M. Mir, “Electrical modeling of the influence of medium conductivity on electroporation.,” *Phys. Chem. Chem. Phys.*, vol. 12, no. 34, pp. 10055–10064, 2010.

[133] T. Kotnik, D. Miklavčič, and T. Slivnik, “Time course of transmembrane voltage induced by time-varying electric fields - A method for theoretical analysis and its application,” *Bioelectrochemistry Bioenerg.*, vol. 45, no. 1, pp. 3–16, 1998.